TRIBOLOGICAL PERFORMANCE OF DIAMOND-LIKE CARBON AND WATER-BASED LUBRICANTS FOR METALWORKING

By

MUHAMMAD SHUHAIMI BIN IBRAHIM

Thesis Submitted to the School of Graduate Studies, Universiti Putra Malaysia, in Fulfilment of the Requirements for the Degree of Master of Science

February 2025

FK 2025 2

Abstract of thesis presented to the Senate of Universiti Putra Malaysia in fulfilment of the requirement for the degree of Master of Science

TRIBOLOGICAL PERFORMANCE OF DIAMOND-LIKE CARBON AND WATER-BASED LUBRICANTS FOR METALWORKING

By

MUHAMMAD SHUHAIMI BIN IBRAHIM

February 2025

Chair : **Mohd Hafis bin Sulaiman, PhD, P. Eng**
Faculty : **Engineering**

Metalworking processes face challenges in extending tool life and eliminating harmful lubricants. This study investigates a new tribosystem that combines Diamond-Like Carbon (DLC) coatings and environmentally friendly water-based lubricants (WBL). The effects are analysed using tribological, machining, and sheet-metal forming. The first objective is to investigate DLC coatings on CNC lathe cutting tools under severe dry friction conditions. Machining was performed on Al6061 aluminum and AISI4340 alloy steel using double-layered (DLC/TiAlSN, DLC/CrN, DLC/TiAlN) and single-layered (TiAlSN, CrN, TiAlN) coatings. The test parameters include a depth of cut of 0.5 mm, a speed of 240 rpm, and a feed rate of 0.15 mm/rev. The results show the superior performance of the double-layered coating, with DLC/TiAlN excelling in cutting force, tool temperature, wear, surface quality, and chip thickness. Adhesive wear was found on machning aluminum, while abrasive wear was observed on alloy steel. The second objective evaluates the effect of additives in WBL. A hybrid additive system combining MXene and Ionic Liquid (IL) was formulated with Carboxyl Methyl Cellulose (CMC) and Xanthan Gum (XG) to improve viscosity and dispersion stability. Block-on-ring tribology tests (ASTM G77) at 500 rpm and 42 N revealed that XG improved WBL stability, while MXene/IL additives significantly reduced friction and wear. WBL formulated with CMC and MXene/IL hybrids were performed in hydrodynamic lubrication regime. The third objective was to evaluate the effect of the optimized DLC/TiAlN and WBL combination on sheet-metal forming in ironing process with 20% reduction thickness. Using DLC/TiAlN coated tools and SUS304 stainless steel sheets, ironing tests showed an 8% reduction in ironing force and less tool wear. Further tribology tests confirmed a 26% reduction in friction and a 7.3% reduction in wear. This study identified an optimal tribosystem, integrating DLC/TiAlN and CMC_MXene/IL, which improves lubricity, reduces wear and improves tool performance in metalworking applications

Keywords: Water-based lubricant, Tribology, Ironing process, DLC double-layered coating, Metal forming.

SDG: GOAL 6: Clean water and Sanitation, GOAL 9: Industry, Innovation and Infrastructure

Abstrak tesis yang dikemukakan kepada Senat Universiti Putra Malaysia
Sebagai memenuhi keperluan untuk ijazah Master Sains

PRESTASI TRIBOLOGI *DIAMOND-LIKE CARBON* DAN PELINCIR BERASASKAN AIR UNTUK KERJALOGAM

Oleh

MUHAMMAD SHUHAIMI BIN IBRAHIM

Februari 2025

Pengerusi : Mohd Hafis bin Sulaiman, PhD, P. Eng
Fakulti : Kejuruteraan

Proses kerja logam menghadapi cabaran dalam memanjangkan jangka hayat alat dan menghapuskan pelincir berbahaya. Kajian ini menyelidiki sistem tribologi baharu yang menggabungkan salutan Diamond-Like Carbon (DLC) dan pelincir berasaskan air yang mesra alam (WBL). Kesan-kesan dianalisis menggunakan tribologi, pemesinan, dan pembentukan kepingan logam. Objektif pertama adalah menyelidiki salutan DLC pada alat pemotong CNC lathe di bawah keadaan geseran kering yang teruk. Pemesinan dilakukan pada aluminium Al6061 dan aloi keluli AISI4340 menggunakan salutan dua lapis (DLC/TiAlSN, DLC/CrN, DLC/TiAlN) dan satu lapis (TiAlSN, CrN, TiAlN). Parameter ujian termasuk kedalaman pemotongan 0.5 mm, kelajuan 240 rpm, dan kadar suapan 0.15 mm/rev. Hasil menunjukkan prestasi unggul salutan dua lapis, dengan DLC/TiAlN cemerlang dalam daya pemotongan, suhu alat, haus, kualiti permukaan, dan ketebalan serpihan. Haus melekit ditemui pada pemesinan aluminium, manakala haus kasar diperhatikan pada aloi keluli.

Objektif kedua menilai kesan tambahan dalam WBL. Sistem tambahan hibrid yang menggabungkan MXene dan Cecair Ionik (IL) diformulasikan dengan Carboxyl Methyl Cellulose (CMC) dan Xanthan Gum (XG) untuk meningkatkan kelikatan dan kestabilan pengedaran. Ujian tribologi block-on-ring (ASTM G77) pada 500 rpm dan 42 N menunjukkan bahawa XG meningkatkan kestabilan WBL, manakala tambahan MXene/IL secara signifikan mengurangkan geseran dan haus. WBL yang diformulasikan dengan CMC dan hibrid MXene/IL dilakukan dalam rejim pelinciran hidrodinamik. Objektif ketiga adalah menilai kesan kombinasi DLC/TiAlN dan WBL yang dioptimumkan pada proses pembentukan kepingan logam dalam proses pengironan dengan pengurangan ketebalan 20%. Menggunakan alat yang dilapisi DLC/TiAlN dan lembaran keluli tahan karat SUS304, ujian pengironan menunjukkan pengurangan 8% dalam daya pengironan dan kurang haus alat. Ujian tribologi lanjut mengesahkan pengurangan 26% dalam geseran dan 7.3% dalam haus. Kajian ini mengenal pasti sistem tribologi optimum, mengintegrasikan DLC/TiAlN dan CMC_MXene/IL, yang meningkatkan kelikatan, mengurangkan haus, dan meningkatkan prestasi alat dalam aplikasi kerja logam.

Kata Kunci: Pelincir berasaskan air, Tribologi, Proses menyeterika, Salutan dwi-lapisan DLC, Kerja logam.

SDG: MATLAMAT 6: Air Bersih dan Sanitasi, MATLAMAT 9: Industri, Inovasi dan Infrastruktur

ACKNOWLEGEMENT

Alhamdulillah, praise to Allah S.W.T for giving me the opportunity and strength to conclude this meaningful journey of my final year thesis even though many obstacles and challenges need to be faced.

I express my deepest appreciation to my project supervisor, Ir. Dr. Mohd Hafis Sulaiman and co-supervisor Associate Professor Dr. Mohd Idris Shah Ismail and Dr. Yazid Yaakob for allowing me to do the project and providing invaluable guidance along the journey. Their vision, sincerity and motivation have deeply inspired me. Working and studying under their supervision was a privilege and an honor. I am grateful for their acceptance and patience with me throughout the project and thesis preparation.

I am very grateful to the Malaysia Ministry of Higher Education for the financial support under the Special Graduate Research Allowance Scheme (SGRA) through the Fundamental Research Grant Scheme (FRGS/1/2022/TK10/UPM/02/9). Additionally, I appreciate Universiti Putra Malaysia and the GP-IPM (UPM/GPIPM/2022/9717500) for the development and testing of DLC coatings for metalworking applications. Special thanks are extended to the Department of Mechanical and Manufacturing Engineering, Faculty of Engineering, Universiti Putra Malaysia, for their invaluable assistance and for making their facilities available at every stage of this research.

I would like to express my deepest gratitude to Mr. Khairuddin for his extraordinary contribution as a team member in this project. His technical expertise, unwavering dedication, and valuable insights have played a significant role in the successful completion of this research. En. Khairuddin 's commitment to overcoming challenges and his collaborative spirit have been a source of motivation and inspiration throughout the journey. I am truly thankful for his hard work and support, and it has been a privilege to work alongside him on this project. I would like to express my heartfelt appreciation to Habib Shah, a dear friend and dedicated group member, for her invaluable support and contributions throughout this project.

I would like to express my deepest appreciation to my team members for their hard work and dedication throughout the predictive maintenance project. Their technical expertise, insightful ideas, and collaborative spirit were instrumental in overcoming the challenges we faced. I am truly grateful for the time and effort they devoted to ensuring the project's success, and I look forward to future opportunities to work together.

Lastly, I would like to express my deepest gratitude to my beloved family, my father Ibrahim and my mother Fatmawati also my siblings for their unwavering support, patience, and encouragement throughout this journey. I am grateful for your unconditional support, which has given me the strength to keep moving forward. This achievement would not have been possible without each and every one of you. Thank you for all your encouragement.

This thesis was submitted to the Senate of Universiti Putra Malaysia and has been accepted as fulfilment of the requirement for the degree of Master of Science. The members of the Supervisory Committee were as follows:

Mohd Hafis bin Sulaiman, PhD
Senior lecturer
Department of Mechanical and Manufacturing Engineering
Universiti Putra Malaysia
(Chairman)

Mohd Idris Shah bin Ismail, PhD
Associate Professor
Department of Mechanical and Manufacturing Engineering
Universiti Putra Malaysia
(Member)

Yazid bin Yaakob, PhD
Senior Lecturer
Faculty of Science
Universiti Putra Malaysia
(Member)

ZALILAH MOHD SHARIFF, PhD
Professor and Dean
School of Graduate Studies
Universiti Putra Malaysia

Date: 8 May 2025

TABLE OF CONTENT

		Page
ABSTRACT		i
ABSTRAK		iii
ACKNOWLEGEMENT		v
APPROVAL		vii
DECLARATION		ix
TABLE OF CONTENTS		xiii
LIST OF TABLES		xiv
LIST OF FIGURES		xiii
LIST OF ABBREVIATIONS		xx

CHAPTER

1	**INTRODUCTION**	
	1.1 Background	1
	1.2 Problem statement	3
	1.3 Objectives of the research	5
	1.4 Scopes and limitations of the study	5
	1.5 Thesis outline	7
2	**LITERATURE REVIEW**	
	2.1 Metal working	8
	2.1.1 Machining in turning operation	8
	2.1.2 Metal forming	14
	2.2 Tribology testing	20
	2.2.1 Friction	20
	2.2.2 Wear	21
	2.2.3 Lubricant	25
	2.3 Tribo testing method	31
	2.3.1 Block on ring	31
	2.3.2 Pin on disk	32
	2.3.3 Four ball	33
	2.3.4 Previous work	34
	2.4 Coating applied to metal working tooling in metal working industry	37
	2.5 Lubrication	42
	2.5.1 Nano additive used in lubricant	42
	2.5.2 Low-dimensional materials	43
	2.5.3 Additive in lubricants	44
	2.5.4 Effect of additives on lubricants	54
	2.5.5 Method to prepare nano additive lubricant	56
	2.6 Research gap	58
3	**METHODOLOGY**	
	3.1 Introduction	60

3.2 Overview of the framework 60
3.3 Material 63
3.3.1 Coating tool 63
3.3.2 Water-based Lubricant 64
3.4 Method to determine the tool coating 69
3.5 Method of tribological testing 74
3.6 Method to evaluate both coating and water-based lubricant 75
3.7 Method to evaluate Wear 77

4 RESULTS AND DISCUSSION
4.1 Introduction 79
4.2 Selection of coating using turning process 80
4.2.1 Effect of coated tool to cutting force 80
4.2.2 Effects of coated tools on surface integrity 85
4.2.3 Wear analysis of coated tools after machining 90
4.2.4 Raman analysis of top-layered DLC coatings 101
4.2.5 Microstructural analysis of DLC/TiAlN coating 103
4.3 Evaluation of water-based lubricant 105
4.3.1 Influence of additive in water-based lubricant 106
4.3.2 Coefficient of friction (COF) 108
4.3.3 Temperature 112
4.3.4 Wear 114
4.3.5 Roughness of sliding surface 116
4.3.6 Film thickness of test WBLs 119
4.4 Combined effect of coating and water-based lubricant in metal working 120
4.4.1 Ironing force 120
4.4.2 Wear on the tool surface 121
4.4.3 DLC/TiAlN and CMC_Mxene/IL testing 124

5 CONCLUSION
5.1 Conclusion 129
5.2 Recommendations 131

REFERENCES 132
APPENDINCES 158
BIODATA OF STUDENT 165
LIST OF PUBLICATIONS 166

LIST OF TABLES

Table		Page
2.1	Previous work on tribology testing method	36
2.2	Previous work of using additive in lubricant	49
2.3	Previous testing methods of tribo testing	52
3.1	Single coating and double coating of cutting tool	64
3.2	Chemical formula and density of additive and surfactant	65
3.3	The properties of Ionic liquid and MXene.	66
3.4	Content of water-based lubricants	67
3.5	Parameter setup for machining AISI4340 and Al6061	70
3.6	Mechanical properties of test workpiece; Al6061 and AISI4340 (MatWeb LLC, 2024).	71
3.7	Chemical composition of workpiece; Al6061 and AISI4340 (MatWeb LLC, 2024).	71
3.8	Material properties of block and ring AISI 52100	74
4.1	Minimum film thickness and λ of lubricants	111
4.2	Summary of surface Roughness (Ra and Sa) on the block after BOR	118
4.3	Wear area for CMC_Mxene/IL with coating DLC/TiAlN and without coating	128

LIST OF FIGURES

Figure		Page
2.1	Effect of cutting speed and feed rate to tool life (Khan et al., 2022).	11
2.2	Basic motion in turning operation (Davim, 2011)	12
2.3	Modern CNC lathe operation (Davim, 2011).	12
2.4	Cutting operation of (a) Orthogonal method and (b) Oblige method (Miracle & Olaleke, 2020).	13
2.5	(a) chip formation during machining, (b) schematic diagram of chip formation where t is depth of cut, t' is thickness of chip and L is surface contact, and (c) force acting during machining (TriboMAN, 2024).	14
2.6	Tribological tests representing the friction conditions in the specific areas of the draw piece	15
2.7	(a) Bending process that involve in deep drawing application and (b) the drawing force at steady state including surface roughness of AISI 304L and surface condition of the coating die (Sulaiman et al., 2019)	17
2.8	(a) Schematics of laboratory test for ironing process, (b) Setup of the ironing process, and (c) surface condition of workpiece AISI 304L and die at temperature 80° under dry condition (Sulaiman et al., 2019).	18
2.9	Force distribution of moving block	21
2.10	Process of adhesive wear	23
2.11	SEM morphology of adhesive wear surface (Podgornik, 2022)	23
2.12	(a) Two body and three body abrasive wear (B. R. Gupta, 2023) and (b) SEM images of the P110 worn casing sample (S0) tested under dry conditions at 115 rpm and 1000 N for 40 min from (Osman et al., 2022).	24
2.13	Process of corrosive wear (Stachowiak & Batchelor, 2013)	25
2.14	The worn surface morphologies of the amorphous coating after the corrosion-wear tests (Liao et al., 2023).	25

2.15	Friction behaviour represent as initial changes in friction with time (Khonsari et al., 2021)	26
2.16	Stribeck curve graph (Y. Wang & Wang, 2013) and stribeck curve with friction data obtained from a range of fluids with varying viscosity from (Xu & Stokes, 2020)	27
2.17	Contact mechanics (a) Contact between two spheres. (b) two cross cylinder and (c) (Popov, 2010)	28
2.18	Block-on-ring diagram (Ideris et al., 2023)	32
2.19	Pin-on-disk diagram (Di Puccio et al., 2024)	33
2.20	Four ball diagrams	34
2.21	Structure of layer coating attach to substrate (Caliskan et al., 2017)	38
2.22	Crack propagation behaviour for each of the common coating structure (Caliskan et al., 2017)	39
2.23	(a) Layer structure of DLC and (b) Surface condition images of the workpiece and tool after screening experiments with dry lubrication at a tool temperature of 80°C (Sulaiman et al., 2017)	40
2.24	a) The friction coefficient curves and b) The wear rates of the N-DLC/DLC, N-DLC, DLC (Sharifahmadian & Mahboubi, 2019)	41
2.25	The contrast of 0D, 1D and 2D materials (Shaw et al., 2021)	43
2.26	(a) COF plots vs. cycle number under load of 0.5 N and 1.0 N; (b) specific wear rate of copper disk with/without Ti3C2 coatings (Lian et al., 2018).	46
2.27	Field Emission Scanning Electron Microscopy (FESEM) images of Ti3AlC2 and HF-etched Ti3C2TX samples prepared over 48 hours (Khatun & Roy, 2022).	47
2.28	Schematic illustration of (a) rolling effect (b) mending effect, (c) polishing effect and (d) protective tribo-film formation (Azman & Samion, 2019; Singh et al., 2020)	54
2.29	Subdivision of preparation methods of nanolubricants. (Morshed et al., 2021)	57
2.30	Schematics of preparation methods of nanolubricants	58

3.1	The main flowchart of this study	61
3.2	The detail of framework for (a) objective 1, (b) objective 2, and (c) objective 3	63
3.3	Chemical structure of (a) Tributyl(methyl)phosphonium dimethyl phosphate (Wijanarko et al., 2022b), (b) Xanthan Gum and (c) Carboxymethyl Cellulose (Michaelis et al., 2023)	65
3.4	Particle of Ti3C2Tx MXene multilayer Nanoflake at (a) 10000 magnification and (b) 25000 magnification	66
3.5	Preparation of WBLs	67
3.6	The SV-10 viscometer	69
3.7	Test setup for machining through orthogonal cutting.	70
3.8	SURFTEST SJ-210 tester to measure the surface roughness.	73
3.9	Tribological test setup following ASTM G77 test standard.	74
3.10	Wear area analysis on the surface of the block	75
3.11	Ironing setup on the press machine.	76
3.12	Dimension of lower die for ironing with 20 percent thickness reduction.	76
3.13	Dimension of uncoated and coated tools for ironing with 20 percent thickness reduction.	77
3.14	Dino-Lite AM4113.	77
3.15	Olympus Digital Microscope DSX1000	78
3.16	SEM machine model JSM-7800F from JEOL	78
4.1	Detail observation in this research	79
4.2	Measured cutting force Fz in steady-state conditions during the orthogonal cutting experiment using both single- and double-layered hard coatings	80
4.3	Measured temperature in steady-state conditions during the orthogonal cutting experiment using both single- and double-layered hard coatings	82

4.4	Measured workpiece roughness after the orthogonal cutting experiment using both single- and double-layered hard coatings	86
4.5	Measured chip thickness t after the orthogonal cutting experiment using both single- and double-layered hard coatings	87
4.6	Comparative Analysis of (a,b) Flank Wear; (c,d) Crater Wear on Al6061 and AISI4340 Workpieces Using Various Coated Cutting Tools, as Observed Under a Microscope	93
4.7	Tool wear indicators according to ISO 3685	94
4.8	Measured a) flank wear VBavg and b) crater wear KBavg of both single- and double-layered coated tools after the orthogonal cutting experiment.	95
4.9	SEM-EDS analysis on both single- and double-layered coated tools after the orthogonal cutting of aluminium Al6061	98
4.10	SEM-EDS analysis on both single- and double-layered coated tools after the orthogonal cutting of AISI4340 alloy steel	100
4.11	Tool wear on uncoated (left) and double-layered DLC/TiAlN (right) coated tools after the orthogonal cutting of aluminium Al6061 using SEM-EDS analysis.	101
4.12	Tool wear on uncoated (left) and double-layer DLC/TiAlN (right) coated tools after the orthogonal cutting of AISI4340 alloy steel using SEM-EDS analysis.	101
4.13	Raman analysis on DLC coating as top-layered to CrN-, TiAlSiN-, TiAlN coatings	103
4.14	A cross-sectional view of the tool surface with deposited DLC/TiAlN coating (Note	104
4.15	Analysis of the elemental composition in DLC/TiAlN coating via SEM-EDX.	105
4.16	Sedimentation test of wate-based lubricants; (a) CMC_IL, (b) XG_IL (c) CMC_Mxene, (d) XG_Mxene (e) CMC_Mxene/IL, and (f) XG_Mxene/IL.	107
4.17	Viscosity of for the test WBLs	108
4.18	COF for all lubricants including dry condition for whole testing (a) 15000 cycle and (b) at steady state.	109

4.19	Average COF for different lubricant at 500 rpm	110
4.20	WLB in region of lubrication with COF and minimum film thickness where viscosity of lubricant is different at 500 rpm and normal load 42 N	112
4.21	Temperature near to sliding surfaces for tribological experiment on block-on-ring test setup until 15,000 cycle.	113
4.22	Measured average and maximum temperature near to sliding surfaces for tribological experiment on block-on-ring test setup until 15,000 cycle.	113
4.23	Area of Wear and the Calculation Formula	114
4.24	Wear scar of the block arranged ascendingly according to the wear area.	114
4.25	Close up of the wear on the block for every additive and surfactant.	116
4.26	Line roughness (Ra) and Area surface roughness (Sa) on the block after BOR	118
4.27	COF and minimum thickness for CMC_Mxene/IL at various speeds.	119
4.28	Force during blanking process every 5 strokes for dry frication and using DLC/TiAlN coating with lubricant CMC_Mxene/IL	121
4.29	Wear visible on punch nose of uncoated tool performed in dry friction condition.	123
4.30	Wear occurred to punch nose for DLC/TiAlN coated punch with dry condition	123
4.31	Wear occurred to punch nose for DLC/TiAlN coated punch lubricated with CMC_Mxene/IL WBL.	124
4.32	Measurement of friction for CMC_Mxene/IL with DLC/TiAlN coated and uncoated.	125
4.33	Average COF for CMC_Mxene/IL with DLC/TiAlN coated and uncoated at 500 rpm.	125
4.34	Average and maximum temperature near to sliding surfaces for WBL CMC_Mxene/IL with coating DLC/TiAlN and without coating.	126

4.35 Wear area on the block using (a) DLC/TiAlN coating with CMC_Mxene/IL, (b) DLC/TiAlN coating with dry condition and (c) Uncoated steel surface. 128

LIST OF ABBREVIATIONS

[THTDP] [Deca]	Trihexyl (Tetradecyl) Phosphonium Decanoate
0D	Zero-Dimensional
1D	One-Dimensional
2D	Two-Dimensional
AADD	Aluminium Alloy Deep Drawing
Al_2O_3	Aluminium Oxide
ASTM	American Society for Testing and Materials
BUE	Build-Up Edge
CDs	Carbon Dots
CMC	Carboxymethyl Cellulose
CNC	Computer Numerical Control
COF	Coefficient Of Friction
CrN	Chromium Nitride
Cu-Be	Copper-Beryllium
DI	Distilled Water
DLC	Diamond-Like Carbon
DPA	Bis(2-Hydroxyethyl) Ammonium Palmitate
EDS	Energy Dispersive Spectroscopy
EDX	Energy Dispersive X-Ray
EP	Extreme Pressure
FESEM	Field Emission Scanning Electron Microscopy
GO	Graphene Oxide
hBN	Hexagonal Boron Nitride

HF	Hydrogen Fluoride
HiPIMS	High Power Impulse Magnetron Sputtering
IL	Ionic Liquid
ILs	Ionic Liquids
KB	Crater Width
KB_{avg}	Average Of Crater Wear
LDMs	Low-Dimensional Materials
MoS_2	Molybdenum Disulfide
NRo	Nanorods
PAO	Polyalphaolefin
Ra	Arithmetical Mean Height
rpm	Revolutions Per Minute
Sa	Arithmetical Mean Height in Area
SEM	Scanning Electron Microscopy
SiO_2	Silicon Dioxide
SPM	Stroke Per Minute
Ti_3C_2	Titanium Carbide
TiAlN	Titanium Aluminium Nitride
TiAlSN	Titanium Aluminum Silicon Nitride
TiO_2	Titanium Dioxide
TMP	Trimethylolpropane
VB	Flank Wear
VB_{avg}	Average Of Flank Wear
WBL	Water-Based Lubricant
WBLs	Water-Based Lubricants

WSD	Wear Scar Diameter
XG	Xanthan Gum
ZrO_2	Zirconium Dioxide

CHAPTER 1

INTRODUCTION

1.1 Background

The term "tribology" is derived from the Greek word "tribos," which mean "rubbing," and is coupled with the suffix "-ology," indicating "the study of." Thus, tribology is the study about surfaces interacting in relative motion, encompassing the science and engineering of wear, lubrication, and friction, as outlined by Dunn et al., (2021). Highlighting its significance, Bhushan, (2013) regards tribology as a discipline that applies operational analysis to solve economically impactful problems, with applications that even reach into the realm of space exploration. This is related to the science of wear, lubrication, and friction is pivotal in various applications where the presence of sufficient friction and wear is essential. For instance, friction allows objects to be grasped securely (Hao et al., 2021) and provides traction between tires and road surfaces, thus preventing skidding. Additionally, high wear rates are beneficial in manufacturing processes like grinding and polishing. However, friction can also lead to energy losses through heat generation (Aleshin & Papangelo, 2020), which is undesirable in many industrial settings. This friction-induced wear results in material loss, contributing to wastage. Remarkably, it is estimated that one-third of a vehicle's fuel consumption is expended in overcoming friction. Research by Zhai et al., (2017) suggests that even a modest reduction of 20% in friction could lead to significant environmental benefits and cost savings. Therefore, minimizing friction and wear is of great interest. One effective method to achieve this is through the application of lubricants, which create a protective film that minimizes contact between surfaces, thereby reducing both friction and wear.

In response to the detrimental environmental effects of Oil-based lubricants (OBLs), Water-based lubricants (WBLs) have been identified as a viable and environmentally friendly alternative. They show great promise across a range of engineering applications such as in electric vehicles, transmission systems, hydropower operations, machining processes, and metal shaping, as noted by Morshed et al., (2021). A notable instance is the collaborative research initiative supported by the Swedish government, which includes contributions from CEVT (an innovation center within the Geely Family), SKF (a renowned Swedish manufacturer of bearings and seals), and the Luleå University of Technology. This collaboration between them is to explore the application of WBLs to boost the performance of electric vehicles, as reported by SKF Group, (2021). Additionally, Klüber Lubrication, a German expert in lubricants, introduced WBLs designed for gearboxes in 2018 and showcased their potential in the lubrication of sliding bearings in hydropower settings, as documented by Klüber Lubrication, (2018).

The development of automated machinery marked a significant turning point in human history, offering a substitute for manual labor (Janssen et al., 2019). These machines, produced to perform tasks that were once human-driven, boast enhanced efficiency and precision, surpassing what is achievable with manual tools. Moreover, they contribute to better time management and a decrease in production errors, which are key aspects of machine innovation.

The efficiency of business operations is directly proportional to the reduction in lead times and errors. Nonetheless, ongoing research is essential to validate the long-term efficiency of these machines. Applying a hard coating to surfaces is a common practice in metal working, particularly for progressive tools that operate under harsh tribological conditions where wear is a risk. However, the use of Diamond-like Carbon (DLC) coatings in this field is not as widespread. While diamond-like carbon (DLC) coatings offer the advantage of reducing friction and enhancing wear resistance (Kashyap et al., 2022), their application in processes like metal cutting and ironing, which involve high normal pressures, necessitates the use of effective yet potentially dangerous lubricants to prevent the coatings from detaching. Therefore, it is crucial to conduct further research on the impact of DLC coatings under extreme tribological conditions, involving high pressure and temperature, to fully understand their benefits and limitations.

1.2 Problem statement

In metal working processes, tool degradation poses a significant challenge that directly affects product quality. This deterioration is characterized by progressive wear on the tool surface, resulting in a reduced tool lifespan. Generally, an alternative approach involves coating the tool surfaces is crucial to minimize tool wear and extend tool life. However, the effectiveness of single-layered coatings compared to double-layered coatings in such extreme conditions for machining ductile and brittle material remains insufficiently explored. Ductile materials tend to cause adhesion-related wear, while brittle materials contribute to abrasive and chipping wear mechanisms, both of which pose challenges to tool longevity (Trzepieciński, 2023). Excessive tool wear leads to dimensional inaccuracies, poor surface finish and increased manufacturing costs due to frequent tool replacement and downtime. Determining which tool coatings are most effective in reducing wear and improving tool life is crucial for optimizing machining performance and durability. Another alternative is by using lubricant. The conventional oil-based lubricants have been widely used in various industries due to their effectiveness in reducing wear and friction as well as reducing wear and improving tool performance. However, their application raises significant environmental concerns, including pollution and challenges in disposal, which contribute to ecological degradation posing environmental and ecological risks (Nowak et al., 2019). With the increasing global emphasis on sustainability, water-based lubricants have emerged as a promising alternative due to their eco-friendly nature and potential to minimize environmental impacts. However, the performance and tribological behavior of water-based lubricants have not yet been fully explored (Aiman et al., 2024). WBLs has emerged as an alternative in specific industrial applications given the environmental issues associated with OBLs and the abundance of water as a natural resource (N. Wang et al., 2020). They offer easy cleaning, better cooling, and a lower environmental impact than OBLs. However, their industrial use is limited by challenges in lubrication performance, stability, and tribological properties (Rahmadiawan & Shi, 2024). Understanding the mechanisms that lead to wear when using water-based lubricants is important for developing strategies to minimize wear and improve tool performance. Although coated tools combined with oil-based lubricants are effective in reducing wear, improper selection of coatings and lubricants can lead to accelerated tool degradation. A mismatch between coating properties and lubricant performance can result in inadequate protection against friction and thermal stress, ultimately reducing tool life and machining efficiency (Trzepieciński, 2023).

1.3 Objectives of the research

This study aims to investigate the tribological performance of protective hard coatings and environmentally friendly water-based lubricants (WBLs) for metalworking applications. The objectives of this study are as follows:

1. To investigate the performance of single- and double-layered coatings deposited on tool surfaces machining ductile and brittle material under tribologically severe dry friction conditions.
2. To analyse tribological performance of ecofriendly water-based lubricants formulated with MXene and Ionic Liquid additives.
3. To evaluate the performance of combined effects between the most promising tool coatings and water-based lubricants to the tool surface in metal working application.

1.4 Scopes and limitations of the study

This study investigated the application of both single and double coatings on tool surfaces, using a CNC lathe to test AISI 4340 as a brittle material and Al6061 as a ductile material. Ductile materials tend to cause adhesion-related wear, whereas brittle materials contribute to abrasive and chipping wear. It examined the performance of water-based lubricants (WBLs) enhanced with

$Ti_3C_2T_x$ MXene multilayer Nanoflake additives and an ionic liquid (Tributyl(methyl)phosphonium dimethyl phosphate), benchmarked against distilled water. In addition, the research explored the role of surfactants, specifically Xanthan gum and Carboxymethyl Cellulose, in improving the dispersion stability and viscosity of WBLs. Tribological evaluations were conducted using a Block-on-Ring test setup according to ASTM G77 standards, maintaining a constant load of 42 N on AISI 52100 bearing steel at room temperature (28°C). Furthermore, ironing tests on SUS304 stainless steel were performed to evaluate the combined effects of the most promising tool coatings and the formulated WBLs, with thickness reductions of up to 20% to mimic real-world tribological contact conditions in the metalworking industry. The study has certain limitations. It focuses on a specific coating type, which may not be representative of all possible coating combinations. The workpiece materials used are limited to AISI 4340 and Al6061, limiting the applicability of the findings to other materials. The lubricant formulations studied are limited to $Ti_3C_2T_x$ MXene and Tributyl(methyl)phosphonium dimethyl phosphate with specific surfactants, excluding other potential additives. In addition, the tribological evaluation was conducted only at room temperature (28°C), without considering extreme temperature conditions that could affect performance. Although the Block-on-Ring test follows the ASTM G77 standard, it may not fully replicate actual machining conditions. The ironing test is limited to SUS304 stainless steel with a maximum thickness reduction of 20%, which may not cover all industrial ironing scenarios

1.5 Thesis outline

Chapter 1 introduces the background, problem, objectives, and scopes of study of this research. Then, Chapter 2 reviews various related journal papers, articles, and other credible sources on types of lubricants, WBLs, additive lubricant, lubrication mechanism, tribology testing method and coating. Afterwards, Chapter 3 explains the methodology involved in this project, including process flow chart, material, preparation and tribology test. Chapter 4 discusses and analyses the results obtained in terms of the characterisation of lubricants, tribology test, lubrication mechanism, and the societal/health/safety impact. Finally, Chapter 5 concludes the project and provides future recommendations for similar projects.

CHAPTER 2

LITERATURE REVIEW

2.1 Metal working

Metalworking is a process that combines various techniques, such as lathe machining and sheet metal forming, each with unique methods and practical uses. Lathe machining is a process dedicated to precise material removal, enabling metal components to be carved into specific configurations. Its important condition in precision machining, facilitating the careful removal of excess material to forge intricate designs. As Mandali et al., (2023), these advanced tools are indispensable to achieve the high level of precision required in complex manufacturing processes. On the other hand, sheet metal forming is the art of turning flat metal sheets into complex shapes through a series of manipulations. Sheet metal forming uses methods such as bending, ironing and deep drawing, effectively minimizing material waste while achieving complex geometries. Both processes are fundamental to the industry, each playing an important role in the creation of metal products with their specific approach and application.

2.1.1 Machining in turning operation

Machining operations require relative motion between the workpiece and the tool to function effectively. This relative motion, the basis of most machining processes, combines various basic motions. The primary motion, known as the cutting speed, is essential for the material removal process involving the rotational speed between the cutting tool and the workpiece. In contrast, the secondary motion, referred to as the feed, advances the tool across the workpiece which is essential for achieving the desired surface finish and extending tool life. When synchronized with this motion, the specific geometry and position of the tool in relation to the workpiece is critical in shaping the final machine surface to meet the desired specifications. Higher cutting speeds tend to increase tool wear due to high temperatures, leading to thermal softening, oxidation and diffusion wear, which ultimately reduces tool life (M. K. Gupta et al., 2022). However, speeds that are too low can cause built-up edge (BUE) formation (Ahmed et al., 2019), which negatively affects tool performance and to surface finishing product. Similarly, higher feed rates increase mechanical stress on the tool, accelerating wear and chipping due to removes more material per revolution cause higher mechanical loading on the cutting tool and resulting to the tool life (Khan et al., 2022). Figure 2.1 illustrates the effect of cutting speed and feed rate to tool life.

The turning process is defined as the machining of a rotating material using a stationary, single-point tool to produce a cylindrical shape with a smooth and accurate outer or inner diameter. It is noted that the cutting tools for turning are single-point and can be classified into two categories: solid tools and insert tools, which may be coated to improve the machining process. Solid cutting tools are constructed from a single solid piece, usually made of high-speed steel or carbide, which increases their strength and lifespan. These tools are designed for heavy-duty applications, offering reliability in extreme conditions due to their robust structure (Stephenson & Agapiou, 2018). They are typically used in machine operations that require high precision and stability, such as milling and turning. Insert cutting tools, on the other hand, feature a clamping mechanism that holds replaceable cutting inserts, allowing customization based on the specific machining task. One of their main advantages is cost-effectiveness, as worn inserts can be replaced without removing the entire tool, thereby reducing costs and downtime (Val et al., 2024). Additionally, insert tools offer versatility, as inserts can be designed with specific geometries and coatings to optimize performance for different materials and cutting conditions (Khatai et al., 2022).

Carbide, high-speed steel (HSS) and ceramic tools are widely used in machining due to their different properties and performance characteristics. Carbide tools, mainly composed of tungsten carbide (WC) with cobalt (Co) as a binder, exhibit high hardness and wear resistance, making them suitable for high-speed machining of hard materials such as stainless steel, cast iron and titanium alloys (C. Chen et al., 2023). However, carbide tools are relatively brittle and prone to chipping under high impact loads (Ren et al., 2023). In contrast, HSS tools, alloyed with elements such as tungsten, molybdenum and chromium (Sami & Wasim, 2023), offer better toughness and impact resistance, enabling them to withstand interrupted cutting conditions. Although HSS tools have lower hardness and wear resistance than carbide, they are widely used in drilling, tapping and milling operations where resharpening of the tool is advantageous. Ceramic tools, on the other hand, mainly composed of aluminum oxide (Al_2O_3) or silicon nitride (Si_3N_4) (J. Guo et al., 2020), provide extreme hardness and superior thermal stability. These tools can operate at much higher cutting speeds than carbide and HSS, making them suitable for high-speed finishing operations, particularly in machining hardened steels and super alloys. The selection of cutting tool material depends on the specific machining application, considering factors such as workpiece material, cutting speed, and tool life requirements.

The basic motions required by turning are provided by a machine tool known as a lathe (Davim, 2011). The basic turning operation illustrated in Figure 2.2 is distinguished by the direction of the feed motion relative to the turning axis and the configuration of the tool. In parallel turning, also referred to as longitudinal turning, the feed moves parallel to the axis of rotation. On the other hand, in facing and parting operations, the feed direction is perpendicular to the axis. For taper turning, the feed approaches the axis at a certain angle, facilitating the creation of a tapered profile on the workpiece. Figure 2.3 illustrates the various turning operations performed on a modern CNC lathe.

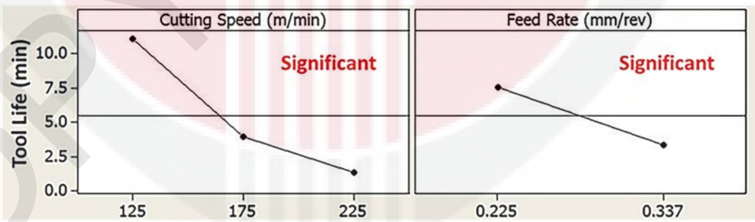

Figure 2.1: Effect of cutting speed and feed rate to tool life (Khan et al., 2022).

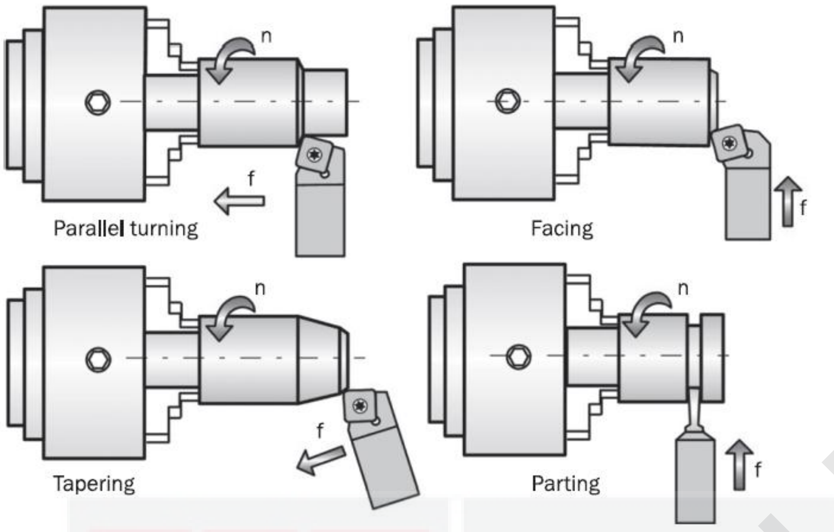

Figure 2.2: Basic motion in turning operation (Davim, 2011)

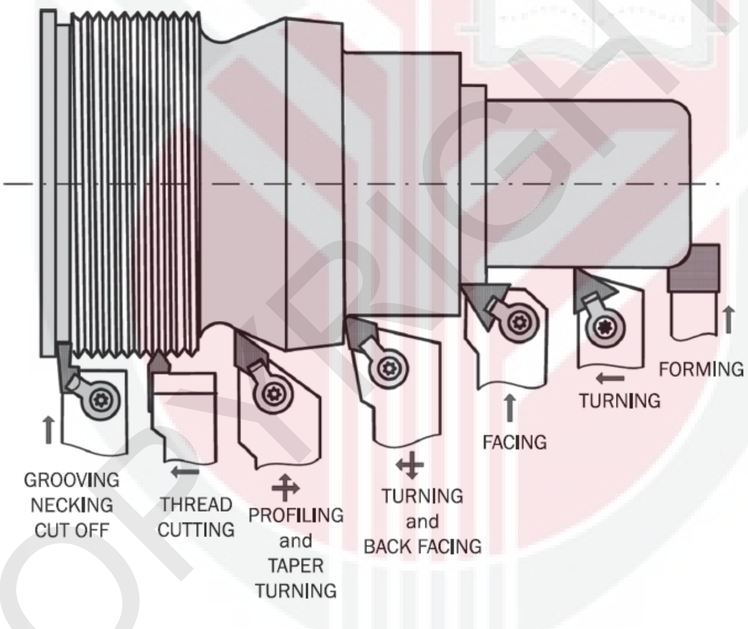

Figure 2.3: Modern CNC lathe operation (Davim, 2011).

Metal cutting operations involve positioning the cutting edge at a certain angle relative to the cutting direction. Orthogonal and oblique cutting are two fundamental machining processes that differ primarily in the geometry of the cutting tool and the mechanics of chip formation. Orthogonal cutting involves the cutting edge being 90° to the cutting direction, resulting in a more efficient cut with less force as in Figure 2.4(a). On the other hand, oblique cutting features an inclined cutting edge, leading to a more complex interaction between the tool and the workpiece as in Figure 2.4(b).

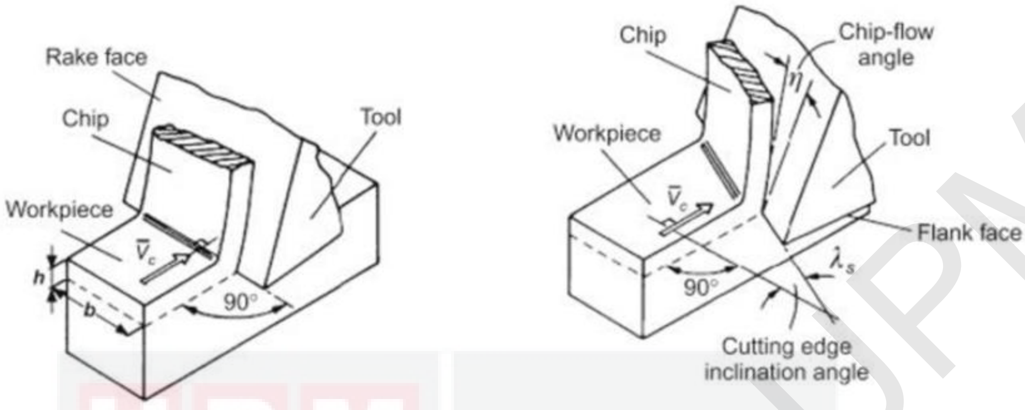

(a) (b)

Figure 2.4: Cutting operation of (a) Orthogonal method and (b) Oblige method (Miracle & Olaleke, 2020)**.**

In orthogonal cutting, directly analyzing the cutting operation is challenging due to the high speed and significant shearing involved. Instead, it was possible to analyze the forces acting on the cutting tool and measure the thickness of the produced chips. By knowing the uncut chip thickness (feed) and comparing it with the chip thickness, the degree of chip compression could be determined. Therefore, an experimental study was performed on a lathe under nearly orthogonal cutting conditions, with ratios between depth of cut and feed (the feed in turning corresponded to the uncut chip thickness) ensuring plane strain conditions (w/t ≥ 10). A cylindrical specimen of an aluminium alloy was used, with a tool having a restricted contact length of about 1 mm and nominal rake and clearance angles of 12° (TriboMAN, 2024).

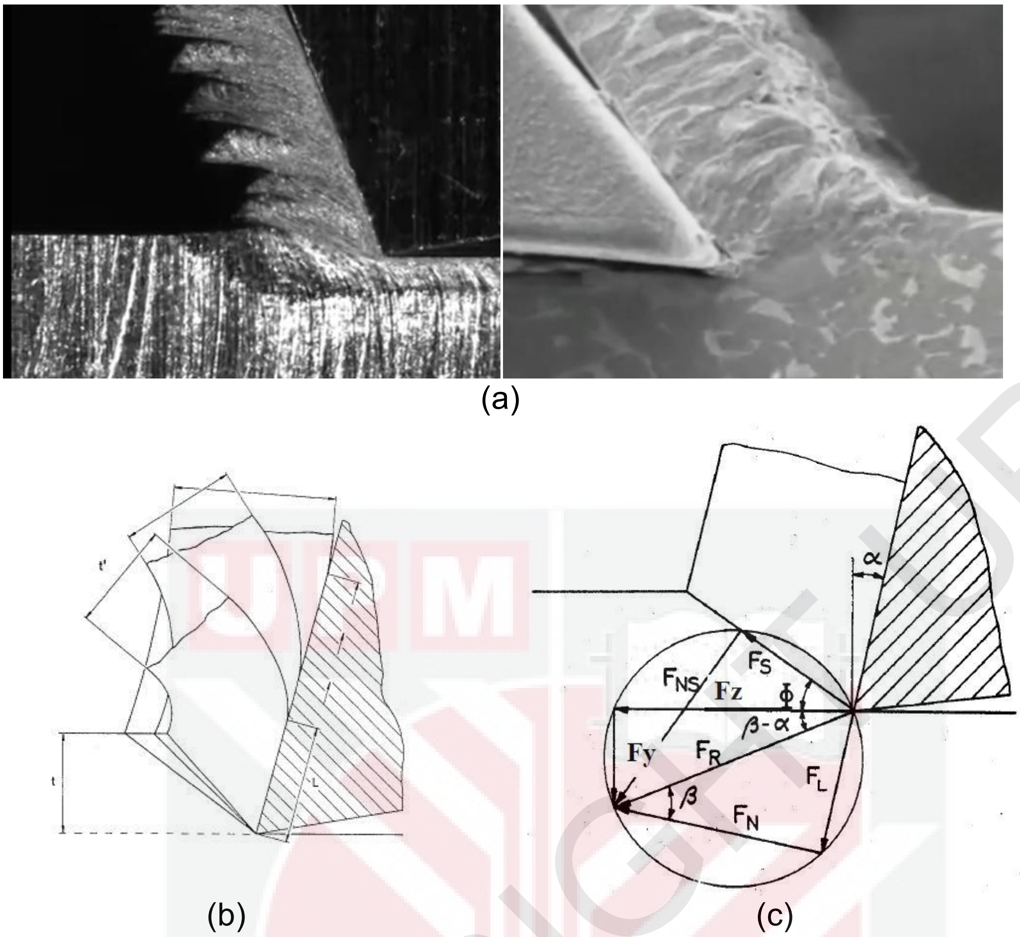

Figure 2.5: (a) chip formation during machining, (b) schematic diagram of chip formation where t is depth of cut, t' is thickness of chip and L is surface contact, and (c) force acting during machining (TriboMAN, 2024)**.**

2.1.2 Metal forming

Sheet metal forming techniques are important in manufacturing as show in Figure 2.6. The field of tribology, which studies the interaction between surfaces in motion, is central to this process. It significantly affects the quality of the final product, the durability of the tool, and the efficiency of the overall procedure. A thorough understanding of tribological factors in sheet metal formation is essential. It leads to the optimization of industrial operations and increased product excellence. This understanding contributes to more durable and high-quality products and promotes sustainable manufacturing practices by reducing waste and extending tool life.

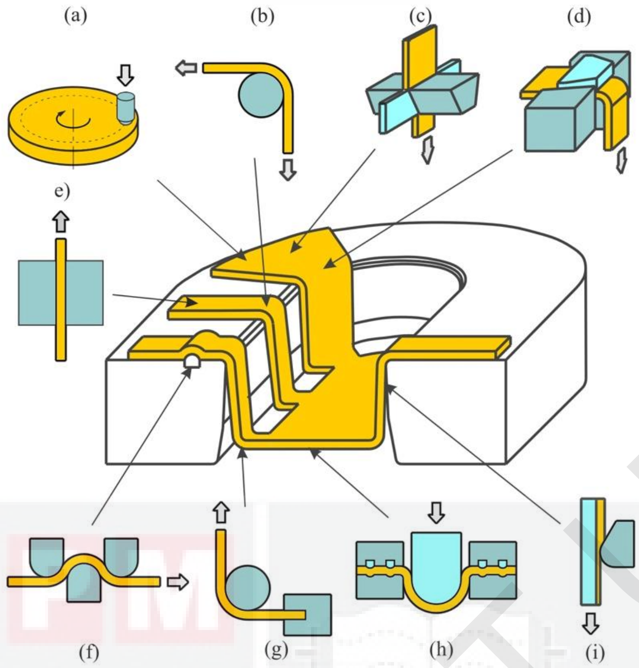

Figure 2.6: Tribological tests representing the friction conditions in the specific areas of the draw piece: (a) pin-on-disc, (b) bending under tension, (c) drawing with tangential compression, (d) bending with tangential compression, (e) strip-drawing test, (f) draw-bead test, (g) strip-tension test, (h) hemispherical stretching, (i) ironing testing (Bay et al., 2008)**.**

Tribological considerations are crucial for manufacturing success in stamping and deep drawing operations. The interface between the workpiece and the tool is subjected to aggressive conditions, including high temperatures and pressures, which can induce significant mechanical and thermal stresses, along with abrasion and adhesion (Schmid, 2013). For example, the coefficient of friction (COF) in hot forging has been noted to decrease with rising temperatures and to increase with heavier loads (Schmid et al., 2020). This interplay between friction, temperature, and load is critical for designing forming processes and choosing suitable lubricants.

Friction in the deep drawing is an important boundary condition that influences the forming quality of aluminum alloy components (Ngaile et al., 2022).

However, the tribological challenges in aluminum alloy deep drawing (AADD) systems are more complex due to the materials' propensity for oxidation and adhesion, compared to traditional steel sheet deep drawing (Ngaile et al., 2022). Consequently, investigating AADD friction is vital to produce high-quality aluminum alloy parts.

The strip bending test described by Sulaiman et al., (2019) simulates the deep-drawing process that simulate industrial sheet-metal forming conditions. This approach helps identify optimal tribological systems for evaluating friction and wear under both dry and lubricated conditions. Figure 2.7(a) illustrates how both experimental setups replicate oil-based forming processes effectively. They measured torque, because it is more sensitive to changes in friction than to drawing loads. The testing was conducted on DLC/TiAlN-coated on the surface die and workpiece was stainless steel AISI 304L under both dry and lubricated conditions. The results indicated that torque measurements were lower and smooth surface for the coated surface than in the dry condition as show in Figure 2.7(b).

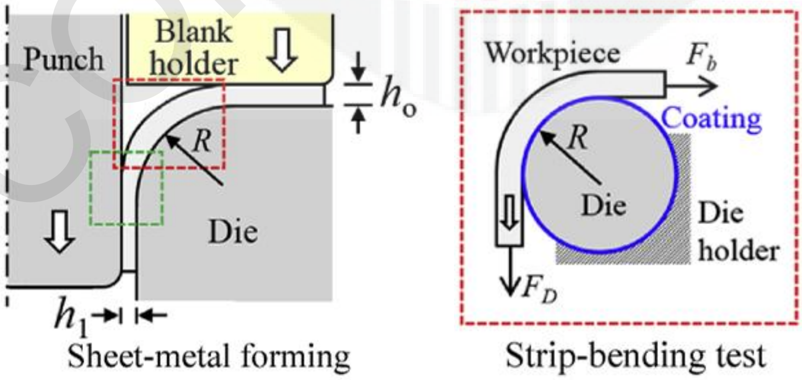

(a)

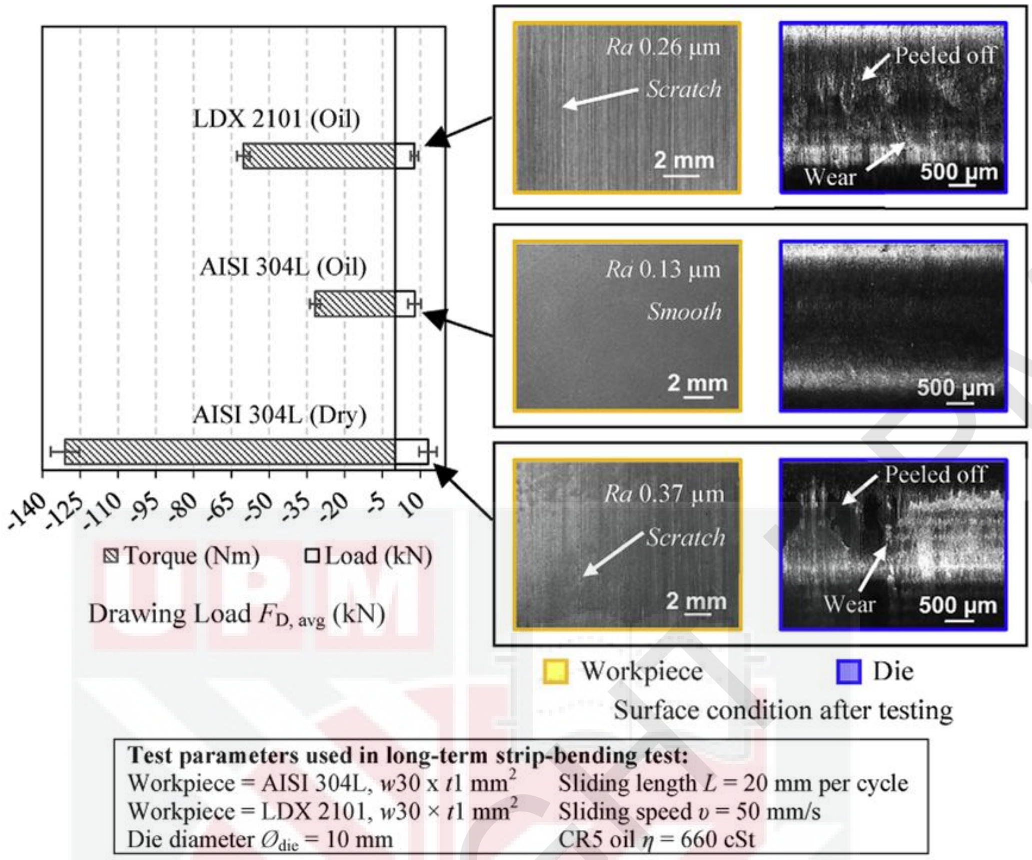

(b)

Figure 2.7: (a) Bending process that involve in deep drawing application and (b) the drawing force at steady state including surface roughness of AISI 304L and surface condition of the coating die (Sulaiman et al., 2019)

Ironing is a pivotal process in sheet metal forming, marked by intense tribological conditions. It is distinguished by high normal pressures, minimal sliding lengths, and considerable surface expansion. The impact of frictional forces within the forming zone is multifaceted. Externally, between the workpiece and the die, these forces amplify tensile stresses. Internally, between the workpiece and the punch, they alleviate the critical section, thereby diminishing stress in the portion of the wall undergoing ironing. The experiment that conducts by Sulaiman et al., (2019), investigate the DLC/TiAlN coating in ironing process of AISI 304L as setup in Figure 2.8(a). In Figure 2.8(b) shows wear on the die surface and workpiece also the setup of the ironing process. The screening test results indicate that DLC/TiAlN outperformed under all test and lubrication conditions, forming a robust protective coating film that reduces forming load and withstands high contact pressure and interface temperature. That why DLC/TiAlN coatings exhibit strong resistance to galling under dry friction and thin film lubrication conditions, while other coatings require thin oil films to function effectively.

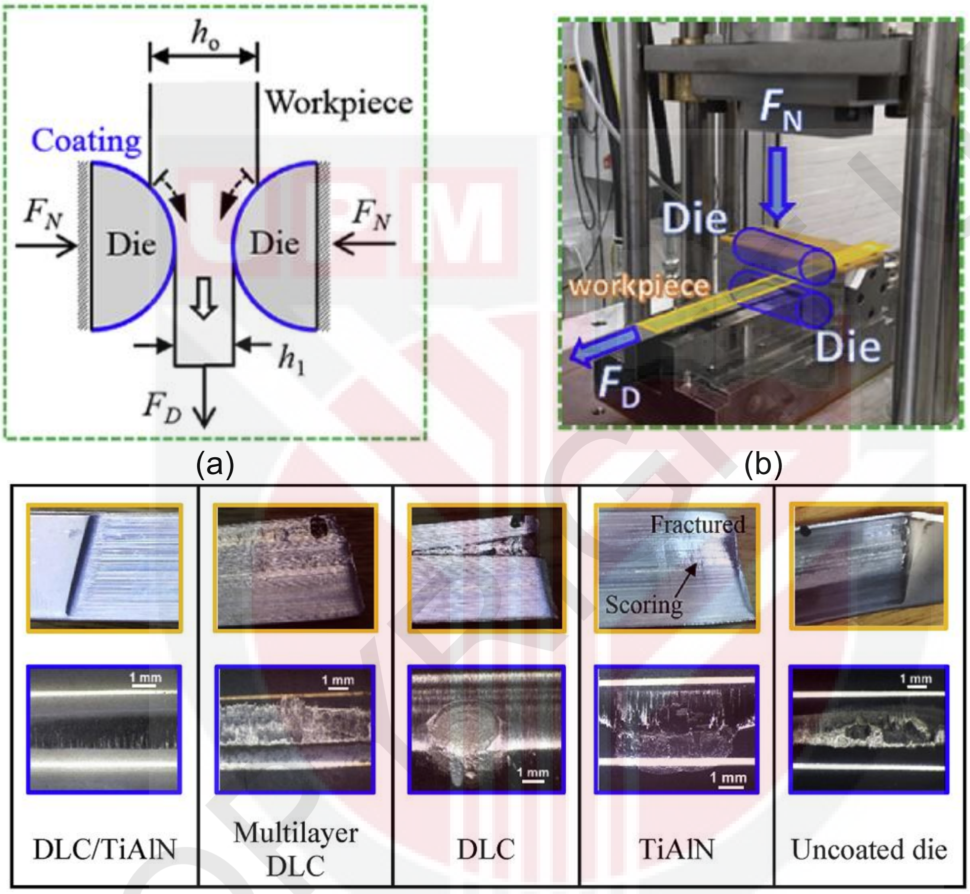

Figure 2.8: (a) Schematics of laboratory test for ironing process, (b) Setup of the ironing process, and (c) surface condition of workpiece AISI 304L and die at temperature 80° under dry condition (Sulaiman et al., 2019)**.**

Friction plays a significant role in the metal forming process, directly affecting metal thinning, material flow, and the occurrence of potential defects such as wrinkles or tears. In the context of strip reduction testing, as discussed by Bay et al., (2008), the effects of friction are particularly pronounced due to the high stresses and surface expansion involved. This test involves applying high normal pressures to the metal strip, simulating the intense contact stresses experienced during the pressing process, which can exceed 1000 MPa. Additionally, the slide length in this test is typically low, reflecting minimal sliding between the tool and the workpiece during pressing. An important aspect of the test is surface expansion, where the metal experiences significant thinning stresses exceeding 25%. Friction between the metal sheet and the mold can cause uneven material flow, causing some areas to be thinner than others (Nguyen & Trung, 2021). This uneven thinning can increase the risk of defects, as areas with excessive thinning are more susceptible to failure. Furthermore, friction affects the way the material flows into the mold during forming. Lower friction allows for easier flow, reducing the risk of thinning and improving formability (Dou & Xia, 2019). Conversely, high friction restricts the flow of material, leading to increased forming forces and the possibility of defects such as wrinkles and tears (Preedawiphat et al., 2020). Wrinkles form when the flow of material is uneven, often due to high friction preventing smooth flow into the mold. Tears occur when the material is overstressed, which can occur if friction prevents adequate material flow, leading to excessive thinning and eventual failure. Therefore, understanding and managing friction is essential to optimizing metal forming processes and minimizing defects.

2.2 Tribology testing

Tribological testing is a critical aspect of understanding the wear, friction, and lubrication characteristics of materials, which is essential for optimizing their performance in various applications.

2.2.1 Friction

Friction is commonly defined as the resistance that one surface or object encounters when moving over another. The frictional force is a tangential force that must be overcome to initiate motion (David et al., 2021). Meanwhile, the coefficient of friction (COF), denoted by the Greek letter μ, is a dimensionless value representing the ratio of frictional force (F) to the normal force (N) exerted by an object. It can be calculated using Equation 2.1 (Cao et al., 2022). This coefficient is crucial in calculating the force required to move an object or to understanding the resistance it would face while in motion.

$$\mu = \frac{F}{N}$$ Equation 2.1

The COF is a standard metric that measures the magnitude of friction between two surfaces in contact, reflecting how severe it is. A lower COF suggests that less force is needed to initiate sliding, and the opposite is true for a higher COF. Certain applications, like brake systems, require a high COF, whereas others benefit from reduced friction to minimize energy loss and prevent potential failure of components due to excessive heat production. The orientation of the forces related to this concept is depicted in Figure 2.9.

.

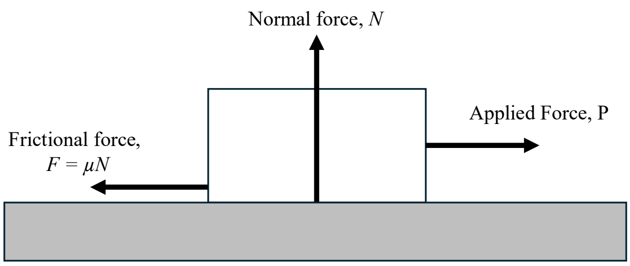

Figure 2.9: Force distribution of moving block

Friction is typically divided into two categories: static and kinetic. Static friction is the resistance encountered at the onset of motion, generally exceeding the kinetic friction experienced during movement. Kinetic friction, on the other hand, occurs when objects are in motion. The foundational theories of friction, proposed by Amontons and Coulomb, initially overlooked the aspect of energy dissipation, leading to their eventual dismissal in favor of more comprehensive models that account for this phenomenon, as noted by Bhushan, (2013).

2.2.2 Wear

Wear refers to the gradual deterioration of material at an interface due to movement. This process involves displacement and changes in material properties at the point of contact, which can occur through rolling, sliding or impact action. Such movement can lead to material transfer and particle detachment (Menezes et al., 2013). This phenomenon can manifest itself in various patterns, indicating the basic wear mechanism. It is common for surfaces to experience multiple wear mechanisms simultaneously (Lijesh & Khonsari, 2020), such as adhesive with corrosive wear, or abrasion with fatigue wear, among others. The wear develops depending on time or with changes in operating conditions. There are different mechanisms of common wear among adhesive wear, abrasive wear and corrasion wear. Adhesive and abrasive wear behave differently in ductile and brittle materials due to their different mechanical properties. In adhesive wear, ductile materials tend to form strong bonds at the contact interface, leading to micro-welding and material transfer when the junction breaks under shear stress (Xu et al., 2023). This results in the formation of wear debris and an increase in surface roughness. In contrast, brittle materials experience minimal adhesive wear because they lack plasticity, causing them to fracture rather than stick. In brittle materials, abrasive wear leads to micro-cracks and chips due to their inability to deform plastically, resulting in sudden material loss and surface damage (Valizade & Farhat, 2024). Overall, ductile materials exhibit wear through plastic deformation and material transfer, while brittle materials primarily experience wear through fracture and chipping.

Adhesive wear

Adhesive wear happens when an adhesive bond develops between two surface asperities, and shearing forces typically cause the softer asperity to adhere to the harder surface. This interaction often leads to the creation of loose wear particles, particularly during further sliding movements (Menezes et al., 2013). Figure 2.10 and Figure 2.11 shows the concept of adhesive wear in a manner that is straightforward and easy to comprehend.

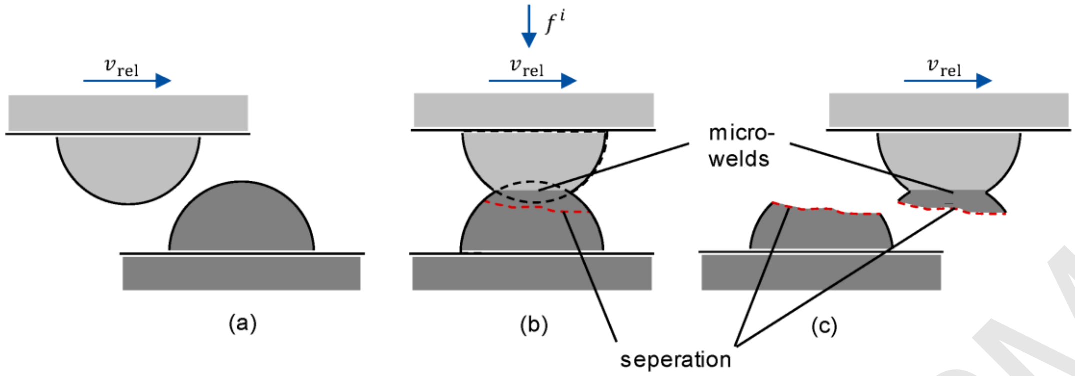

Figure 2.10: Process of adhesive wear: (a) before contact; (b) during contact; (c) after contact (Terwey et al., 2020)

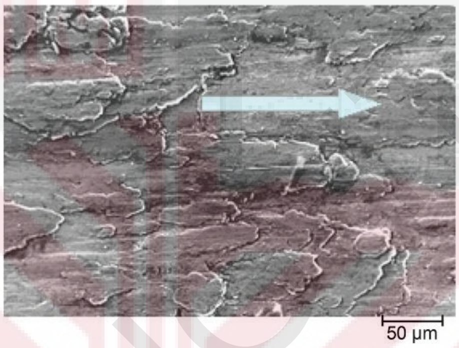

Figure 2.11: SEM morphology of adhesive wear surface (Podgornik, 2022)

Abrasive wear

Abrasive wear is the process where a rough and hard surface slides over a softer one, leading to material degradation. Defined by ASTM International, this phenomenon results from the friction caused by hard particles that move across and exert pressure on a solid surface. The nature of the contact between surfaces dictates the type of abrasive wear, which is categorized into two-body and three-body wear. In two-body wear, the hard particles directly erode the material from a single surface. Conversely, three-body wear involves particles that move freely and abrade the surface without any restrictions (Bhushan, 2013). This wear can manifest itself in two main ways: as two-body abrasive wear, where the materials are in direct contact; and as three-body abrasive wear, where there is an intermediate material, as illustrated in Figure 2.12.

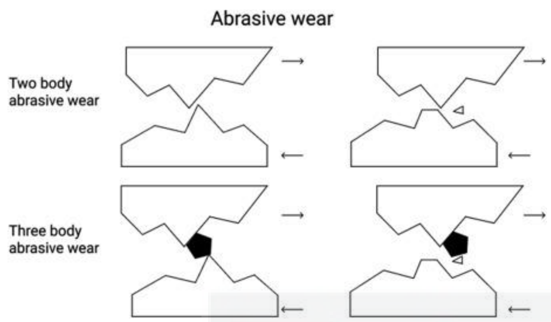

(a)

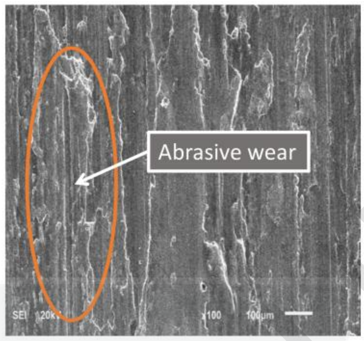

(b)

Figure 2.12: (a) Two body and three body abrasive wear (B. R. Gupta, 2023) **and (b) SEM images of the P110 worn casing sample (S0) tested under dry conditions at 115 rpm and 1000 N for 40 min from** (Osman et al., 2022)**.**

Corrosive wear

Chemical wear, also known as corrosive wear (Alojali & Benyounis, 2016), occurs when materials move against each other in a corrosive setting. Oxygen is a common corrosive agent, leading to what is specifically referred to as oxidative wear. In the absence of movement, a protective oxide layer forms on the surface of the material. However, this protective layer is removed during sliding, exposing the material to further corrosion. Therefore, it is observed that the phenomenon of corrosive wear requires the simultaneous presence of both corrosion and abrasive motion (Menezes et al., 2013). Figure 2.13 illustrates the corrosive wear, which occurs due to chemical reactions between the material and its environment.

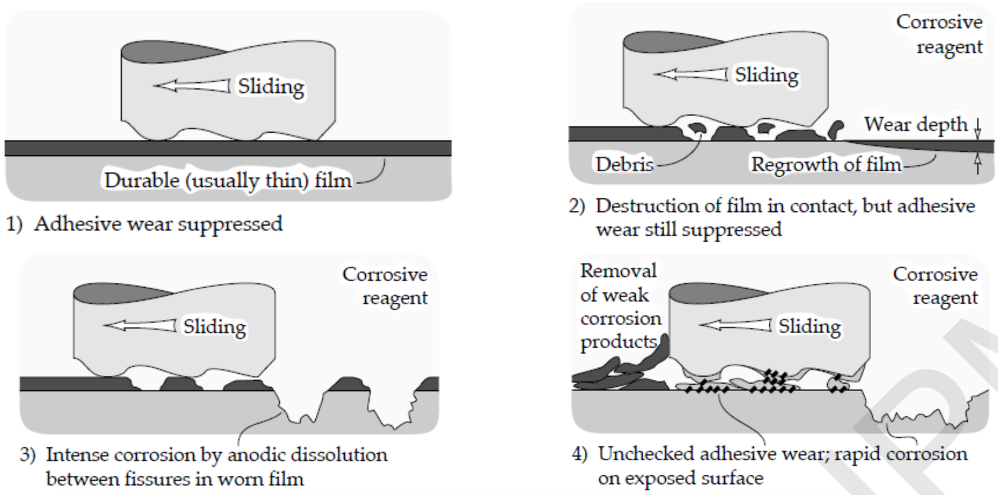

Figure 2.13: Process of corrosive wear (Stachowiak & Batchelor, 2013)

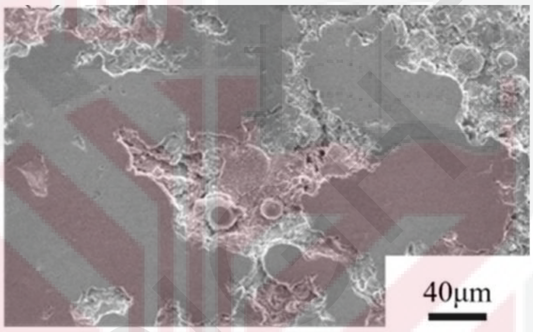

Figure 2.14: The worn surface morphologies of the amorphous coating after the corrosion-wear tests (Liao et al., 2023).

2.2.3 Lubricant

In many applications, excessive friction and wear can have severe negative consequences to product and environment. To deal with this issue, the use of lubricants is very effective. The main function of lubricants is to reduce wear and friction between moving parts. In addition, it plays an important role in heat dissipation, removal of contaminants, and extending the operational life of mechanical systems (Menezes et al., 2013). An important example of the importance of lubricants occurred in North America in 1979. It is estimated that about one-third of the $200 billion spent on machine maintenance could be saved using sufficient lubricants (Bannister, 1996). Lubricants are generally classified into three categories: solid, liquid and gas.

At the beginning of the experiment, each lubricant undergoes an initial run-in phase, which transitions to an equilibrium phase where the COF value is stable and remains relatively unchanged. The running-in phase is characterized by the initial contact between the two surfaces under the load, moving against each other, which usually results in rapid wear at the beginning of the experiment. This was caused by the lack of lubricating layer between the mating surfaces in the early stages of the experiment, leading to severe asperity contact occurred and material removal took place (Arinbjarnar et al., 2022). This period is important because it involves the removal of high points or asperities on the surface, which leads to an increase in the actual contact area. As the experiment progresses and loads are applied, the relative motion between the surfaces smooths them out, contributing to more consistent COF values (Blau, 2005). Significant changes in micro-asperities observed at the start of the sliding test can correspond to variations in the COF throughout the running-in phase. The configuration of the runout curve can provide the investigator with insight into the events that occur during the initial stages of the tribological test. Figure 2.15 shows example initial stages of tribology test.

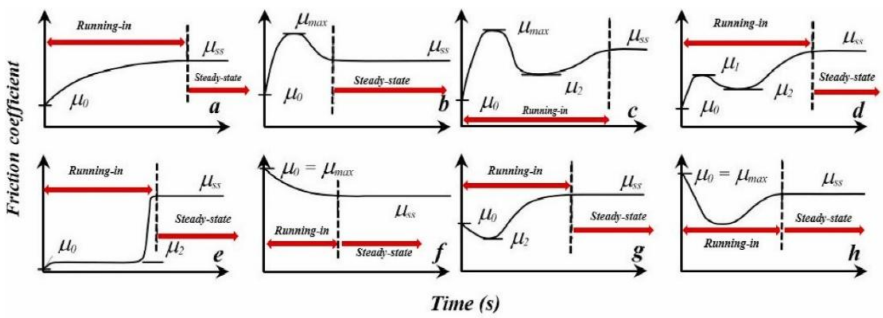

Figure 2.15: Friction behaviour represent as initial changes in friction with time (Khonsari et al., 2021)

During the contact phase, various lubrication modes exhibit the formation of different fluid film thicknesses. The phase includes three main stages: boundary lubrication, mixed lubrication, and hydrodynamic lubrication. Typically, the lubrication regime, as illustrated by the Stribeck curve, determines the friction and wear characteristics of the component, as show in Figure 2.16. Lubrication performance is basically affected by three factors: load, lubricant viscosity, and velocity. These elements collectively determine the effectiveness of the lubrication process. A widely used approach to identify the lubrication regime is the Stribeck curve. This method involves plotting the COF against a dimensionless parameter, commonly referred to as the Hersey number or Stribeck number (Menezes et al., 2013) that can be found using Equation 2.2.

$$Hersey's\ number = \frac{\eta v}{\mathrm{P}} \qquad \text{Equation 2.2}$$

Where η is the viscosity of the lubricant, v is the sliding velocity and P is the load per unit length.

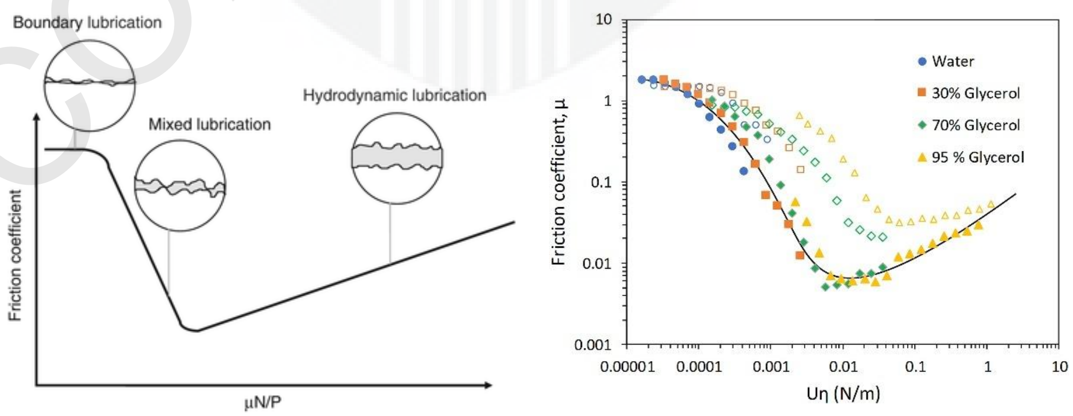

(a) (b)

Figure 2.16: Stribeck curve graph (Y. Wang & Wang, 2013) **and stribeck curve with friction data obtained from a range of fluids with varying viscosity from** (Xu & Stokes, 2020)

Hertzian stress plays an important role in tribological evaluation. Theoretically, the interaction between two parallel cylinders forms a line relationship, while the engagement between two intersecting spheres or cylinders forms a point relationship, as illustrated in Figure 2.17. Such contact generates infinite pressure, potentially leading to immediate surface yielding. However, in practice, the actual contact area, although small, arises from elastic deformation, significantly reducing stress. However, the resulting stress can be very high, giving rise to the risk of multiple failure modes, which holds great importance in tribological studies.

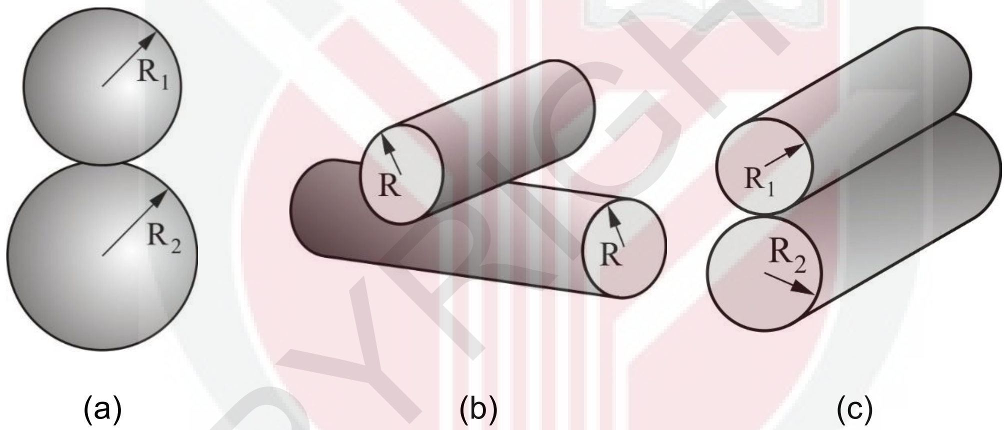

Figure 2.17: Contact mechanics (a) Contact between two spheres. (b) two cross cylinder and (c) (Popov, 2010)

The Hertzian stress for block-on-ring test with cross cylinders and point contact can be computed as follows (Sidh et al., 2023):

$$E' = \left[\frac{1 - \upsilon^2}{E}\right]^{-1}$$ **Equation 2.3**

$$a = \sqrt{\frac{8 \times F_N \times R_x}{E' \times \pi \times L}}$$ **Equation 2.4**

$$P_o = \frac{2 \times F_N}{\pi \times a \times L}$$ **Equation 2.5**

Where:

E' = Equivalent elastic modulus

v = Poisson's ratio

E = Elastic modulus

a = Hertzian contact half width

F_N = Normal load

Rx = Effective radius

L = width of block

P_o = Hertzian pressure

The ration of roughness and film thickness, denoted as λ, is an important parameter in evaluating lubricants during tribological testing. The value of λ enables the prediction of the lubrication regime (Menezes et al., 2013): λ greater than 3.0 indicates a hydrodynamic lubrication regime; λ between 1.0 and 3.0 suggests a mixed lubrication regime; and λ less than 1.0 points to the boundary lubrication regime, as illustrated in the Stribeck curve shown in Figure 2.16. In the boundary lubrication regime, the lubrication film is minimal, which leads to significant contact between surface asperities and results in increased friction levels. The mixed lubrication regime has a slightly thicker lubrication film, but it is not thick enough to separate the contacting surfaces. On the other hand, the hydrodynamic lubrication regime is characterized by a large lubrication film that effectively separates the surfaces, thus minimizing the contact between the asperities (Zhang et al., 2020). The λ parameter applicable to the block-on-ring test, which involves cross-cylinder configurations and point contacts, is calculable through the application of the Dowson-Higginson equation (Sidh et al., 2023).

$$G_* = \alpha \times E' \quad \textbf{Equation 2.6}$$

$$U_* = \mu_0 \times \frac{u_1 + u_2}{E' \times R_x} \quad \textbf{Equation 2.7}$$

$$W_* = \frac{F_N}{E' \times R_x \times L} \quad \textbf{Equation 2.8}$$

$$h_{min} = 0.985 \times (U_*)^{0.7} \times (G_*)^{0.6} \times (W_*)^{-0.11} \quad \textbf{Equation 2.9}$$

$$\lambda = \frac{h_{min}}{\sqrt{R_{q1}^2 + R_{q2}^2}} \quad \textbf{Equation 2.10}$$

Where:

G*, U*, W* = dimensionless parameter

α = Pressure viscosity coefficient

μ_0 = dynamic viscosity

R_x = Effective radius

L = width of block

F_N = Normal load

u = velocity of block and ring

hmin = minimum film thickness

λ = Ratio film thickness and roughness

R_q = Peak-to-valley surface roughness

E' = Equivalent elastic modulus

2.3 Tribo testing method

Advanced tribometers are outfitted with sophisticated instruments that facilitate the measurement of various parameters, such as wear rates, friction forces, coefficients of friction, and the vibrations, noise, and temperature of a system (Valdes et al., 2020). To assess the tribological performance of newly developed WBLs several testing methods are predominantly employed. These include the four-ball (Du et al., 2018), pin-on-disk (Verma et al., 2022), and block-on-ring (Huang et al., 2021) techniques, which are instrumental in evaluating the effectiveness of these lubricants under different conditions.

2.3.1 Block on ring

In the block-on-ring setup illustrated in Figure 2.18, the block is pressed against a rotating ring with a certain load. The COF between the block and the ring is measured as the ring rotates at a set speed. Block-on-ring tribometers are widely used for the analysis of nanolubricants (Huang et al., 2021), coatings (Ideris et al., 2023) because of their effectiveness in simulating real-world wear conditions. This tribometer design is good at evaluating wear and COF for interacting sliding surfaces, including lubricating films, rings and bearings, providing valuable insight into their performance and durability.

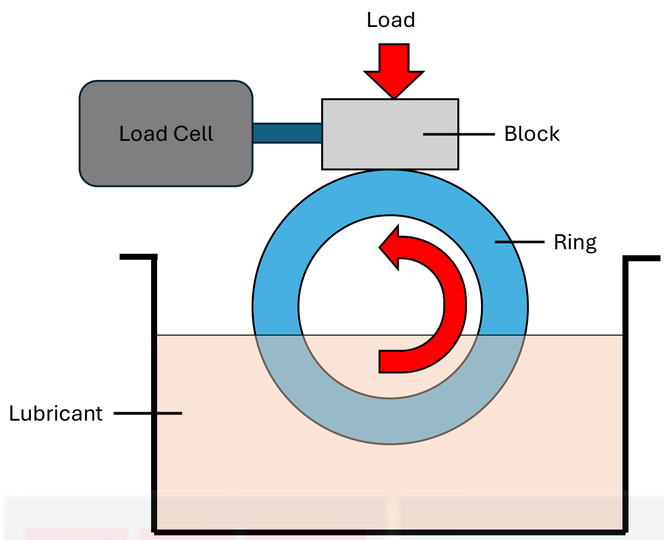

Figure 2.18: Block-on-ring diagram (Ideris et al., 2023)

2.3.2 Pin on disk

The pin-on-disk tribometer, depicted in Figure 2.19, operates in compliance with established testing protocols. This system comprises a stationary pin above a rotating disk, creating a circular sliding track on the disk's surface. Load cells and sensors are employed to record the frictional forces and tangential stresses exerted by the stationary pin. A loading force is applied to the pin, positioned at a specific distance from the center of the disk. The disk's rotation is powered by a servo motor, which operates at a predetermined speed measured in revolutions per minute (rpm). Typically, the pins used are cylindrical with ends that may be flat, truncated, or spherical in shape. Pin wear is assessed by tracking changes in its dimensions, such as pin length, wear scar diameter (WSD) of the contact area, or through weight loss measurements. In instances where weight loss is minimal and difficult to measure, it can be deduced or assessed by analyzing the wear area, which is determined from the surface profile using a 3D microscope.

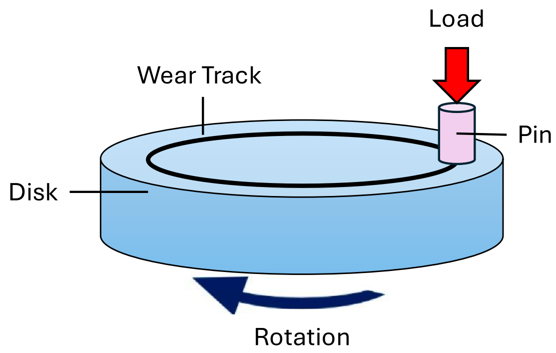

Figure 2.19: Pin-on-disk diagram (Di Puccio et al., 2024)

2.3.3 Four ball

The four-ball tribometer, a prevalent instrument for assessing lubricant efficacy, is depicted in Figure 2.20. This structure consists of three balls fixed in a lubricant bath. The rotating ball is placed above the three fixed balls (Valdes et al., 2020). During tribological testing, this rotating ball is subjected to a consistent pneumatic force, which escalates until the balls fuse due to the generated frictional heat. This device is versatile, enabling the measurement of the WSD and COF, as well as evaluating the lubricant's load-bearing capacity and extreme pressure (EP) attributes. Adherence to the ASTM D2783 standard is maintained throughout the testing process. EP qualities are determined by measuring the PB (the last non-seizure load where the scar diameter does not exceed 5% of the baseline value) and the PD (the weld point, or the minimum load at which the surfaces bond). Generally, higher PB and PD values suggest superior EP characteristics. The capability to assess EP properties is a distinctive aspect of the four-ball test, setting it apart from other tribological test configurations.

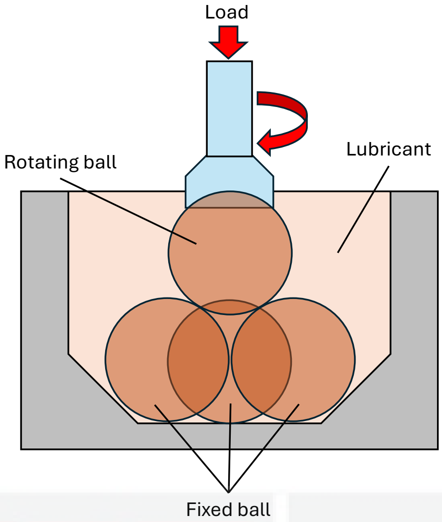

Figure 2.20: Four ball diagram

2.3.4 Previous work

In recent studies, various tribological testing methods have been employed to evaluate the effectiveness of different nanoadditives in reducing friction and wear. The block-on-ring method has been used to assess the performance of ZrO_2/TiO_2 and GO-Al_2O_3 nanoadditives. Huang et al., (2021) reported that ZrO_2/TiO_2 achieved a 25% reduction in friction and 65% wear reduction at a sliding speed of 400 mm/s under a 100 N load. Meanwhile, Huang et al., (2019) investigated GO-Al_2O_3 over a broader range of speeds (100–400 mm/s) and forces (10–30 N), demonstrating a friction reduction of 47–64%, though wear reduction was not specified. Similarly, pin-on-disk tribometry has been used to evaluate graphene oxide (GO) and hexagonal boron nitride (hBN) as lubricating additives. Elomaa et al., (2015) found that GO at a low speed of 0.02 m/s and a 10 N load reduced friction by 57%. In contrast, (He et al., 2019) reported that hBN at 300 rpm and 400–600 N led to a 29.1% friction reduction and a 14.6% decrease in wear. The four-ball method has also been explored, with Bai et al., (2020) demonstrating that hBN at 120–440 rpm and 100 N resulted in a 60% friction reduction and 95.73% wear reduction. Tang et al., (2019) further investigated carbon dots-ionic liquid (CDs-IL) at 600 rpm under 30–80 N loads, achieving 57.5% friction reduction and 64% wear reduction. These studies highlight the potential of nanoadditives in improving tribological performance across different testing configurations, emphasizing their effectiveness in minimizing friction and wear under various operating conditions. All has summary in Table 2.1.

Table 2.1: Previous work on tribology testing method

Tribo testing method	Ref	Nanoadditive	Parameters		Result	
			Speed	Force	Friction reduction	Wear reduction
Block on ring	(Huang et al., 2021)	ZrO_2/TiO_2	400 mm/s	100 N	25%	65%
	(Huang et al., 2019)	GO-Al_2O_3	100 to 400 mm/s	10 to 30 N	47–64%	-
Pin-on-disk	(Elomaa et al., 2015)	GO	0.02 m/s	10 N	57%	-
	(He et al., 2019)	hexagonal boron nitride (hBN)	300 rpm	400–600 N	29.1%	14.6%
Fourball	(Bai et al., 2020)	hexagonal boron nitride (hBN)	120–440 rpm	100 N	60%	95.73%
	(Tang et al., 2019)	Carbon dots-Ionic liquid (CDs-IL)	600 rpm	30–80 N	57.5%	64%

2.4 Coating applied to metal working tooling in metal working industry

The evolution of tool coatings in the metalworking industry has been driven by the constant quest for enhanced tool performance, extended tool life, and optimized machining operations (Yogesh Dileep Lande, 2024). Advanced coatings like TiAlTaN have significantly improved tool life and surface quality in cutting processes, particularly in materials like Cu-Be alloys (Nogueira et al., 2023). The shift towards green machining has spurred the development of coatings to replace cutting fluids, aiming to improve machining accuracy and efficiency while reducing costs (Qian et al., 2020). To meet the increasing demands of modern machining environments, researchers have been enhancing coating structures with functional alloy elements to create high-performance coatings that are wear-resistant, self-lubricating, and oxidation-resistant (Qiang et al., 2020). Innovations in coating technology have led to the creation of hard coatings with specific layer compositions to enhance tool durability and performance, showcasing a continuous evolution in the field of tool coatings in the metalworking industry (Isaka, 2020).

Coatings can be tailored specifically to meet specific application requirements by manipulating their architecture and composition. This customization allows precise control over the microstructure and its mechanical properties. Various coating designs are available, each applied to substrates to improve performance across a broad spectrum of applications (Sousa et al., 2021).

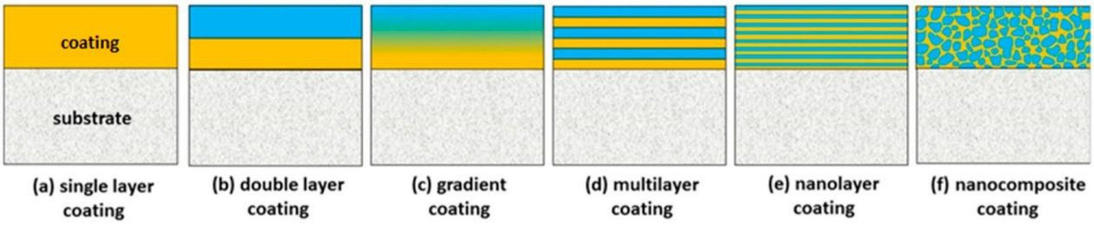

Figure 2.21: Structure of layer coating attach to substrate (Caliskan et al., 2017)

Various coating designs are applied to substrates for a wide range of applications, as shown in Figure 2.21. Various coating structures are selected to address different challenges. For example, using a multi-layer coating can significantly improve the properties of a tool with a single-layer coating. Multi-layer coatings are particularly effective in increasing crack propagation resistance compared to their single-layer counterparts. The effectiveness of coating is often linked to the number of layers it contains; in addition, a greater number of layers can also improve other characteristics, such as hardness (Caliskan et al., 2017; Shuai et al., 2020). Double-layer coatings are widely used in research and industrial applications to improve material performance by combining the benefits of two different layers. The main advantage of using two-layer coatings is the ability to increase wear resistance, where the base layer provides hardness and durability, while the top layer reduces friction and prevents surface damage (Liu et al., 2022). This combination also improves lubricity, as a well-designed top layer, such as diamond-like carbon (DLC), can significantly reduce friction, improving the tribological behavior of the coated surface. In addition, two-layer coatings offer increased heat and oxidation resistance, making them suitable for high-temperature environments. The base layer, such as titanium aluminum nitride (TiAlN), provides excellent heat resistance and oxidation protection, allowing the coating to maintain its integrity under extreme conditions (Sebbe et al., 2024). Another major benefit is the synergistic effect between the two layers, where each contributes unique properties that work together to improve overall performance beyond what a single-layer coating can achieve. The behavior of crack propagation in relation to the coating structure is illustrated in Figure 2.22.

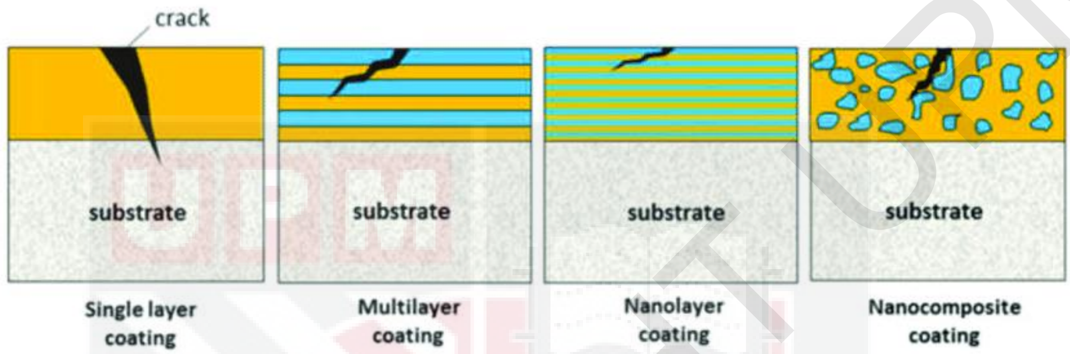

Figure 2.22: Crack propagation behaviour for each of the common coating structure (Caliskan et al., 2017)

Sulaiman et al., (2017) conducted an experiment on the ironing process of AISI 304L, investigating different structures of diamond-like carbon (DLC) coatings with a thickness reduction of r = 15 – 25%. Three types of DLC coatings were tested: single layer (Type A), double layer (Type B), and multi-layer (Type C), as shown in Figure 2.23(a). Their findings indicated that DLC Type B exhibited the best adhesion to the tool substrate, as seen in the light optical microscope images in Figure 2.23(b).

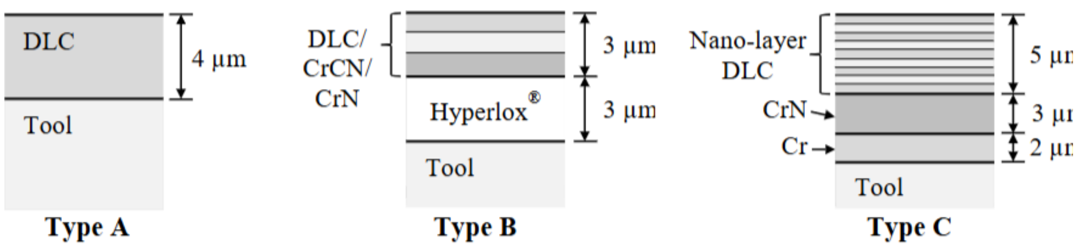

(a)

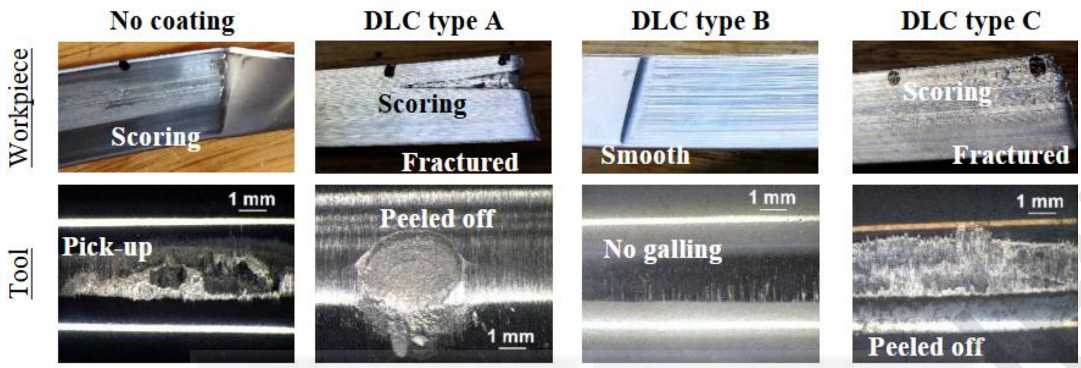

(b)

Figure 2.23: (a) Layer structure of DLC and (b) Surface condition images of the workpiece and tool after screening experiments with dry lubrication at a tool temperature of 80°C (Sulaiman et al., 2017)

Sharifahmadian & Mahboubi, (2019) conducted a study on the tribological properties of N-DLC/DLC double-layer coatings versus single-layer DLC coatings, using a ball-on-disk test up to a sliding distance of 500 meters. The N-DLC/DLC coating demonstrated superior wear resistance compared to single-layer coatings. Figure 2.24 summarizes the friction coefficient and wear rate from the study. Key characteristics of the double-layer coating include high stability and a low friction coefficient of around 0.15. The N-DLC/DLC sample showed the lowest wear rate, approximately 6.52 × 10−5 mm^3/N m. The study found that the gradient in mechanical and chemical properties of the N-DLC/DLC coating enhances tribological performance and substrate adhesion over single-layer coatings.

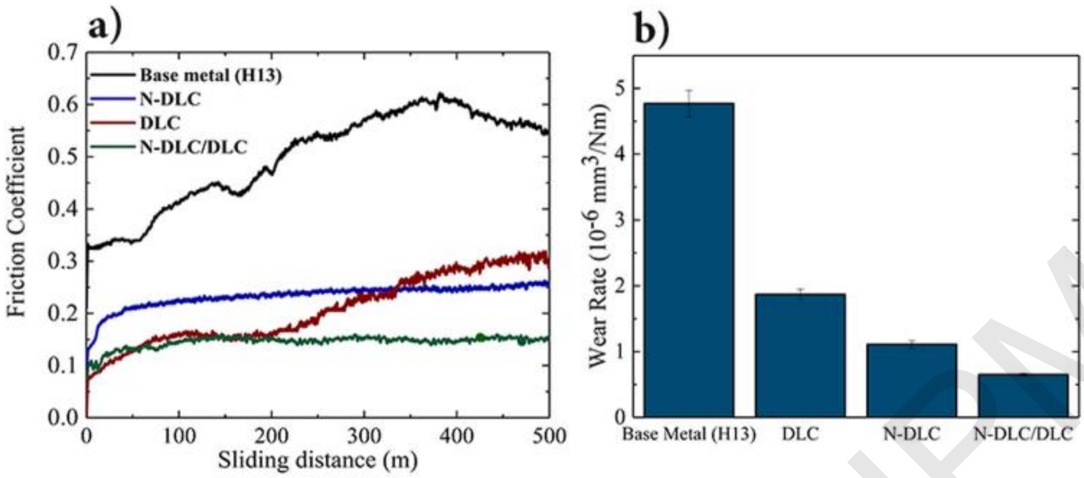

Figure 2.24: a) The friction coefficient curves and b) The wear rates of the N-DLC/DLC, N-DLC, DLC (Sharifahmadian & Mahboubi, 2019)

Diamond-Like Carbon (DLC), and Titanium Aluminum Nitride (TiAlN) are commonly used in machining and tribological applications due to their distinct properties that enhance tool performance. DLC coatings are known for their very low coefficient of friction, high hardness, and excellent wear resistance (Goti et al., 2023). These properties make DLC suitable for applications that require minimal heat generation and wear reduction, such as in tribological testing and biomedical tools. However, DLC has lower thermal stability compared to TiAlN, limiting its effectiveness in high-temperature machining. TiAlN, with its higher aluminum content, provides superior thermal stability (Sousa et al., 2021) and oxidation resistance (Wu et al., 2024). At high temperatures, it forms a protective aluminum oxide layer that increases heat resistance, making it suitable for high-speed and dry machining applications. This coating is commonly used in cutting, drilling, and grinding hard materials. While TiAlN offers greater durability in high-temperature conditions. Overall, the selection of this coating depends on the machining conditions, with DLC being preferred for low-friction applications, and TiAlN for high-temperature and high-speed operations (Moreno et al., 2021).

2.5 Lubrication

2.5.1 Nano additive used in lubricant

Lubricants play a crucial role in reducing friction and wear between moving surfaces, ensuring the efficient and reliable operation of machinery. The incorporation of nanoparticle additives has emerged as a promising approach to further enhance the tribological properties of lubricants (I. Ali et al., 2019; Radhika et al., 2021). Nanoparticles, with their small size and unique properties, offer several advantages when used as lubricant additives. Their ability to penetrate the contact interfaces and form a protective boundary film is particularly beneficial in high-pressure contacts (Waqas et al., 2021). Among the various nanoparticle materials investigated, tungsten disulfide (WS_2) nanoparticles have received significant attention due to their effectiveness in reducing friction and wear, as well as their thermal and chemical stability (Ratoi et al., 2013). One of the key factors influencing the performance of nanoparticle additives in lubricants is their size, shape, and surface functionalization. The size of the nanoparticles, for instance, determines their ability to access and fill the gaps between contact asperities, while the surface properties can influence their adsorption and interaction with the lubricant (I. Ali et al., 2019). In addition to nanoparticles, other carbon-based nanomaterials, such as carbon nanotubes and graphene, have also been explored as lubricant modifiers. These materials have shown promising results in reducing friction and wear, while also being environmentally friendly and non-toxic (I. Ali et al., 2019).

2.5.2 Low-dimensional materials

Low-dimensional materials (LDMs) are categorized as 0D, 1D, or 2D, based on their size and aspect ratios. This classification reflects the number of dimensions in which these materials exhibit significant physical properties. Figure 2.25 provides a visual summary of LDMs, illustrating their various antimicrobial mechanisms

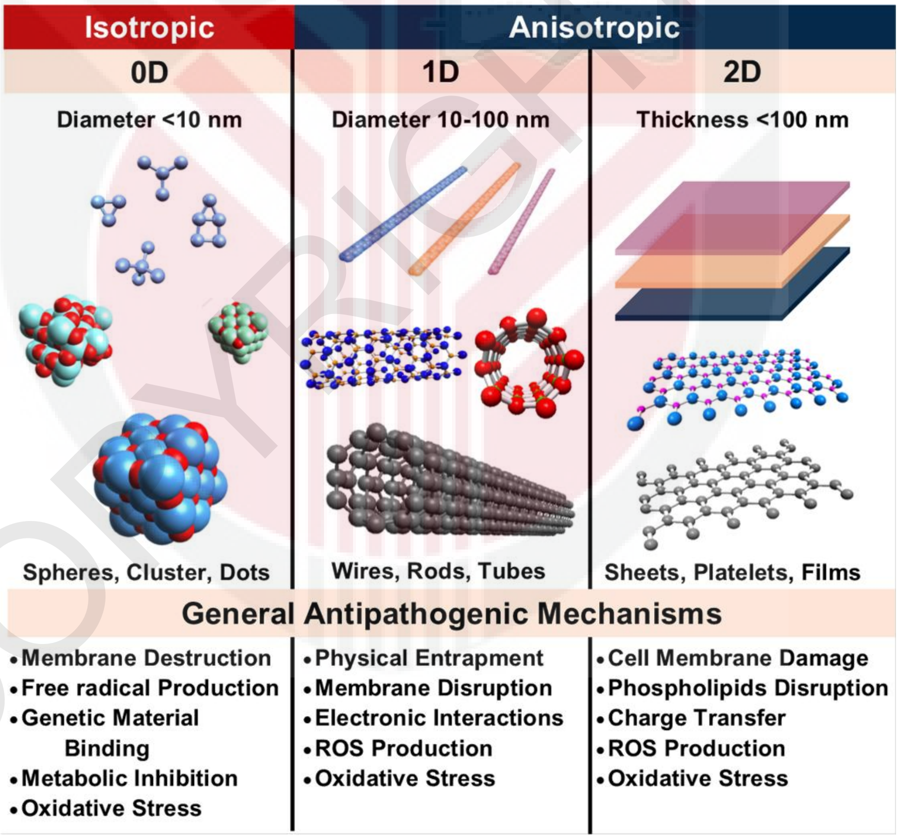

Figure 2.25: The contrast of 0D, 1D and 2D materials (Shaw et al., 2021)

Zero-dimensional materials, or 0D materials, are defined by their confinement within the nanoscale across all three dimensions, typically comprising just a few atoms and boasting an average size below 10 nm, which bestows them with consistent, isotropic properties (Hwang et al., 2020). Quantum dots are one example, crystalline aggregates of semiconductor materials (Mir et al., 2018), whereas nanoclusters and nanodots encompass a broader spectrum of sub-10 nm materials.

One-dimensional (1D) materials are defined by their confinement to the nanoscale in two dimensions, while extending into the microscale in the third. These materials typically manifest as cylindrical structures with diameters ranging from 10 to 100 nm and lengths usually under 12 μm (E. J. Kim et al., 2019). Nanorods (NRo) are distinguished by their solid, low aspect ratio structures, contrasting with nanowires, nanotubes, nanoribbons, and nanofibers, all of which exhibit higher length to width aspect ratios (Y. Xu et al., 2018).

Two-dimensional (2D) materials are characterized by confinement to the nanoscale in one dimension, while the other two dimensions extend from the microscale to several centimeters (H. Khan et al., 2020). These materials typically form nanosheets, also known as nanoflakes, which may exhibit a random shape (Li et al., 2019). In cases where the materials possess a uniform and controlled shape with defined edges, they are referred to as nanoplatelets. If these structures display rounded edges, they are termed nanodisks (T. Lu et al., 2016). Notably, both nanosheets and nanoplatelets maintain a thickness less than 3 nm, equivalent to 1–2 atomic layers (Zhang et al., 2019).

2.5.3 Additive in lubricants

MXenes have gained significant attention in the field of tribology due to their potential as lubricant additives. MXenes are two-dimensional materials with excellent mechanical and tribological properties. The covalent functionalization of MXenes has been explored for tribological purposes, with a focus on enhancing their performance as lubricants. Parra-Muñoz et al., (2022) provided a critical review of the existing state-of-the-art regarding MXenes' covalent functionalization, emphasizing tribological properties and needs. In addition to MXenes, other materials such as ionic liquids and nanoparticles have also been investigated for their potential as lubricant additives. Tang et al., (2018) synthesized ionic liquid functionalized graphene oxides and studied their tribological properties under water lubrication. Sharma et al., (2018) developed a hybrid nano-lubricant with improved tribological properties by mixing MoS2 nanoparticles with alumina nanoparticles in an oil-water emulsion base fluid. Furthermore, the influence of water on the tribological properties of lubricant additives has been studied. Fatima et al., (2015) evaluated the effect of water on the performance of additives in automatic transmission fluid, while W. Chen et al., (2021) investigated the ultralow friction of copper using a green WBL containing phytic acid. Wijanarko et al., (2022b) studied the tribological performance of ionic liquids as lubricant additives in water-based and PAO lubricants, with BMP showing the best performance in non-polar lubricant media. Overall, research in the field of lubricant additives for tribological applications continues to explore novel materials and formulations to improve lubrication performance under various conditions, including WBL. The development of MXenes and other advanced materials as lubricant additives holds great promise for enhancing the efficiency and durability of mechanical systems.

Lian et al., (2018) conducted a systematic study of the tribological properties of MXenes as solid lubricant coatings. In their research, they prepared a 200 nm thick Ti_3C_2 MXene coating on a copper disk using a spray coating method. The Figure 2.26 were the resulting Ti_3C_2 coatings showed coefficients of friction (COF) of 0.15 and 0.19 at normal loads of 0.5 and 1.0 N, respectively. This value is lower than the uncoated copper disc. Correspondingly, the wear rate follows the same trend. Further investigation into the lubrication mechanism of the Ti_3C_2 coating revealed the formation of carbon and graphitic carbon transferred films on steel balls. MXene can reduce friction and wear, which is attributed to its properties of ultrathin multilayered structure and high surface area. This structure provides an advantage by facilitating easy shear and promoting the formation of a protective tribofilm on contact surfaces (X. Lu et al., 2023).

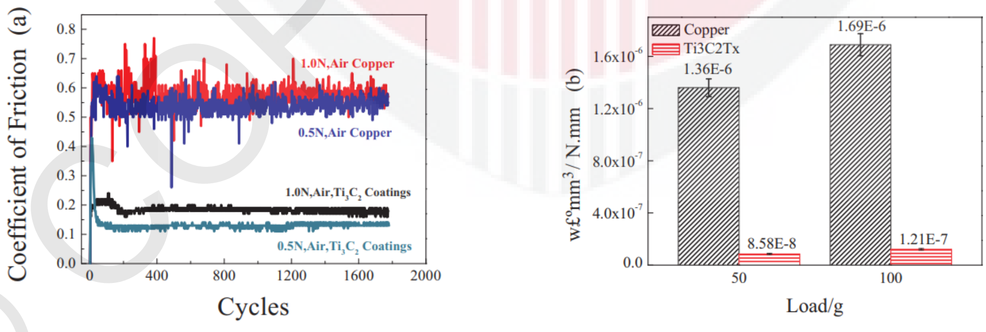

(a) (b)

Figure 2.26: (a) COF plots vs. cycle number under load of 0.5 N and 1.0 N; (b) specific wear rate of copper disk with/without Ti_3C_2 coatings (Lian et al., 2018)**.**

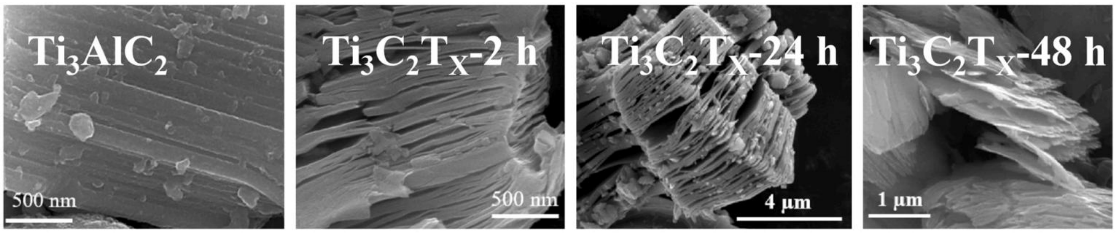

Figure 2.27: Field Emission Scanning Electron Microscopy (FESEM) images of Ti_3AlC_2 and HF-etched $Ti_3C_2T_X$ samples prepared over 48 hours (Khatun & Roy, 2022)**.**

In study Khatun & Roy, (2022) explored the optimal etching duration, ranging from 2 to 48 h, for the preparation of $Ti_3C_2T_X$ MXenes. Findings indicated that shorter etching periods did not sufficiently remove aluminum, and a 24-hour etching period was identified as the most effective for preparing $Ti_3C_2T_x$ MXenes. In contrast, etching for 48 hours resulted in damage to the MXenes structure as shown in Figure 2.27.

Ionic liquids (ILs) have emerged as promising additives in lubricants due to their unique physiochemical properties and lubricating capabilities. Research has shown that ILs can significantly reduce friction coefficients and wear rates in various tribological systems (Avilés et al., 2022; Jiménez et al., 2022; Lee-Niinioja, 2022). The molecular structure of ILs plays a crucial role in their lubrication mechanisms, with specific IL compositions demonstrating superior performance in reducing friction and enhancing durability (Jieming et al., 2023; B. Wang et al., 2022). For instance, ILs containing fluorinated segments and hydroxyl endgroups have shown exceptional thermal stability and lubricity, outperforming traditional lubricants like perfluoropolyether (PFPE) in hard disk drives (B. Wang et al., 2022). Additionally, the addition of certain ILs as lubricant additives has been found to mitigate abrasive wear mechanisms and improve overall lubricating performance, making them a viable option for next-generation lubricants in various applications (Avilés et al., 2022). Rohlmann et al., (2021) found ionic facilitates the formation of a protective boundary layer on metal surfaces, significantly reducing friction and improving lubrication. Its phosphate anions promote the formation of a tribofilm, which helps minimize material loss and extend the life of machine components.

Table 2.2: Previous work of using additive in lubricant

Type additive	Ref	Additive	Properties	Advantage	Mechanism
Solid nanoparticle additives	(H. T. Nguyen & Chung, 2020)	Titanium Carbide (Ti_3C_2)	Nominal and lateral sizes of the Ti_3C_2 flakes: (0.2–3 μm) and (<1 μm to several μm) accordingly	Friction and wear decreased with increasing concentration until 5 wt.%. Afterward, friction increased again	Mechanism: Ti_3C_2 flakes hindered direct contact of the tribo-pair, especially at the edges of the contact interface
	(Cui et al., 2020)	TiO_2	Solid nano additive Size: 100 nm High dispersity and stability in pure wate	Power consumption could be lowered during the drilling process using this nanoparticle additive Improves the load-carrying ability of water	TiO_2 forms a dynamic deposition film on the worn surface (observed using SEM, EDS) and separates the contacting surfaces.

				Friction reduction compared to only water Wear reduction compared to only water	
Ionic liquid-based additives	(Avilés et al., 2021)	Ammonium ionic liquids: bis(2-hydroxyethyl) ammonium palmitate (DPA)	DPA is an ionic liquid crystal with two mesomorphic phase transitions. At 42.1 °C, it experiences a transition from crystalline solid to liquid crystalline, and at 105.2 °C it melts to isotropic liquid	Reduced sapphire-steel COF by 80% compared to water Maintained the friction, even after the evaporation of water from the solution	The lubricant film acted as friction and wear reducer. As per the surface characterization, active groups from the lubricant were observed, indicating the presence of lubricant film.

	(Del Sol et al., 2019)	Trihexyl (tetradecyl) phosphonium decanoate [THTDP] [Deca]	This is a halogen-free ionic liquid	Friction was reduced over 70% compared to only water	Long alkyl chain helps adsorption film formation and thus, reduces friction

Table 2.3: Previous testing methods of tribo testing

Ref	Based oil	Additive	Condition	Optimal content	Lubricant performance	
					Friction	Wear
(H. T. Nguyen & Chung, 2020)	Water	Ti_3C_2	Ball (Martensitic SS)-on-disk (Austenitic SS) tribometer, Specimen radius 10 mm, Sliding distance 0.063 m, Rotation speed 120 rpm, Normal force 3-10 N, Temperature 24-26 °C	5.0 wt%	20 % decrease	48 % decrease
(Yi et al., 2021)	Water/Glycecol	TiC2Tx	Ball (Si_3N_4)-on-disk (sapphire) tribometer, Normal load 1-4 N, Rotating speed 10-990 rpm,	1.0 wt%	96.90% decrease	97.87% decrease

			Temperature 25 ° C			
(J. Chen & Zhao, 2021)	Water	Ti_3C_2Tx	Ball (SiC)-on-flat (316 steel) friction test, Normal load 5 N, Frequency 2 Hz, Time 20 min, Wear track length 5 mm	0.08 wt%	34.74% decrease	45.58% decrease

2.5.4 Effect of additives on lubricants

There are few mechanisms of additive often reported by previous researchers that act to improve tribological performance of lubricants. These include rolling effect, mending effect, polishing effect and protective tribo-film formation. These mechanisms are illustrated in Figure 2.28. The improved tribological performance of lubricants does not derive from a single lubrication mechanism but can result from multiple lubrication mechanisms (Azman et al., 2024).

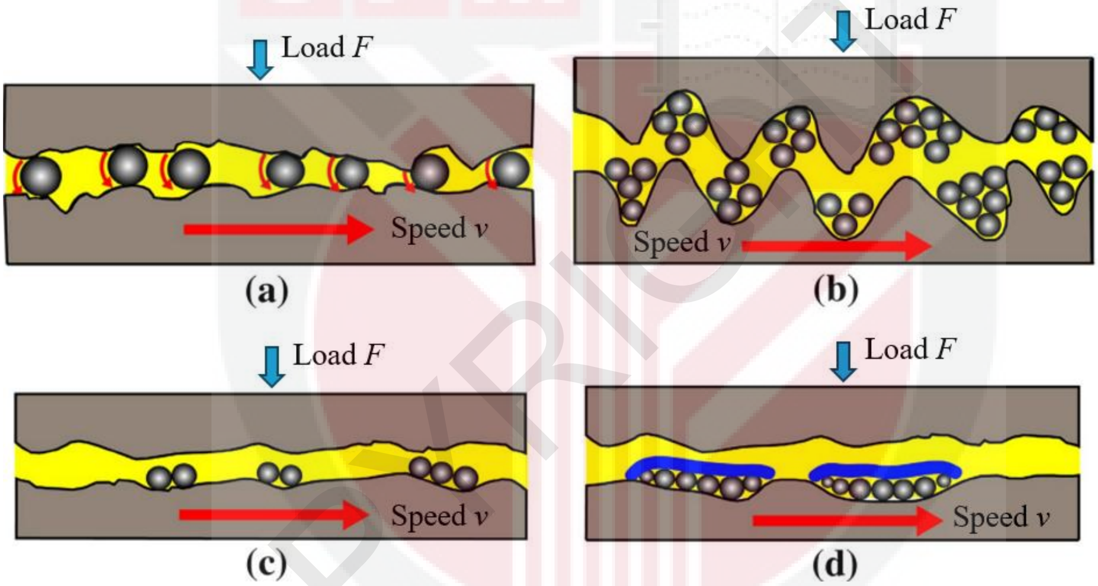

Figure 2.28: Schematic illustration of (a) rolling effect (b) mending effect, (c) polishing effect and (d) protective tribo-film formation (Azman & Samion, 2019; Singh et al., 2020)

The spherical of additive can provide the rolling mechanism between two surfaces that sliding (Figure 2.28(a)). It changes the sliding friction to rolling that allows reducing the friction and wear. The rolling effect depends on the film thickness. When the diameter of the nanoparticles approaches the thickness of the film, the nanoparticles maintain their shape, allowing the rolling mechanism to dominate (Azman et al., 2018). If the diameter of the additive less than film thickness, it would be formed a transfer film (Azman & Samion, 2019).

The mending effect (Figure 2.28(b)) occurs when the additive fills the grooves on the surface, balances for the mass loss and forms a layer on the contact surface. This process works to reduce surface roughness and minimize contact asperities (R. N. Gupta & Harsha, 2018). Essentially, it improves surface integrity and functionality by creating a smoother interface, which can be critical in reducing wear and extending the life of mechanical components. The study conducted by A. Ali et al., (2016), the researchers measured the surface roughness of worn piston rings and demonstrated the remedial effects of Al_2O_3 and TiO_2 particles in engine oil. They provided a comparison with the use of engine oil devoid of these additives.

Polishing effect when the additve make the surface smooth (Figure 2.28(c)). The hard additive can serve as a polishing agent that reduces the roughness of the contact surface. This not only enhances the aesthetic appeal by creating a smoother finish but also minimizes friction, potentially extending the lifespan of the material (Singh et al., 2020). Gulzar et al., (2017) found that friction reduces because of surface enchantment through the mending effect and polishing effect during oil lubrication using additive in their study about investigating TiO_2/SiO_2 in Trimethylolpropane (TMP) ester.

Tribo-film formation (Figure 2.28(d)) is a significant mechanism in reducing friction and wear in sliding contacts. This protective layer can be established either by the deposition and adsorption of nanoparticles onto the sliding surfaces or through the tribochemical reactions of nanoparticles with the contact surface. These processes contribute to the longevity and efficiency of mechanical systems by minimizing direct surface contact and thus, the wear and tear typically experienced during operation. Nanoparticles exhibit mechanical unstable under conditions when high contact pressure and shear stress. This often leads to the delamination and exfoliation of the nanoparticles, which become the prevailing phenomena (Dai et al., 2016).

2.5.5 Method to prepare nano additive lubricant

The development of nano lubricants is a significant advancement towards establishing a stable and long-lasting nanofluid system. In the realm of nanofluid synthesis, there are primarily two approaches employed, known as the single-step and the two-step methods (Ali & Xianjun, 2020; Azman & Samion, 2019; Babar & Ali, 2019; Yang et al., 2020). These techniques are foundational in the production of nanofluids, each with their own set of processes and benefits, contributing to the field of nanotechnology and its application in various industries. Figure 2.29 show the method to prepare the nanolubricant and Figure 2.30 show the different one step and two step method.

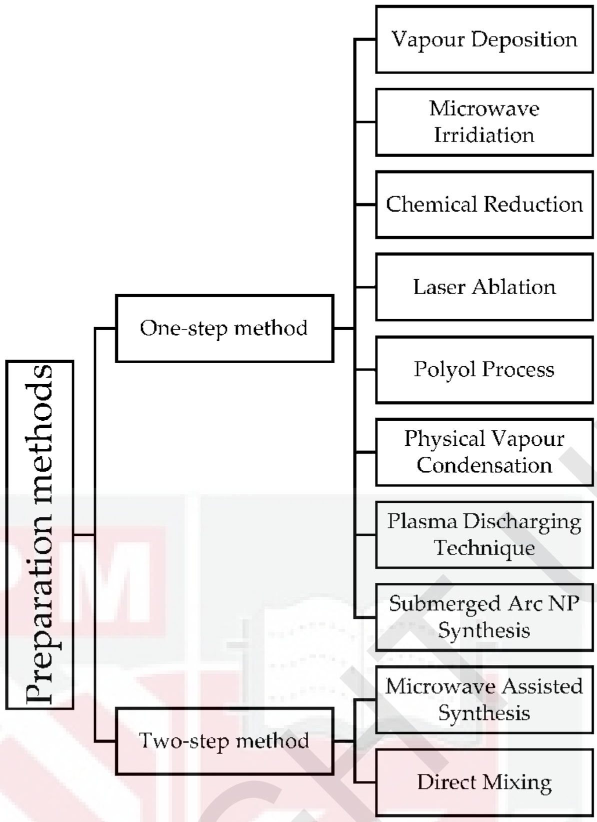

Figure 2.29: Subdivision of preparation methods of nanolubricants. (Morshed et al., 2021)

The single-step method synthesizes nanoparticles directly in the base fluid alongside a suitable dispersing agent to create nano lubricants. This synthesis can be achieved through various techniques, including physical vapor deposition, liquid chemical methods, laser ablation, and submerged arc synthesis systems (Asadi et al., 2019). Despite its direct approach, the single-step method is often constrained by its expensive nature and limited production capacity (Mello et al., 2020).

The two-step method involves an initial separate preparation of nanoparticles, followed by their incorporation into the base fluid with a dispersing agent. This second phase employs several techniques, such as magnetic stirring, probe sonication, bath sonication, homogenization, high shear mixing, and planetary ball milling. Due to its cost-effectiveness and suitability for mass production, the two-step method is the preferred choice for many researchers in the production of nanolubricants (Ali & Xianjun, 2021).

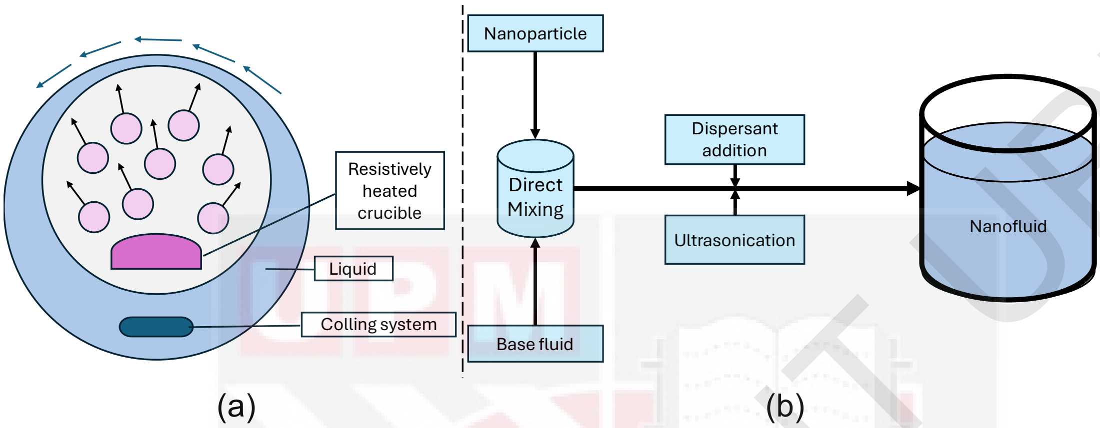

Figure 2.30: Schematics of preparation methods of nanolubricants: (a) one-step method (vapour deposition) (Choi & Eastman, 2001)**, and (b) two-step method (direct mixing technique)** (Angayarkanni & Philip, 2015)

2.6 Research gap

The metalworking industry is constantly looking for ways to increase tool life and reduce reliance on hazardous lubricants (Abdelrazek et al., 2020). Traditional lubrication systems, including oil-based lubricants, raise environmental and health concerns, driving the need for sustainable alternatives (Ijaz Malik et al., 2023). Although DLC coatings have been extensively studied for their superior tribological properties, limited research has explored their performance under severe dry friction machining conditions, especially when combined with novel water-based lubricants (WBLs). Furthermore, most studies on DLC coatings have focused on single-layer structures, while the benefits of two-layer DLC-based coatings in machining remain underexplored.

In addition, the development of hybrid WBL formulations incorporating advanced additives such as MXene and Ionic Liquids (ILs) has received attention to improve lubrication performance. However, the tribological mechanisms of MXene/IL-based WBLs under metal forming operation are not well documented. Although previous tribological studies have focused on block-on-ring tests, their direct impact on actual metal forming processes, such as ironing process, remains unclear. Furthermore, the synergy between optimized DLC coatings and WBL in reducing tool friction and wear in both machining and sheet metal forming has not been systematically analysed.

This research addresses this gap by evaluating the combined effects of a two-layer DLC coating and an advanced MXene/IL-based WBL in CNC lathe machining and sheet metal forming. It aims to provide a deeper understanding of the tribological performance of this tribo-system, optimizing tool life and surface quality while promoting sustainable metalworking practices.

CHAPTER 3

METHODOLOGY

3.1 Introduction

This chapter describes the systematic approach and experimental methodology used in the research. The main objectives are to evaluate the effectiveness of double-layer coating, which Diamond-like Carbon (DLC) as a top layer of tool coating in the turning process using a CNC lathe and to evaluate Water-based Lubricants (WBLs) with additives through a block-on-ring apparatus. The synergy of the coating and the WBLs are further examined in metal forming applications, specifically within the ironing process, to determine their combined effectiveness.

3.2 Overview of the framework

Figure 3.1 shows the framework of the proposed work conducted for this research and detail in Figure 3.2. The first phase is conducting the CNC machine in turning process to investigate the coating under severe conditions. The tool coating is used is single layered (CrN, TiAlN and TiAlSN) and double layered (DLC/CrN, DLC/TiAlN and DLC/TiAlSN). This testing runs under dry friction and machining the soft aluminum and brittle steel alloy.

The second phase is conducting tribological testing using block-on-ring tests using different WBLs. New development formulation of WBLs has been proposed which is enhance with additive Mxene and Ionic Liquid. Lubricants have been improving their properties by adding surfactant carboxymethyl cellulose and xanthan gum.

The third phase is conducting the metal forming application which is ironing process of stainless steel. The experimental setup will use effective coating in first phase and WBLs in second phase. The testing was conducted for 40 strokes.

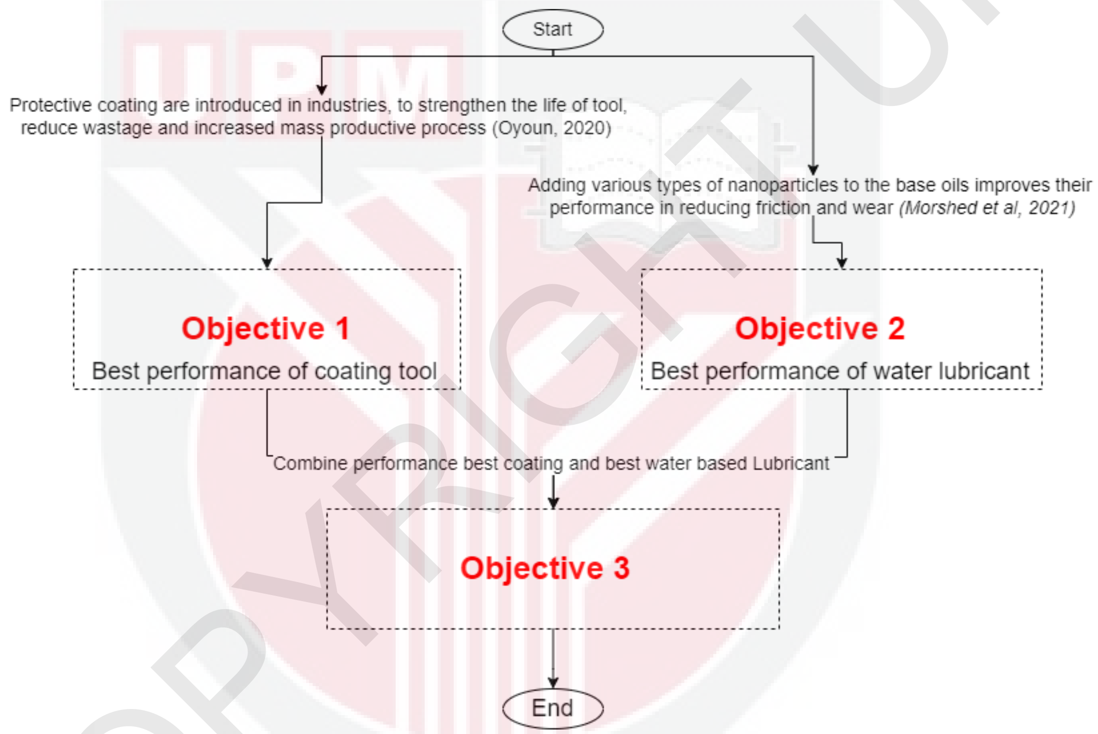

Figure 3.1: The main flowchart of this study

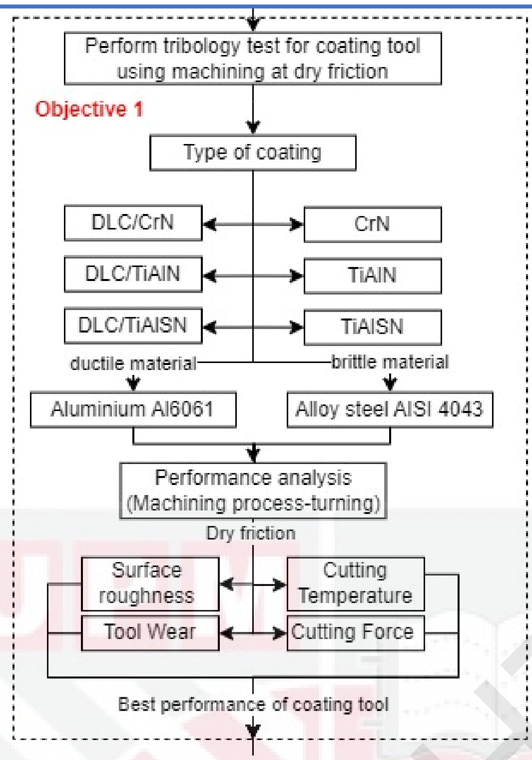
Perform tribology test for coating tool using machining at dry friction
Objective 1
Type of coating
DLC/CrN
CrN
DLC/TiAlN
TiAlN
DLC/TiAlSN
TiAlSN
ductile material
brittle material
Aluminium Al6061
Alloy steel AISI 4043
Performance analysis (Machining process-turning)
Dry friction
Surface roughness
Cutting Temperature
Tool Wear
Cutting Force
Best performance of coating tool

(a)

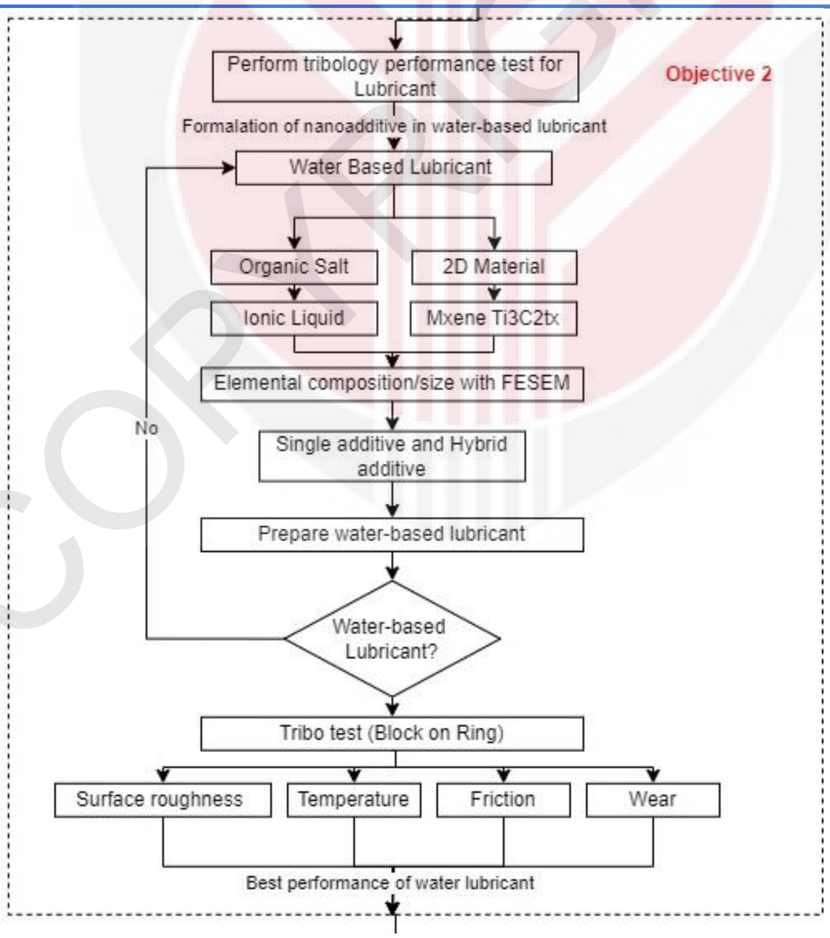
Perform tribology performance test for Lubricant
Objective 2
Formalation of nanoadditive in water-based lubricant
Water Based Lubricant
Organic Salt
2D Material
Ionic Liquid
Mxene Ti3C2tx
Elemental composition/size with FESEM
No
Single additive and Hybrid additive
Prepare water-based lubricant
Water-based Lubricant?
Tribo test (Block on Ring)
Surface roughness
Temperature
Friction
Wear
Best performance of water lubricant

(b)

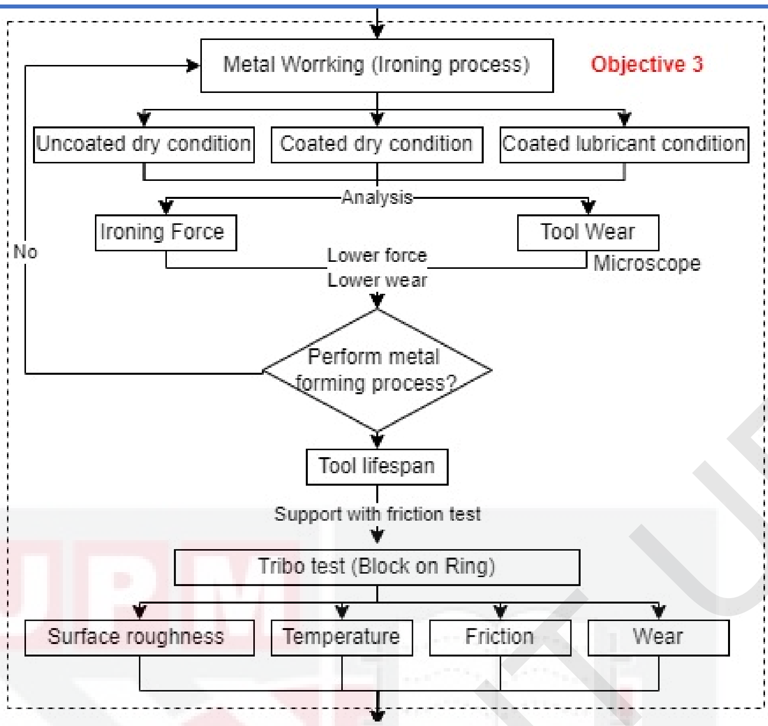

Figure 3.2: The detail of framework for (a) objective 1, (b) objective 2, and (c) objective 3

3.3 Material

3.3.1 Coating tool

The tool surfaces were coated with single and double hard coatings using the High-Power Impulse Magnetron Sputtering (HiPIMS) technique, through the support from CemeCON Scandinavia A/S. For single-layered coatings, materials such as CrN, TiAlSiN, and TiAlN were deposited onto the tool surfaces. In the case of double coatings, combinations of DLC/CrN, DLC/TiAlSiN, and DLC/TiAlN were all deposited on tool surfaces, with the DLC coating serving as the top layer. The average thickness of the test coatings ranged from 3 to 4 μm. The information about coating strategies on the tool surfaces and the measurement of thickness of all test coatings is listed in Table 3.1.

Table 3.1: Single coating and double coating of cutting tool

Coating		Thickness (μm)
Single layered tool coating	CrN	3 ± 0.2
	TiAlSiN	3 ± 0.2
	TiAlN	3 ± 0.2
Double layered tool coating	DLC/CrN	4 ± 0.4
	DLC/TiAlSiN	4 ± 0.4
	DLC/TiAlN	4 ± 0.4

3.3.2 Water-based Lubricant

Commercialized Ti_3C_2Tx MXene multilayer Nanoflake with Purity 99.9 % (Nanoshell, India) and ionic liquid tributyl(methyl)phosphonium dimethyl phosphate with >95 % (Tokyo Chemical Inc, Japan) were used as additive in this research. The nominal size of the Ti_3C_2Tx was < 10 μm. Figure 3.4 shows the FESEM image of Ti_3C_2Tx. The high magnification FESEM image clearly layered the structure of Ti_3C_2Tx. The chemical formula and density of additive and surfactant are shown in Table 3.2 and Table 3.3 show the properties of additives. Polysaccharide/Xanthan Gum (abbreviated XG) and Carboxymethyl Cellulose (abbreviated CMC) were used as viscosity modified/surfactant that purchase from DChemie, Malaysia. Figure 3.3 shows the chemical structure of (a) Tributyl(methyl)phosphonium dimethyl phosphate, (b) Xanthan Gum and (c) Carboxymethyl Cellulose.

Table 3.2: Chemical formula and density of additive and surfactant

Abbr	Chemical Name	Chemical formula / Molecular weight	Density (g/cm^3)
IL	Tributyl(methyl)phosphonium dimethyl phosphate	$C_{15}H_{36}O_4P_2$ = 342.4	1.004
Mxene	Ti_3C_2Tx Mxene Multilayer Nanoflake (Titanium Carbide)	Ti_3C_2 = 167.62	4.12
XG	Xanthan Gum	$C_8H_{14}Cl_2N_2O_2$ = 241.11	1.5
CMC	Carboxymethyl Cellulose	[C6H7O(OH)3−x(OCH2COOH)x]n = 240.21	1.6

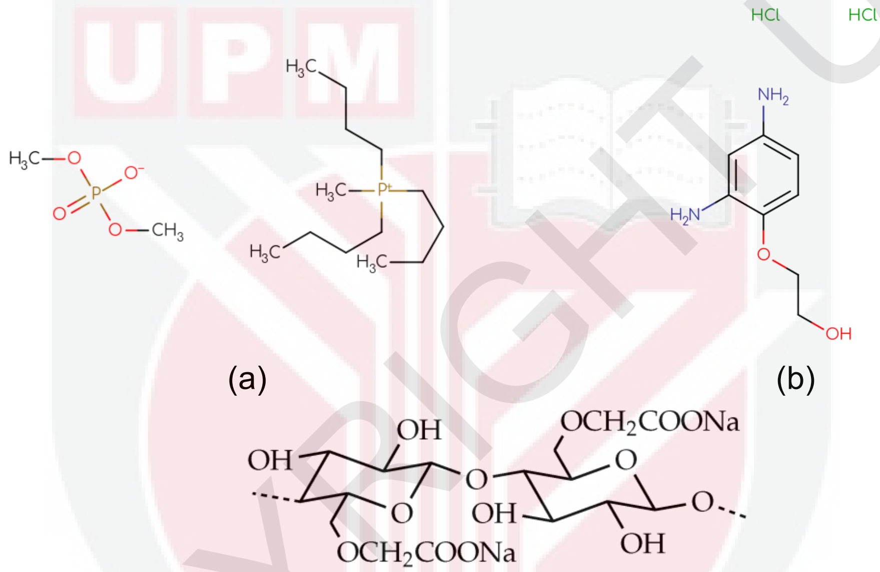

(a) (b) (c)

Figure 3.3: Chemical structure of (a) Tributyl(methyl)phosphonium dimethyl phosphate (Wijanarko et al., 2022b)**, (b) Xanthan Gum and (c) Carboxymethyl Cellulose** (Michaelis et al., 2023)

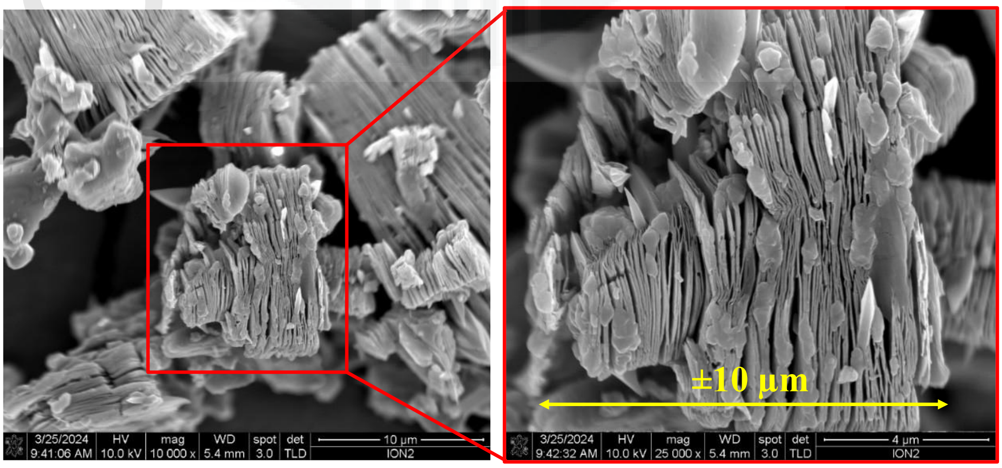

(a) (b)

Figure 3.4: Particle of Ti3C2Tx MXene multilayer Nanoflake at (a) 10000 magnification and (b) 25000 magnification

Table 3.3: The properties of Ionic liquid and MXene.

Property	Tributyl(methyl)phosphonium Dimethyl Phosphate (TBMP-DMP)	$Ti_3C_2T_x$ MXene Multilayer Nanoflake
Chemical Formula	$C_{13}H_{32}O_4P_2$	$Ti_3C_2T_x$ (T_x = –OH, –O, –F, etc.)
State	Liquid at room temperature	Solid (Multilayer nanoflakes)
Melting Point	Low / Room-Temperature Ionic Liquid (RTIL)	Decomposes before melting
Thermal Stability	>250°C	>1000°C (stable in inert conditions)
Electrical Conductivity	Moderate (ionic conductivity)	High (~10^3 to 10^4 S/cm)
Solubility in Water	Highly hydrophilic, water-soluble	Hydrophilic but disperses in water
Viscosity	Moderate to high	Not applicable (solid)
Lubrication Performance	Low friction, forms tribofilm	Reinforces lubricants, reduces wear
Mechanical Strength	N/A	High strength, flexible layers
Chemical Stability	Stable in aqueous and polar solvents	Stable but oxidizes over time
Surface Functional Groups	No active surface groups	–OH, –O, –F, etc. (functionalized)

The preparation of WBLs involves the use of nano additives, distilled water as oil based, and surfactants to increase the stability of the nano particle dispersion. The selected surfactants are Xanthan Gum (XG) and Carboxyl Methyl Cellulose (CMC). Nano additives are first dispersed in distilled water using a magnetic stirrer. Afterwards, surfactant was added to the mixture to increase the viscosity and ensure stable dispersion, with continuous stirring at 1000 rpm for 30 minutes at 50°C. The mixture was then processed in a homogenizer for 5 minutes at 8000 rpm, repeated twice. Figure 3.5 illustrates the production process of WBLs, while Table 3.4 details the content in the lubricant.

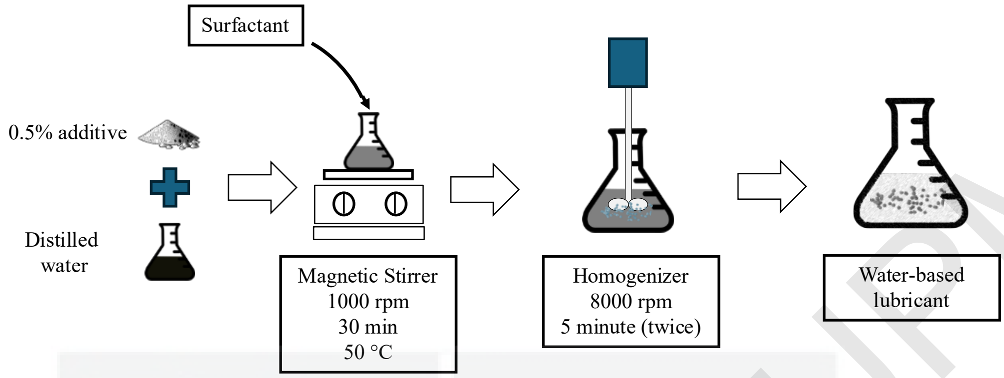

Figure 3.5: Preparation of WBLs

Table 3.4: Content of water-based lubricants

Label	Lubricant content
CMC_IL	0.5 % IL + 0.5 % CMC + Distilled Water
CMC_Mxene	0.5 % Mxene + 0.5 % CMC + Distilled Water
CMC_Mxene/IL	0.25 % Mxene + 0.25 % IL + 0.5 % CMC + Distilled Water
XG_IL	0.5 % IL + 0.5 % XG + Distilled Water
XG_Mxene	0.5 % Mxene + 0.5 % XG + Distilled Water
XG_Mxene/IL	0.25 % Mxene + 0.25 % IL + 0.5 % XG + Distilled Water

Characteristics of water-based lubricants, focusing on their dispersion stability and viscosity. Dispersion stability is an important factor in ensuring uniform distribution of lubricant additives, which directly affects performance and longevity. Meanwhile, viscosity determines the ability of the lubricant to reduce friction and wear under different operating conditions. The sedimentation analysis method offers a straightforward and cost-effective approach to assess the dispersion stability of water-based lubricants. Following the preparation of each lubricant, an immediate sample collection is conducted for analysis. These samples are then systematically photographed at 24-hour intervals over a span of 4 days. Subsequently, observations are made regarding the sedimentation of nanoparticles and the development of a supernatant layer. Viscosity is a critical characteristic of lubricants, defined by the fluid's resistance to shear flow. Within the scope of this study, viscosity is a key factor affecting the integrity of the lubricant film and its capacity to prevent direct surface contact, thereby influencing the lubricant's tribological performance. A viscosity that is too low will result in the lubricant shearing under pressure, leading to metal-on-metal contact, which in turn increases friction and wear. Conversely, excessively high viscosity necessitates greater force to initiate shear, resulting in increased friction, heat generation, and energy loss. Therefore, selecting a viscosity level that ensures a robust lubricant film and surface protection is of utmost importance.

The SV-10 viscometer as in Figure 3.6, manufactured by A&D in Japan, has two thin sensor plates. These plates oscillate in antiphase at a consistent sine wave frequency, like a tuning fork, driven by an electromagnetic force. This electromagnetic mechanism precisely controls the vibration of the sensor plate to ensure a stable amplitude. The driving electric current, functioning as an excitation force, is measured by the resistance it encounters, which is the viscosity produced between the sensor plate and the sample liquid. The viscosity coefficient is then calculated based on the relationship between the drive current and this resistance. Accurate temperature measurement is important because viscosity is highly dependent on temperature. It can measure viscosity ranging from 0.3 to 10,000 mPa·s.

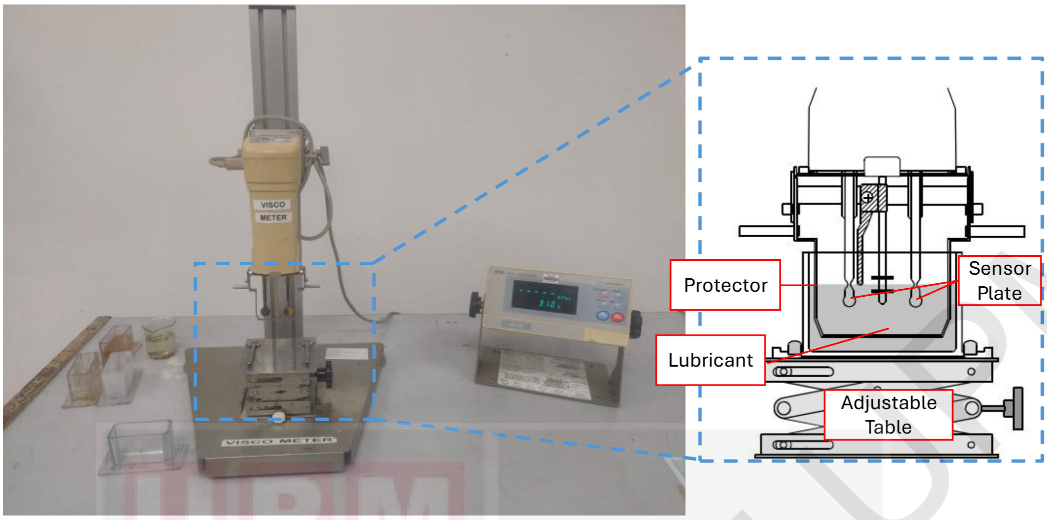

Figure 3.6: The SV-10 viscometer

3.4 Method to determine the tool coating

In this section, the turning process has been chosen to determine the suitable coating to be used for finding the most promising combined effects of coating and WBLs. The setup included an orthogonal cutting arrangement and a Mazak 200MY Computer Numerical Control (CNC) lathe, depicted in Figure 3.7. This CNC lathe can reach a maximum speed of 5000 rpm, with a power output of 26 kW. The machine input parameters are detailed in Table 3.5, with running in dry friction condition at 6° of rake angle and 95° of clearance angle on the tool. The testing was conducted under severe tribological conditions, characterized by dry contact without the presence of lubrication, utilizing orthogonal cutting methods. This rigorous evaluation aimed to simulate severe operational environments to understand the wear behaviors of the materials involved.

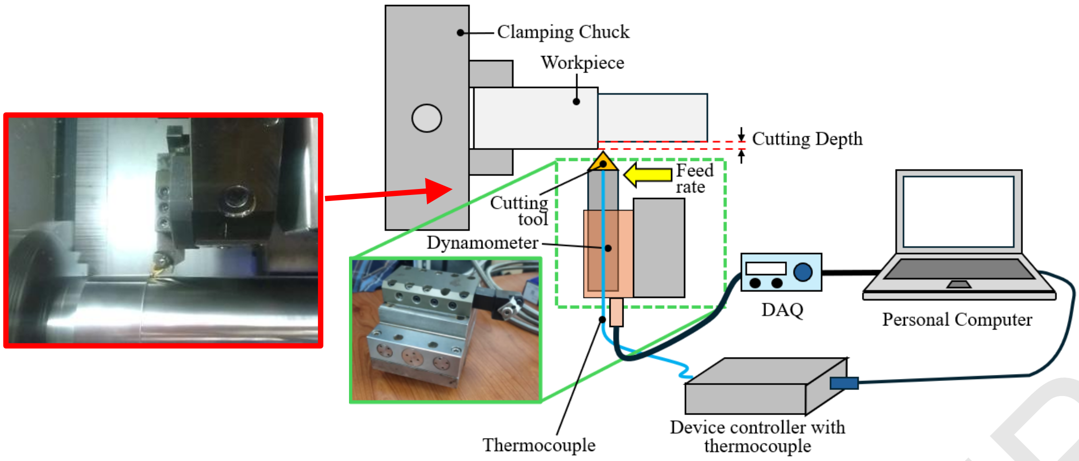

Figure 3.7: Test setup for machining through orthogonal cutting.

Table 3.5: Parameter setup for machining AISI4340 and Al6061

Parameters	Description
Cutting Speed (rev/min)	240
Feed Rate (mm/rev)	0.15
Cutting Depth (mm)	1
Condition	Dry friction condition
Rake angle (°)	6°
Clearence angle (°)	95°

The CNC lathe orthogonal cutting was studied on ductile and brittle workpiece material characteristics. The soft and ductile workpiece material was Al6061 aluminium, meanwhile the hard and brittle workpiece material was AISI4340 alloy steel. Both workpiece material was selected to examine the ductile and britle behaviors in machining, to distinguish the types of tool wear, ie. adhesive and abrasive wear, resulting from the machining process. This allowed for comparative analysis on mechanism material characteristics that influence tool degradation. 300 mm long with external diameter of 100 mm bars are used in this testing. Chemical composition and mechanical properties of workpiece materials are specified in Table 3.6 and Table 3.7.

Table 3.6: Mechanical properties of test workpiece; Al6061 and AISI4340 (MatWeb LLC, 2024).

Material property	Al6061	AISI4340
Yield Strength	55.2 MPa	862 MPa
Ultimate tensile strength	124 MPa	1282 MPa
Modulus of elasticity	68.9 GPa	200 GPa
Hardness	30 HB	363 HB

Table 3.7: Chemical composition of workpiece; Al6061 and AISI4340 (MatWeb LLC, 2024).

Material	Element (%)				
Al6061	Al	Cr	Cu	Fe	Mg
	95.8-98.6	0.04 - 0.35	0.15 - 0.40	<= 0.70	0.80 - 1.2
	Mn	Si	Ti	Zn	
	<= 0.15	0.40-0.80	<= 0.15	<= 0.25	
AISI4340	C	Cr	Fe	Mn	Mo
	0.37-0.43	0.70-0.90	95.195-96.33	0.60-0.80	0.20-0.30
	Ni	P	Si	S	
	1.65-2.0	<= 0.035	0.15-0.30	<= 0.040	

The cutting force was accurately measured utilizing a Kistler 3-Component dynamometer, model 9129AA. This system was interfaced with a multichannel charge amplifier, model 5070A, which in turn was connected to a computer operating Kistler DynoWare software. The roughness of the workpiece was assessed with a SURFTEST SJ-210 tester (Figure 3.8) both prior to and following each machining process, providing an indication of the surface quality post-machining. The Dino-Lite Digital Microscope AM4117 was used to analyzed the type of wear on tool edge (Flank wear and crater wear) and a model JSM-7800F from JEOL Scanning Electron Microscope (SEM) with Energy Dispersive X-ray (EDX) analysis. Both pieces of equipment proved sufficient to characterize flank wear (*VB*) and crater wear (*KB*), providing critical indicators of the tool surface condition post-machining. This analysis included examining the composition of material on the tool surface and analyzing the elevation of material composition peaks, which correlates to the quantity of chemical elements present in the tested coated cutting tools. The SEM machine as illustrate in Figure 3.16 in Section 0

Figure 3.8: SURFTEST SJ-210 tester to measure the surface roughness.

3.5 Method of tribological testing

Tribological tests were performed to evaluate the wear characteristics and friction coefficients of tribological pairs when lubricated. In this project, reference has been made to the ASTM G77-98 standard, which is a recognized method for evaluating the resistance of materials to sliding wear against metals, using a block-on-ring apparatus as in Figure 3.9. Figure 3.8show the material properties of block and ring.

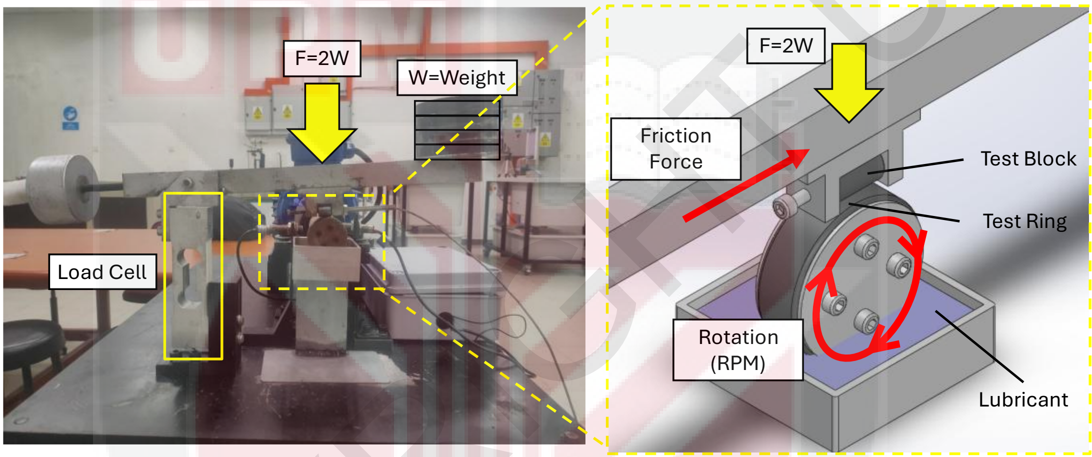

Figure 3.9: Tribological test setup following ASTM G77 test standard.

Table 3.8: Material properties of block and ring AISI 52100

Specimen	Block	Ring
Roughness (µm)	*Ra* = 0.0363 (± 0.0004) *Rq* = 0.0455 (± 0.0004)	*Ra* = 0.6453 (± 0.0004) *Rq* = 0.8317(± 0.0004)
Elastic modulus (GPa)	210	
Yield strength (MPa)	1800	
Ultimate tensile strength (MPa)	2400	
Chemical composition	Fe-96.5%, Cr-1.6%, C-1.1%, Mn-0.45%, Si-0.3%, P-0.025%, S-0.025%	

The wear surface area was accurately measured with the Dino-Lite AM4113, a leading digital microscope, as depicted in Figure 3.14 in Section 0. The wear surface area was calculated using Equation 3.1 and Figure 3.10. Utilizing this microscope allowed for the capture of detailed images of the wear surface profiles. Subsequently, the dimensions of the wear surface were meticulously measured and analysed using the accompanying software, DinoCapture 2.0.

$$A = \frac{\pi}{4} ab \qquad \textbf{Equation 3.1}$$

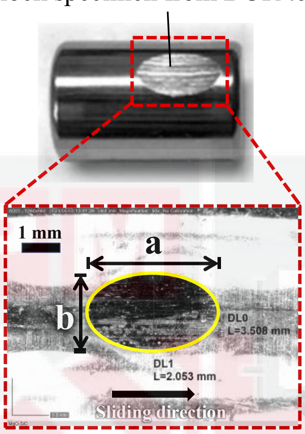

Figure 3.10: Wear area analysis on the surface of the block

3.6 Method to evaluate both coating and water-based lubricant

Ironing has been selected to evaluate the combined effect of coating and WBL. Testing was conducted using an ironing tool coated with a double layer of DLC/TiAlN, which was also applied with WBL CMC_Mxene/IL. The setup of the machine is shown in Figure 3.11. The workpiece used stainless steel SUS304 had a thickness of 1 mm and a diameter of 8 mm. The wear on the tool will be observed using a digital microscope, as detailed in Section 0. The ironing process had a 20% reduction of thickness workpieces. The ironing tool used has a diameter of 4.4 mm and a nose radius of 1 mm. The die used has a diameter of 6 mm and an upper radius of 1.5 mm. The dimensions of the die and the tool are depicted in Figure 3.12 and Figure 3.13, respectively. The operation is carried out at a consistent speed, with each stroke executed at a rate of 250 strokes per minute (SPM).

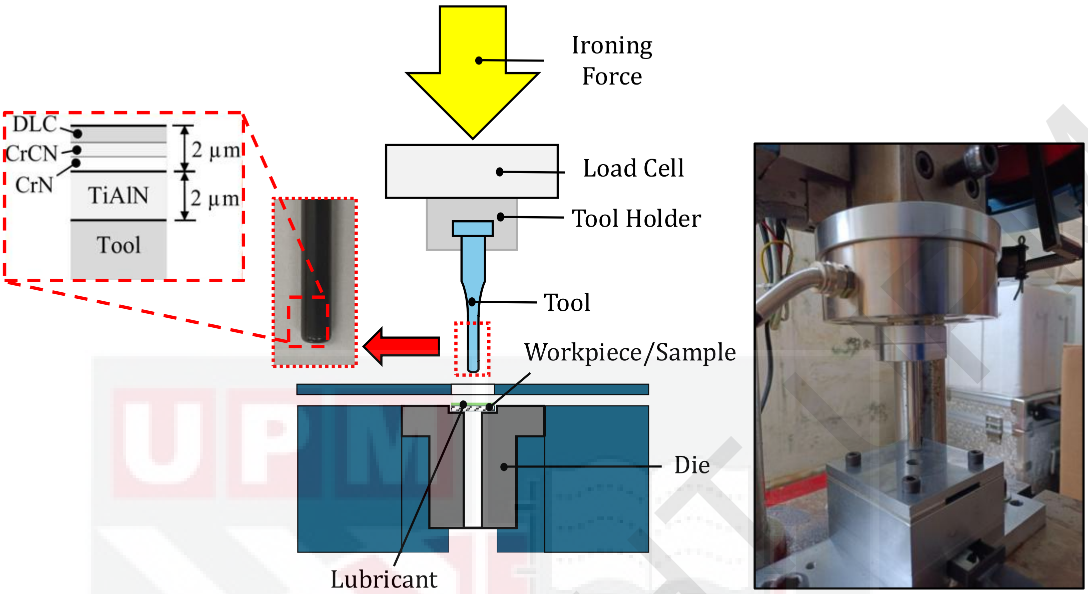

Figure 3.11: Ironing setup on the press machine.

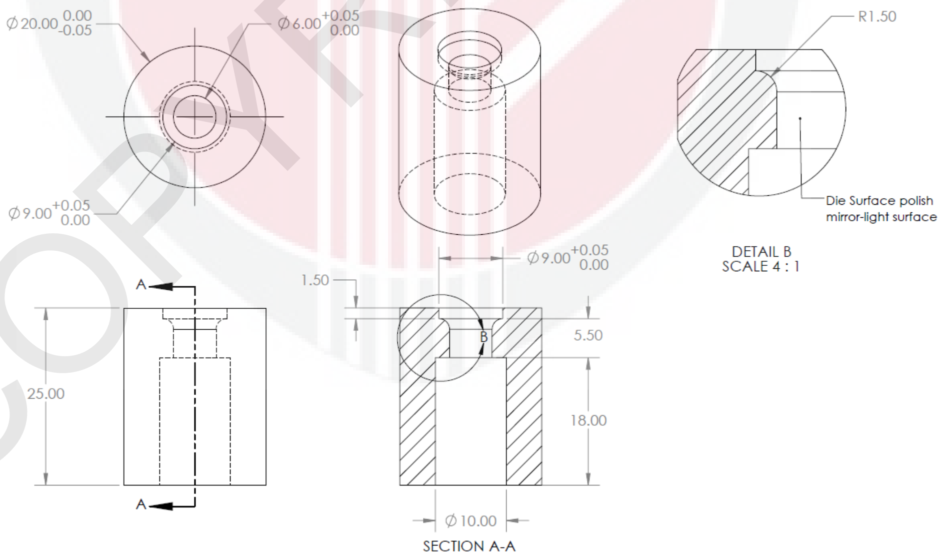

Figure 3.12: Dimension of lower die for ironing with 20 percent thickness reduction.

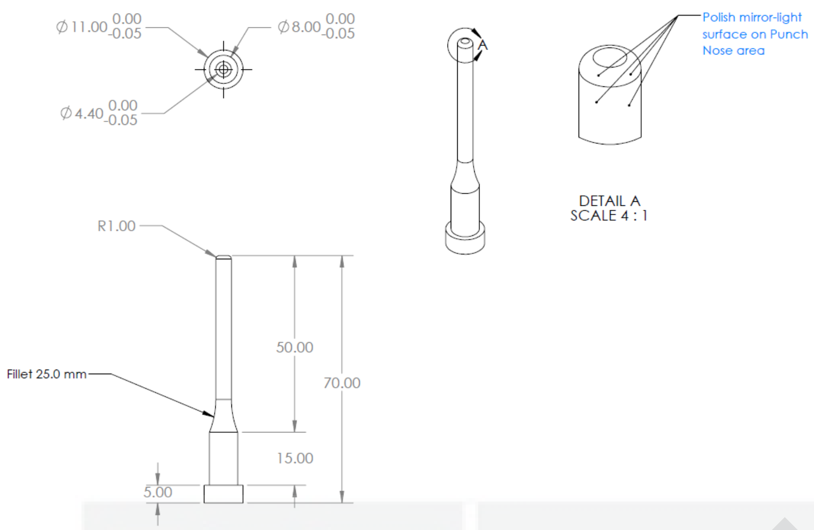

Figure 3.13: Dimension of uncoated and coated tools for ironing with 20 percent thickness reduction.

3.7 Method to evaluate Wear

The assessment of the wear surface is conducted using the Dino-Lite AM4113, a digital microscope of superior quality, as show in Figure 3.14. This advanced instrument enables the acquisition of detailed images that reveal the contours of the wear surface. Following this, the dimensions of the wear area are meticulously measured and analyzed with the aid of the specialized software, Dino Capture 2.0.

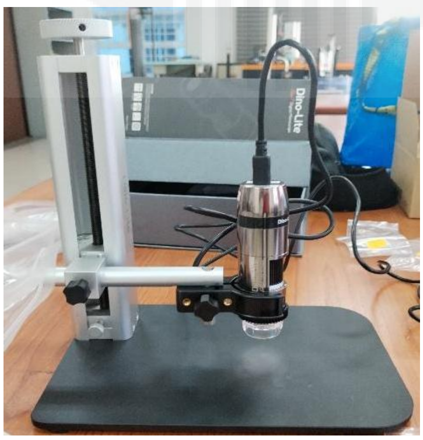

Figure 3.14: Dino-Lite AM4113.

Surface roughness is measured using the Olympus Digital Microscope DSX1000 (Figure 3.15), which offers high-resolution imaging capabilities for detailed surface analysis. This advanced instrument provides accurate and reliable data, essential for quality control in various manufacturing processes.

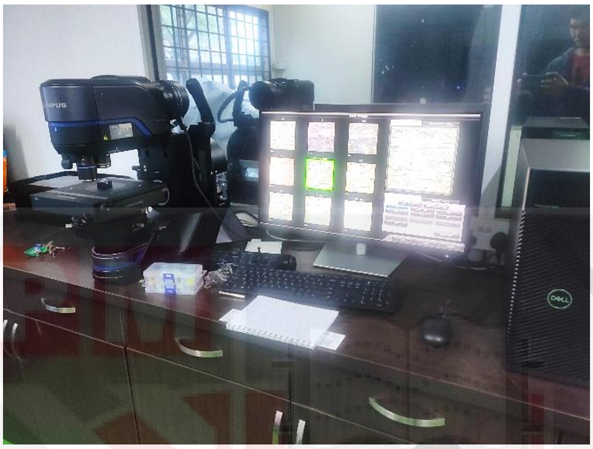

Figure 3.15: Olympus Digital Microscope DSX1000

The Scanning Electron Microscope-Energy Dispersive X-ray Spectroscopy (SEM-EDX) analysis of the coating tool was conducted using the JSM-7800F model from JEOL as illustrate Figure 3.16. This instrument was utilized to measure the elemental composition and microstructural characteristics of the coating.

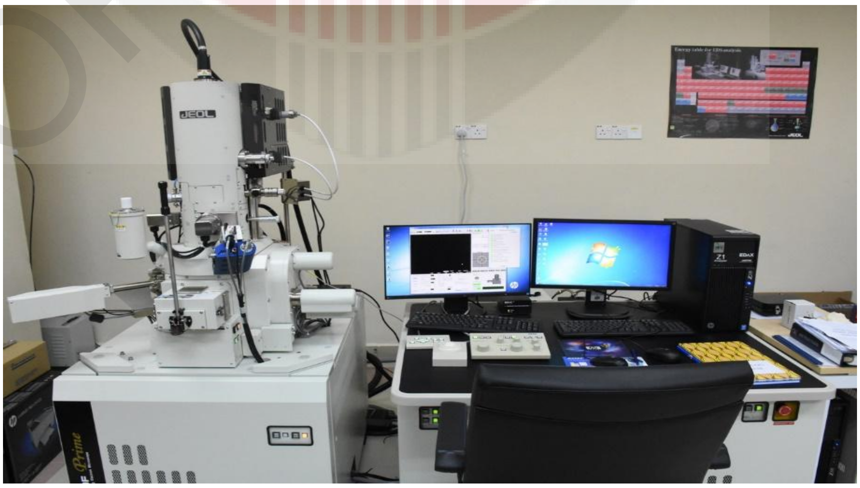

Figure 3.16: SEM machine model JSM-7800F from JEOL

CHAPTER 4

RESULTS AND DISCUSSION

4.1 Introduction

This chapter explains the finding of the evaluation single and double layered coating and investigation of new developments of WBLs with additive Mxene and Ionic Liquid. Figure 4.1 shows the finding section in this research.

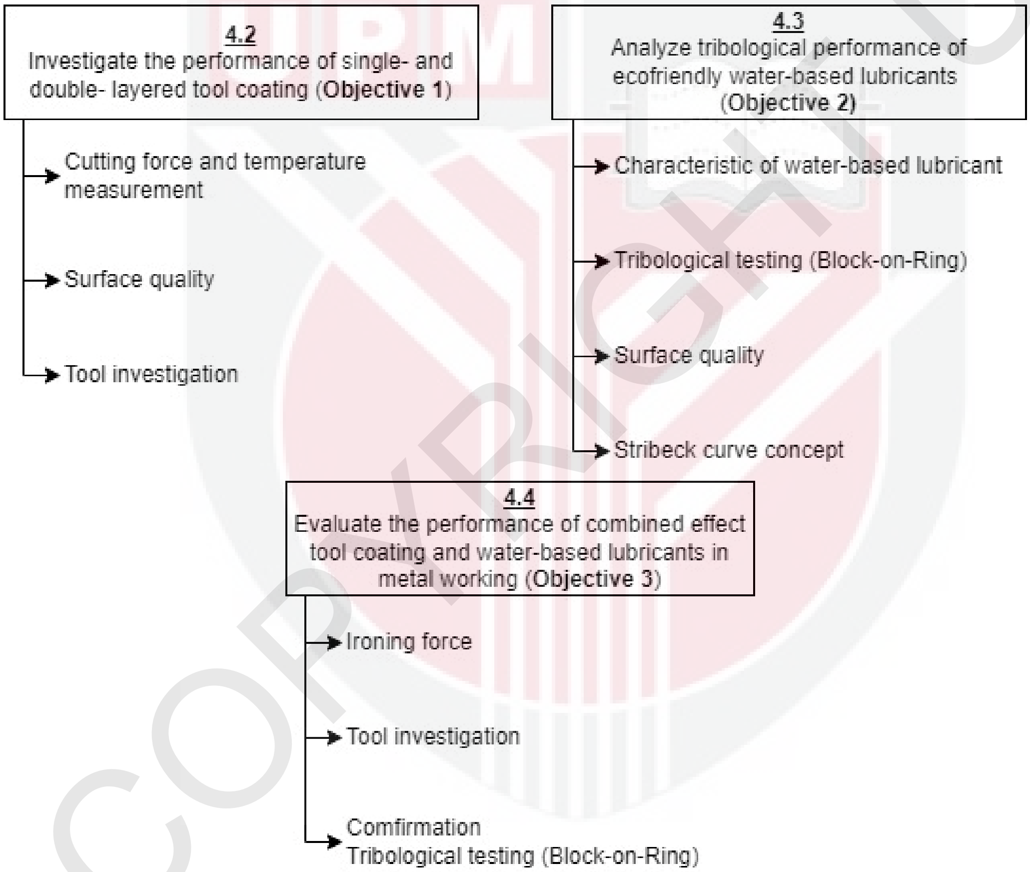

Figure 4.1: Detail observation in this research: (4.2) Investigate the performance of coating, (4.3) analyze tribological performance of WBLs and (4.4) evaluate effect of coated tool and WBL.

4.2 Selection of coating using turning process

The objective 1 involves performing turning operations on a CNC machine to evaluate the coatings performance under severe conditions. The tool coatings used include single-layered (CrN, TiAlN, and TiAlSN) and double-layered (DLC/CrN, DLC/TiAlN, and DLC/TiAlSN) types which diamond-like carbon (DLC) as top layer. The tests are conducted under dry friction conditions while machining soft aluminum and a brittle steel alloy.

4.2.1 Effect of coated tool to cutting force

These findings are presented briefly in Figure 4.2 depicts the cutting force and Figure 4.3 for temperature. After machining, all types of coated tools resulted in lower cutting forces and temperatures for both workpieces, Al6061 and AISI4340, compared to uncoated tools. The study revealed that, after machining, each coated tool variant achieved a reduction in cutting force during the machining of Al6061 and AISI4340 workpieces, in contrast to their uncoated counterparts.

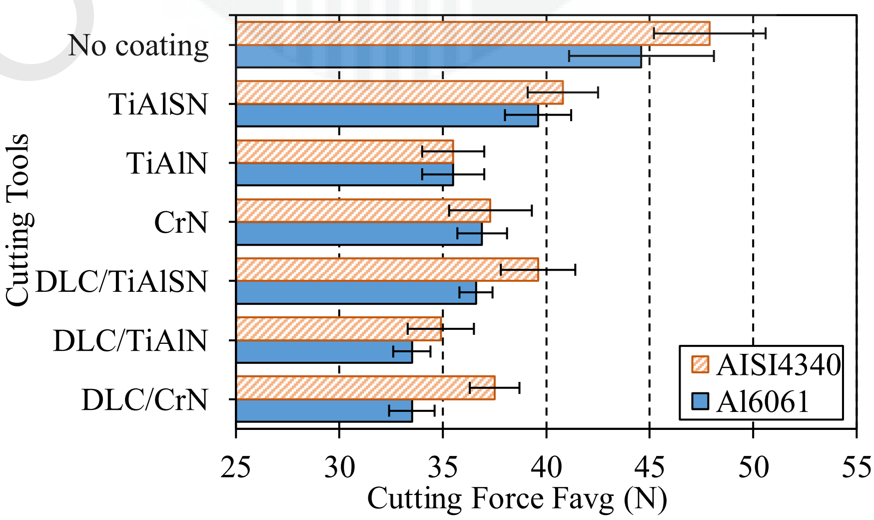

Figure 4.2: Measured cutting force *F*z in steady-state conditions during the orthogonal cutting experiment using both single- and double-layered hard coatings

When machining Al6061, a cutting force of 44.6 N was recorded, while machining AISI4340 produced a cutting force of 47.9 N for uncoated tool. The average cutting force for Al6061 is around 33.5 N, which is reduced by about 25% when using DLC/TiAlN and DLC/CrN double coatings, compared to uncoated tools. This coating produced the lowest cutting force values among all types tested. A DLC/TiAlSN coating was observed to produce a cutting force of 36.6 N, marking the highest record value among dual-layer coatings. In contrast, the TiAlN coating showed the most efficient performance in single-layer applications, with a minimum cutting force of about 35.5 N. This was closely followed by CrN at 36.9 N and TiAlSN at 39.6 N. Among the various tool coatings, TiAlN emerged as the second most effective in reducing cutting forces, surpassing only DLC/TiAlN and DLC/CrN combinations when used in machining Al6061.

In the machining process of AISI4340, all types of coating produced higher cutting forces than those recorded for Al6061, except for the TiAlN single coating. On the other hand, when machining Al6061, the DLC/TiAlN double coating showed the lowest cutting force in all tested coatings, with values of 34.9 N. This represents a 27% reduction in cutting force when compared to uncoated tools. For the double coating, the cutting force was 37.5 N for DLC/TiAlN, followed by 39.6 N for both DLC/CrN and DLC/TiAlSN. Regarding the single coating on AISI4340, the trend is like Al6061, with TiAlN showing the lowest cutting force at 35.5 N, followed by CrN at 37.5 N and TiAlSN at 40.8 N.

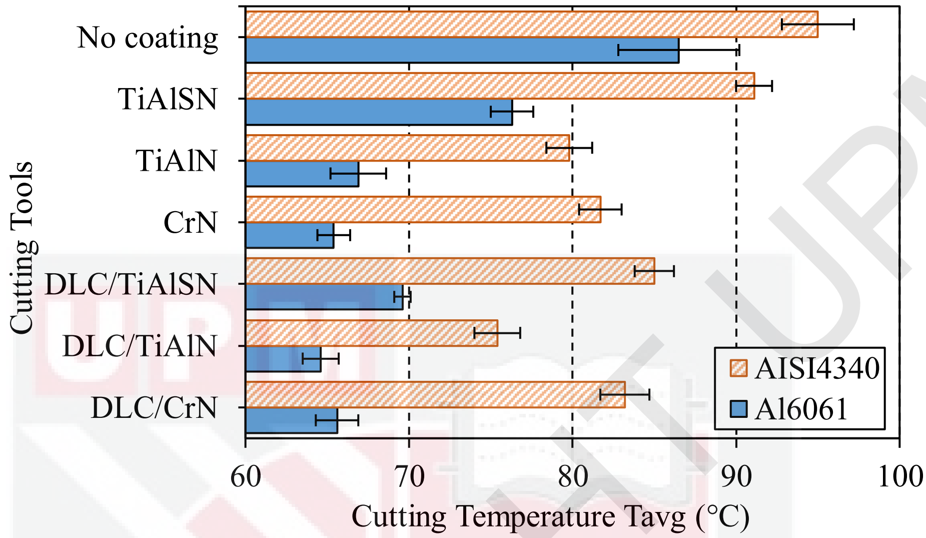

Figure 4.3: Measured temperature in steady-state conditions during the orthogonal cutting experiment using both single- and double-layered hard coatings

For uncoated tool the temperature was recorded at 86.5 °C during the machining of Al6061, while the machining temperature of AISI4340 reached 95 °C. The average cutting force shows that DLC/TiAlN and DLC/CrN double coatings outperform all other types of coatings, producing the lowest values compared to uncoated tools. Temperature measurements show variation between the two instruments; DLC/TiAlN recorded a lower temperature of 64.6 °C compared to DLC/CrN. Among the double coatings, DLC/TiAlSN recorded the highest temperature at 69.6 °C. The single coating presents different temperature profiles: CrN at 65.4 °C, TiAlN at 66.9 °C, and TiAlSN at a higher temperature of 76.3 °C. These findings highlight the effect of coating type on both temperature and cutting force during the machining process.

During the machining of Al6061, the DLC/TiAlN double coating showed the lowest temperature among the tested coatings, recording a temperature of 75.4 °C. This represents a 20% temperature reduction compared to an uncoated tool. Following DLC/TiAlN, DLC/CrN and DLC/TiAlSN coatings recorded temperatures of 83.2 °C and 85 °C, respectively. Similarly, when a single coating is applied to AISI4340, the results are parallel to Al6061. The TiAlN coating showed the lowest temperature, followed by CrN and TiAlSN, with temperatures of 79.8 °C, 81.7 °C and 95 °C, respectively.

Single and double coating reduce forces primarily by decreasing the coefficient of friction (COF) between surfaces. Coatings, such as Diamond-Like Carbon (DLC) coatings, create a protective layer that minimizes direct contact between materials, reducing friction and wear. For example, DLC coatings can lower the COF to values as low as 0.1–0.2, even under extreme conditions. This reduction in frictional forces translates to less energy required for movement, improved durability, and resistance to wear and heat generation in components like seals, shafts, or cutting tools (Kovalčík et al., 2022). Double coatings or multi-layered coatings further enhance these effects by combining properties like increased surface hardness and reduced adhesion, offering superior performance in demanding environments (Kovalčík et al., 2022) Comparing aluminium and alloy steel is necessary because these materials exhibit different mechanical properties, such as hardness, ductility, and corrosion resistance. Aluminium is softer but has lower strength compared to alloy steel. Alloy steel, on the other hand, is stronger propertie. These differences influence how coatings interact with each material. Additionally, the forces experienced during machining or sliding differ due to variations in material hardness and surface roughness. Coated tools may demonstrate different cutting forces when used on aluminium versus alloy steel because of these intrinsic material characteristics (Kovalčík et al., 2022)

According to the data, when machining Al6061, the DLC/TiAlN and DLC/CrN double coatings showed the lowest cutting forces, followed by the TiAlN single coating. DLC/TiAlN showed the lowest cutting forces in the AISI4340 machining case, followed by TiAlN and CrN, respectively, by increasing order of cutting force value. This implies that the cutting force experienced during the machining of these materials is significantly influenced by the coating selection. According to the observation, the DLC/TiAlN coating exhibits the lowest cutting temperature when brittle steel and soft aluminum are machined. According to L. Wang et al., (2022), they state that DLC coatings are well-known for their superior anti-adhesive properties and low friction coefficient. These features facilitate the workpieces sliding movement during the cutting process, which lowers the temperature and cutting force. The reduction in forces can lead to benefits for the materials involved. For instance, lower forces result in less deformation and stress on the workpiece, which helps maintain its dimensional accuracy and surface finish (Ercetin et al., 2023). Additionally, reduced forces can extend the tool life by minimizing wear and tear, as lower forces reduce the friction and heat generated during the cutting process (Kovalčík et al., 2022)

Thermal analysis revealed that coatings significantly affect the temperature profile of cutting tools in the turning process. Single-layer coatings, such as TiAlSiN, CrN and TiAlN, exhibit varying degrees of heat resistance, with TiAlSiN showing superior temperature resistance, making it suitable for high-speed machining. The addition of a DLC top layer further enhances the effectiveness of these coatings. In particular, the synergy between DLC and TiAlSiN results in the highest temperature resistance, suggesting improved surface hardness and reduced friction. However, this combination also leads to high temperatures, indicating that while DLC coatings extend tool life by minimizing wear, they simultaneously require an efficient cooling strategy to manage the resulting thermal load. According to Ai et al., (2022), two-layer coatings improve the high-temperature resistance of tools, making them suitable for both dry and semi-dry machining conditions. Advances in this coating technology not only extend the operational life of tools but also ensure their efficiency across a wide range of environmental conditions. Furthermore, the presence of aluminium in the coating composition plays a key role in inhibiting grain growth, leading to the formation of a continuous, adherent, and thermally stable alumina layer even at high temperatures (Pereira Falcón et al., 2019). These properties are important for improving the durability and performance of cutting tools in high-temperature environments, making such coatings invaluable for industries that require superior temperature resistance and adaptability to different lubrication conditions.

4.2.2 Effects of coated tools on surface integrity

The study also revealed that the quality of the workpiece can be evaluated by the surface roughness obtained after machining. For each cutting tool used, the resulting surface roughness for Al6061 and AISI4340 materials is depicted in Figure 4.4. The surface quality of the machined part is largely determined by the surface roughness parameter (İşleyen & Karamanoğlu, 2019). (Otsuki et al., 2022) reported that lower surface roughness values correlate with higher surface quality. An uncoated tool was used as a standard for comparison, resulting in a surface roughness value of 2.513 μm for Al6061 and 2.516 μm for the AISI4340 workpiece.

The use of dual DLC/TiAlN coating on the surface resulted in significantly reduced roughness for both Al6061 and AISI4340 materials, with measurements of 1.241 μm and 1.451 μm, respectively. This represents a roughness reduction of approximately 50% for Al6061 and 42% for AISI4340 when compared to machining with uncoated tools. In Al6061 machining, the second lowest roughness was achieved using a single CrN coating, followed by a double DLC coating, with values of 1.617 μm and 1.819 μm, respectively. In contrast, the TiAlN coating produced the poorest surface quality, exhibiting the highest roughness value among all coated tools, outperforming the uncoated tool by about 10%.

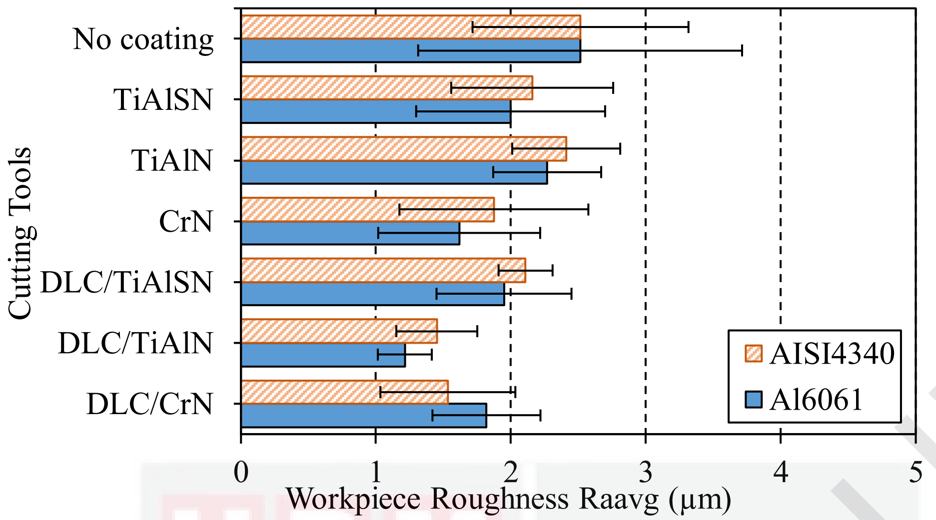

Figure 4.4: Measured workpiece roughness after the orthogonal cutting experiment using both single- and double-layered hard coatings

The use of DLC/TiAlN coatings has been proven to produce the best surface finish in workpieces when processing materials such as mild aluminum and brittle steel. This is same report by Sulaiman et al., (2019), which investigated the effect of this coating on reducing friction and wear during sheet-metal forming and reported significant improvements in surface quality across various scenarios. The coating is known for its strong adhesion and its effectiveness in minimizing wear, as indicated by the low surface roughness measurement of the workpiece. This evidence shows a smooth finish and a strong bond between the DLC, TiAlN and the substrate. Further research from (Ajay et al., 2024) on dual-layer DLC coatings, found that the surface roughness can be reduced to around 0.1 µm. This improvement is credited to the upper DLC layer, which smooths the surface of the workpiece, supporting the findings from (Kapsiz et al., 2023).

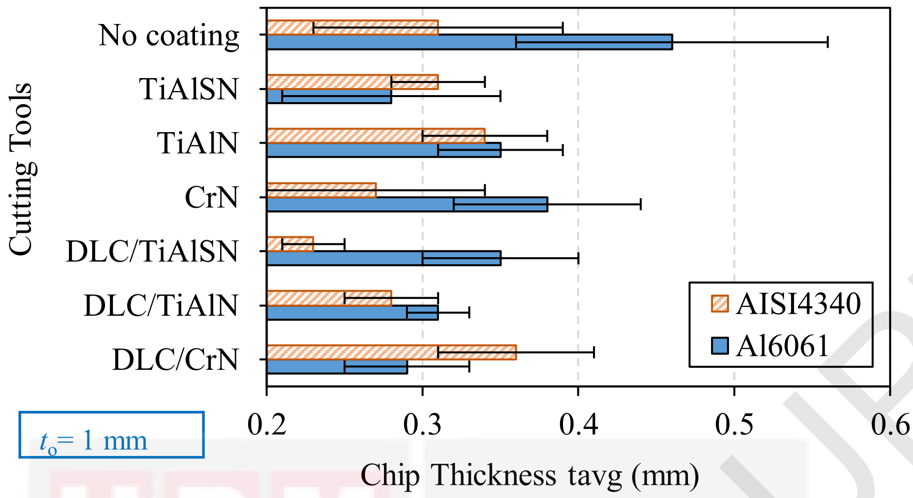

Figure 4.5: Measured chip thickness *t* after the orthogonal cutting experiment using both single- and double-layered hard coatings

AISI4340 alloy steel and Al6061 aluminum alloy were the two different workpiece materials for which the average chip thickness produced during the turning process was examined. Various cutting tools and coatings were used to achieve this. Figure 4.5 shows the measurements for both Al6061 and AISI4340 materials, illustrating the comparison results. Al6061 had the thickest uncoated chip when both materials were machined. In particular, the average chip thickness for AISI4340 was 0.31 mm, but the average for Al6061 was marginally higher at 0.46 mm. When compared to uncoated tools, TiAlSN coated tools yielded chips that were noticeably thinner when a single coating was applied. The average chip thickness was 0.31 mm for AISI4340 and 0.28 mm for Al6061. The typical chip thicknesses produced by TiAlN coatings were 0.34 mm for AISI4340 and 0.35 mm for Al6061. Conversely, for single-coated AISI4340, CrN coatings showed the lowest chip thickness at 0.27 mm, and for Al6061, it was the greatest at roughly 0.38 mm. DLC/TiAlSN coatings, which have DLC as the top layer, reduced chip thickness more significantly than

AISI4340, which has the thickest double coating at 0.23 mm, and Al6061, which has the thickest at 0.35 mm. Chip thicknesses of 0.28 mm for AISI4340 and 0.31 mm for Al6061 were achieved via DLC/TiAlN coatings. Lastly, double-coated AISI4340 produced the largest average chip thickness with DLC/CrN coatings, measuring 0.36 mm, whilst Al6061 maintained an average of roughly 0.29 mm. These results demonstrate how different coatings affect chip thickness during machining operations.

The effect of workpiece properties on chip formation is evident in the differences observed between AISI4340 and Al6061. AISI4340 with a high-strength alloy steel, exhibits greater resistance to plastic deformation due to its higher hardness (Silva et al., 2020). As a result, it produces thinner chips because the material is less prone to extensive flow under cutting forces. In contrast, Al6061 with a softer and more ductile aluminum alloy, allows greater material flow, leading to thicker chip formation(Shailesh & Rao, 2024). This difference highlights the influence of material properties on chip morphology, which is a key factor in machining performance. In addition, the role of coatings in machining further influences chip formation. Coated tools typically reduce friction at the tool-chip interface due to their low coefficient of friction and high hardness. This reduction in friction minimizes material adhesion, thereby preventing the formation of built-up edges (BUE) (Chowdhury et al., 2021). As a result, chip thickness tends to decrease due to smoother chip detachment and reduced material resistance. On the other hand, with a higher coefficient of friction experience greater wear and adhesion, leading to increased material deformation. This often results in thicker chips due to excessive shear stress and energy dissipation in the cutting zone (Öpöz & Chen, 2016).

4.2.3 Wear analysis of coated tools after machining

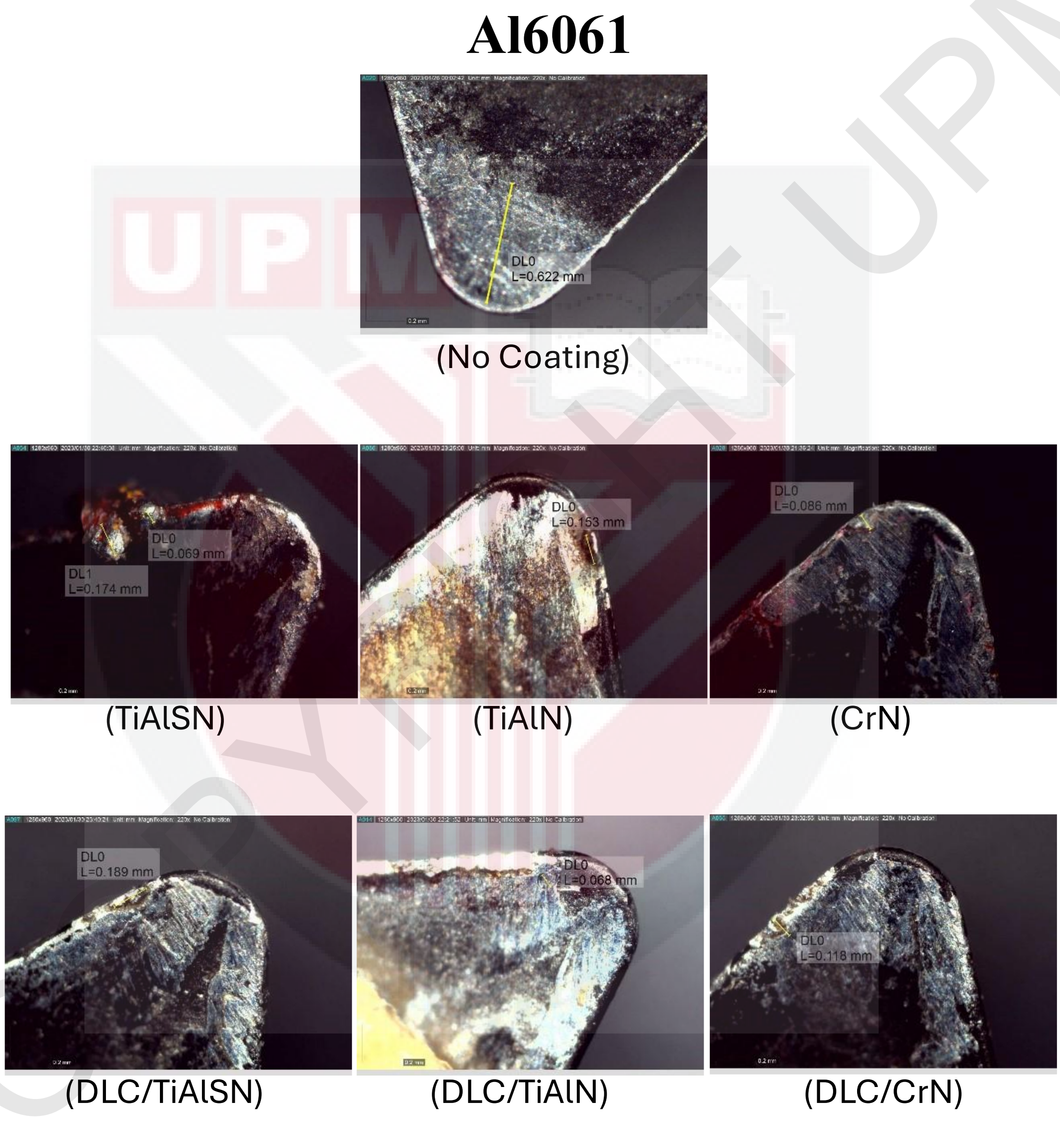

(a)

AISI4340

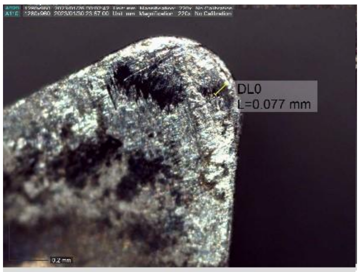

(No Coating)

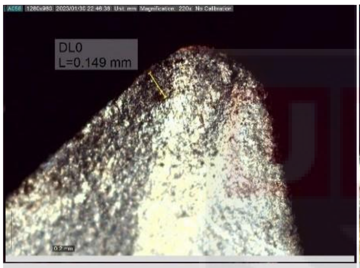

(TiAlSN)

(TiAlN)

(CrN)

(DLC/TiAlSN)

(DLC/TiAlN)

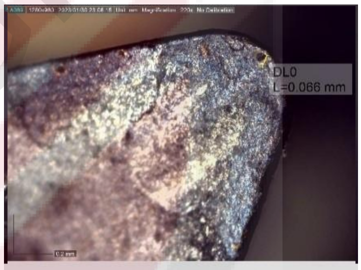

(DLC/CrN)

(b)

Al6061

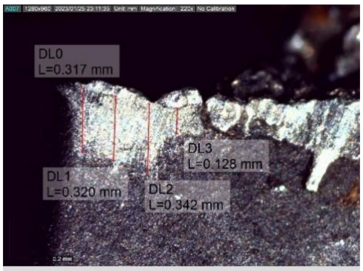

(No Coating)

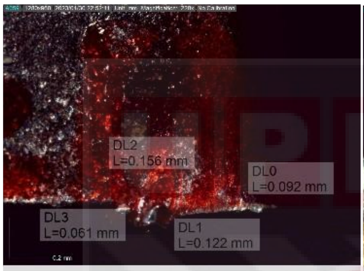

(TiAlSN)

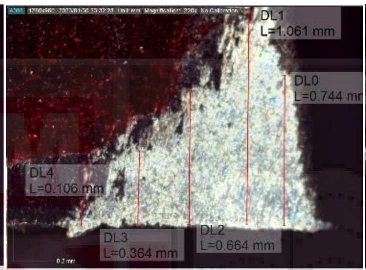

(TiAlN)

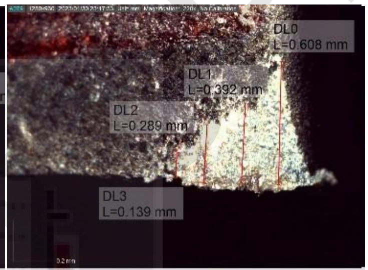

(CrN)

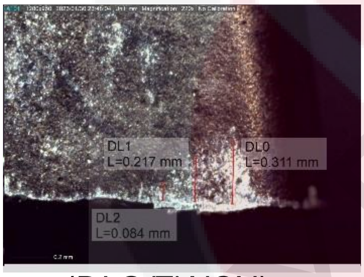

(DLC/TiAlSN)

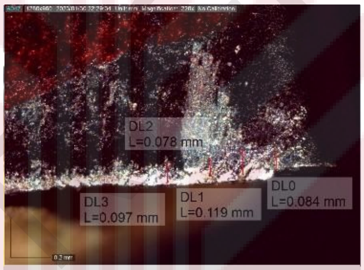

(DLC/TiAlN)

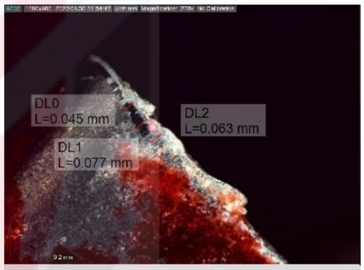

(DLC/CrN)

(c)

AISI4340

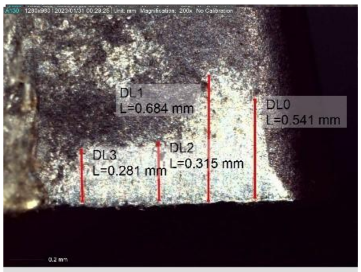

(No Coating)

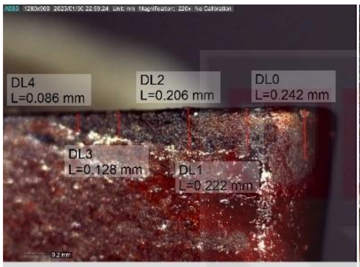

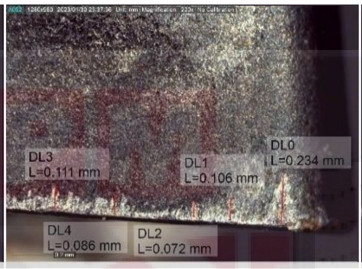

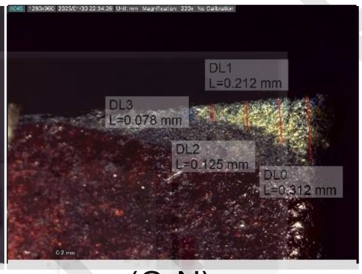

(TiAlSN) (TiAlN) (CrN)

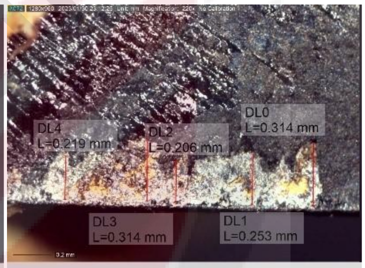

(DLC/TiAlSN) (DLC/TiAlN) (DLC/CrN)

(d)

Figure 4.6: Comparative Analysis of (a,b) Flank Wear; (c,d) Crater Wear on Al6061 and AISI4340 Workpieces Using Various Coated Cutting Tools, as Observed Under a Microscope

Figure 4.6 displays microscopic images of flank wear and craters on each cutting tool, while Figure 4.8 provides a summary of these observations. According to ISO 3685:1993, detailed in Figure 4.7, measurements average of flank wear (*VB_{avg}*) and average of crater wear (*KB_{avg}*) were carried out to classify the type of tool wear encountered after machining (Cappellini & Abeni, 2022).

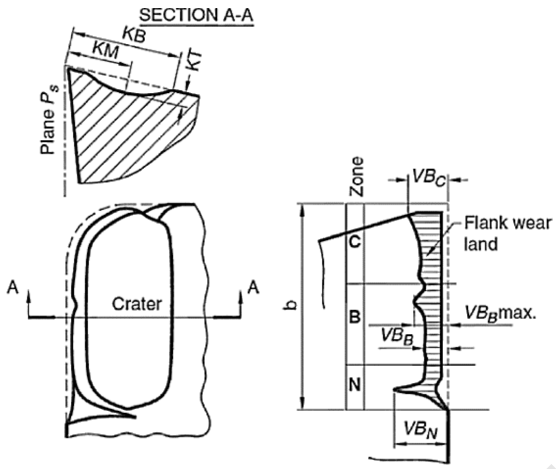

Figure 4.7: Tool wear indicators according to ISO 3685:1993

The observation of reduced flank wear indicates that the cutting tool undergoes minimal degradation. It has been observed that the use of dual-layer DLC/TiAlN coating is most effective in reducing the wear of both ribs and craters, as evidenced in workpieces made of Al60631 and AISI4340. DLC is identified as a wear-resistant coating category that increases the longevity and efficiency of cutting tools, as supported by reference L. Wang et al., (2022). Titanium Aluminum Nitride (TiAlN) is a widely used coating for cutting tools, known for its hardness and ability to work under high temperatures. Ternary metal nitrides have shown better mechanical properties and greater corrosion resistance (Huang et al., 2022). When combined with DLC in a duplex coating, there is a significant increase in wear resistance for cutting tools used in machining AISI 4340 steel and Al6061 aluminum. This dual-layer coating significantly improves resistance to crack propagation compared to a single-layer coating. The increased durability is likely due to multiple layers, with additional layers further strengthening the properties of the coating. The dual layer complex structure acts as an effective barrier against crack progression, thus increasing the material durability and overall performance (Sousa et al., 2021). The DLC coating with TiAlN, together with the composite layer, has the potential to significantly increase the resistance of the substrate surface to wear and change the wear regime to avoid the occurrence of the mixed regime (Xiao et al., 2022).

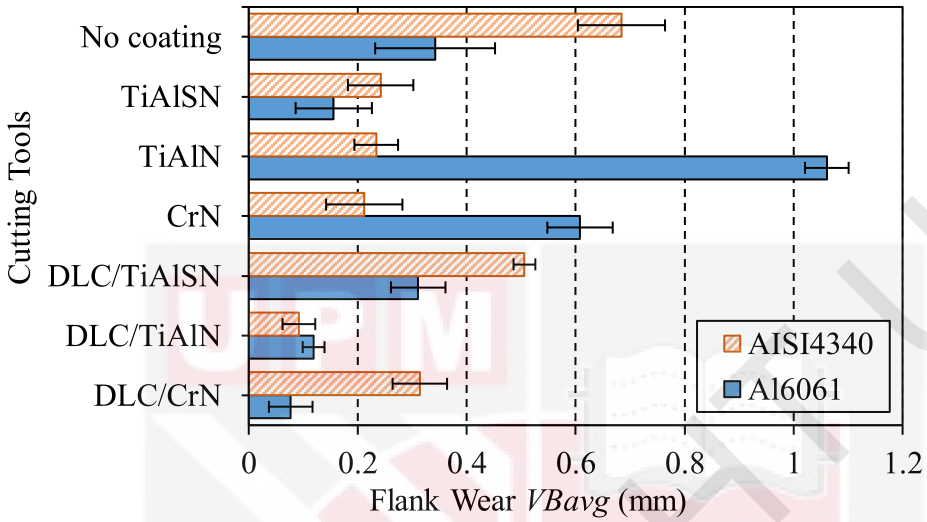

c

(a)

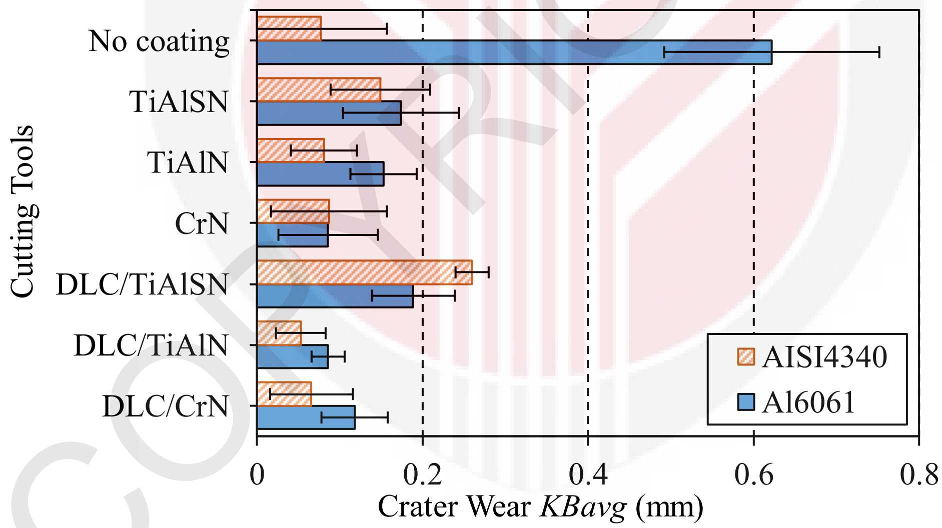

(b)

Figure 4.8: Measured a) flank wear VB_{avg} and b) crater wear KB_{avg} of both single- and double-layered coated tools after the orthogonal cutting experiment.

The high flank wear observed with TiAlN coatings when machining Al6061 can be attributed to the high affinity of titanium for aluminum at the high temperatures generated during the cutting process, which leads to increased adhesion, material removal, and abrasive wear. In addition, the higher hardness and brittleness of TiAlN compared to other coatings can cause it to fracture and wear more quickly under certain cutting conditions (Moreno et al., 2023). The uncoated sample exhibited the highest crater wear because it had no protective coating. Coatings are designed to reduce friction and wear by providing a barrier between the tool and the workpiece. Without this barrier, the tool material is directly exposed to the high temperatures and stresses of the cutting zone, leading to increased dissolution, diffusion, and ultimately, crater wear.

A Scanning Electron Microscope (SEM) was used to analyze the wear mechanism of cutting tools under various layers. The SEM-EDS analysis, illustrated in Figure 4.9 and Figure 4.10, examines the wear on tools used to machine Al6061 and AISI4340 materials. Figure 4.9 presents the SEM and EDS elemental analyses of the Al6061 workpiece, which exhibits ductile properties, followed by Figure 4.10, which depicts the analysis of the AISI 4340 workpiece, which is known for its brittle properties. Both EDS elemental reveal a high concentration of platinum (Pt), as the cutting tool is coated with platinum to allow analysis under high magnification scopes. This platinum coating is applied only after the turning process to help distinguish the chemical composition of the tool wear. The friction between the tool and the workpiece generates heat during the turning process. Al6061, as a ductile material, experiences a temperature increase during cutting, causing the cutting tool to undergo plastic deformation and forming adhesive wear on the tool (Parida et al., 2020). The greater the ductility of the workpiece, the stronger the adhesive effect on the cutting tool. To confirm the adhesion effect of the Al6061 alloy workpiece on the tool, EDS elemental analysis was carried out on the suspected adhesion zone, revealing a high aluminum content. Due to the combination of heat generation and the ductility of aluminum, the coated cutting tool exhibits a very high adhesive effect. Like brittle materials that generate heat, adhesion to the tool occurs due to material deformation. This phenomenon is evident in EDS analysis, which reveals the presence of material transfer, indicating adhesion at the tool-workpiece interface. The cutting tools with two-layer DLC coating experienced a reduced impact on adhesive wear. This can be attributed to DLC serving as the outer layer in a multi-layer coating configuration. Moreover, the robust bonding of elements in the DLC layer reveals the superior surface characteristics of the coated tool, improving its tribological performance against wear. This improvement is due to the combination of graphite and diamond properties in the DLC coating.

Uncoated

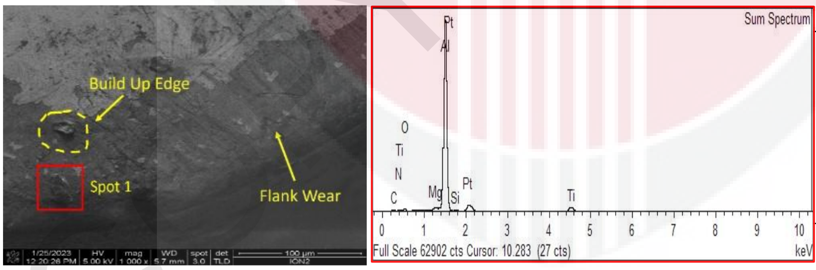

Element	Weight%
C	5.75
N	4.37
O	4.30
Mg	0.64
Al	65.80
Si	0.50
Ti	6.87
Pt	11.77

TiAlSN

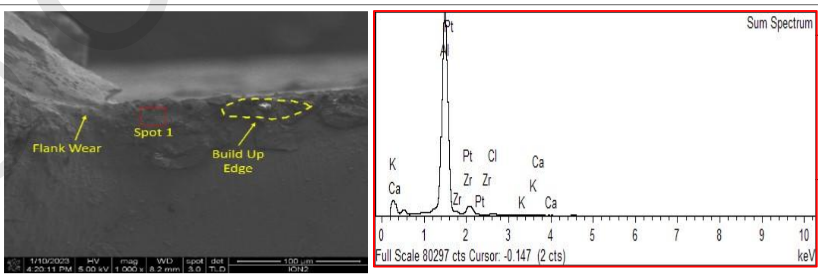

Element	Weight%
Al	81.34
Cl	1.27
K	0.76
Ca	0.53
Zr	0.00
Pt	16.10

TiAlN

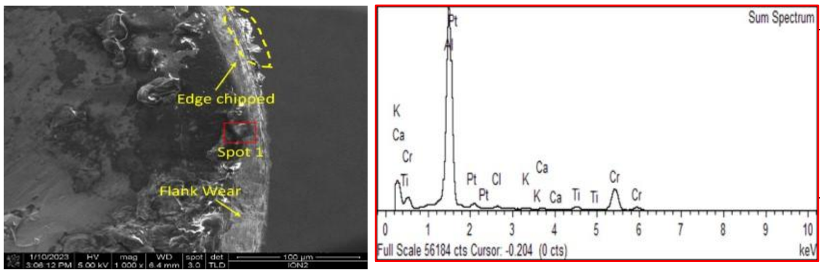

Element	Weight%
Al	59.77
Cl	1.34
K	0.90
Ca	0.48
Ti	2.57
Cr	29.82
Pt	5.13

CrN

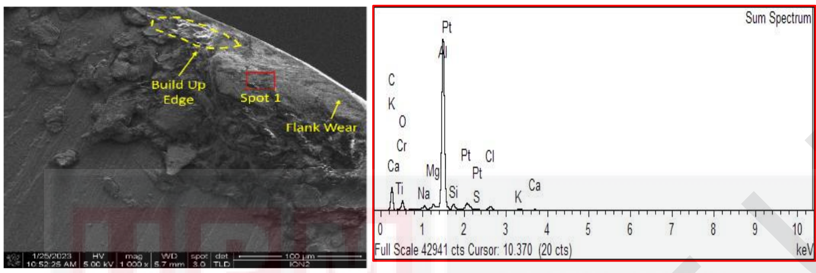

Element	Weight%
C	31.47
O	10.73
Na	0.86
Mg	0.96
Al	41.87
Si	1.99
S	0.27
Cl	1.69
K	0.60
Ca	0.41
Ti	0.24
Cr	0.67
Pt	8.24

DLC/TiAlSN

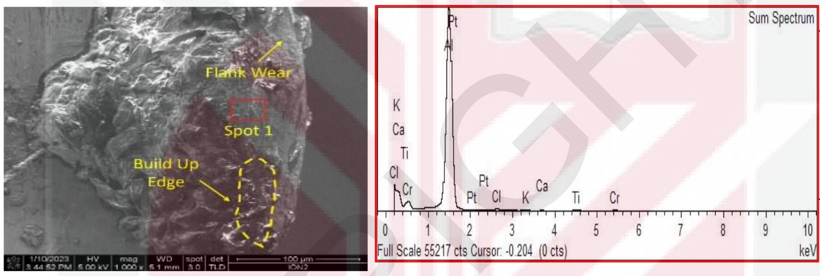

Element	Weight%
Al	92.06
Cl	1.48
K	0.56
Ca	0.43
Ti	2.07
Cr	1.94
Pt	1.47

DLC/TiAlN

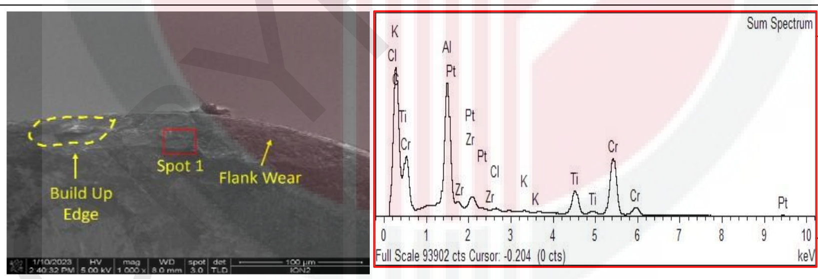

Element	Weight%
C	66.90
Al	8.09
Cl	0.26
K	0.19
Ti	4.77
Cr	17.71
Zr	0.00
Pt	2.10

DLC/CrN

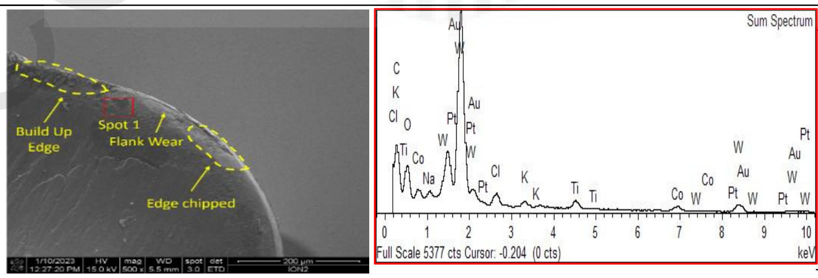

Element	Weight%
C	39.49
O	14.05
Na	0.65
Cl	1.62
K	0.79
Ti	1.67
Co	2.48
W	36.67
Pt	1.87
Au	0.70

Figure 4.9: SEM-EDS analysis on both single- and double-layered coated tools after the orthogonal cutting of aluminium Al6061

Uncoated

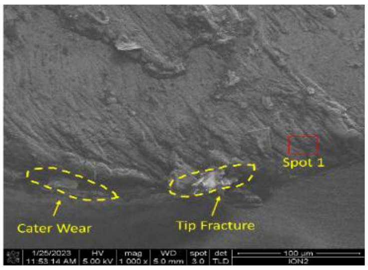

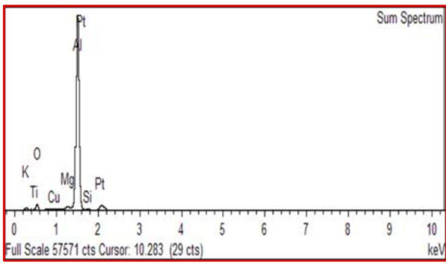

Element	Weight%
O	8.51
Mg	0.78
Al	76.61
Si	0.90
Cl	0.58
K	0.28
Ti	1.29
Cu	0.00
Pt	11.05

TiAlSN

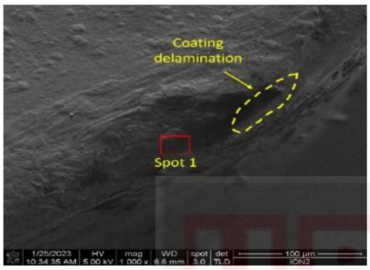

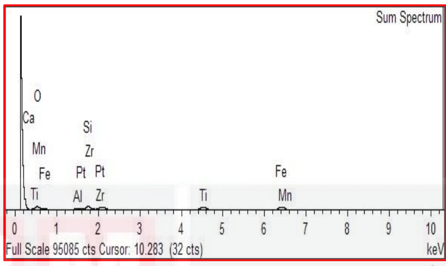

Element	Weight%
O	29.63
Al	1.93
Si	5.71
Ca	1.22
Ti	14.06
Mn	3.40
Fe	29.39
Zr	0.00
Pt	14.66

TiAlN

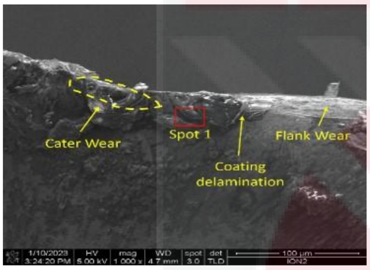

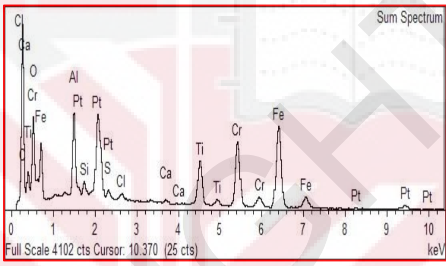

Element	Weight%
C	27.46
O	10.60
Al	3.39
Si	0.60
S	0.31
Cl	0.35
Ca	0.28
Ti	5.89
Cr	12.61
Fe	26.40
Pt	12.11

CrN

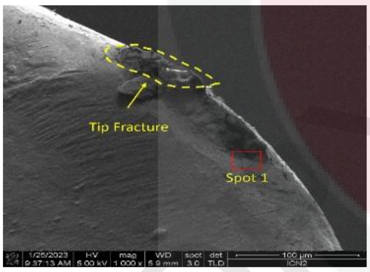

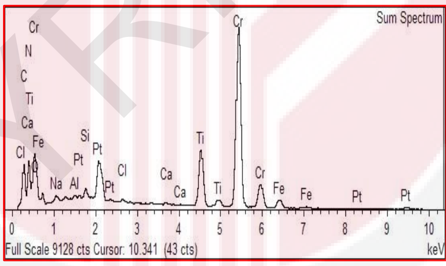

Element	Weight%
C	8.19
N	9.13
O	5.18
Na	0.51
Al	0.22
Si	0.57
Cl	0.29
Ca	0.22
Ti	10.21
Cr	53.29
Fe	3.74
Pt	8.45

DLC/TiAlSN

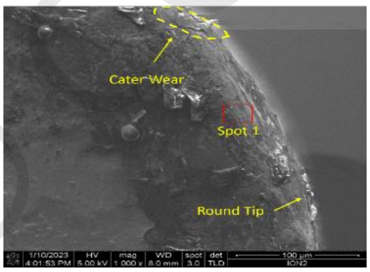

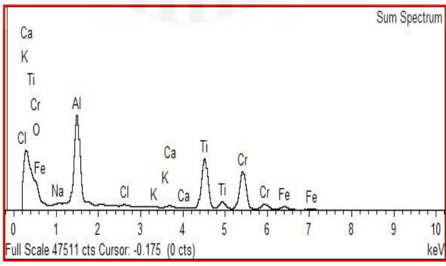

Element	Weight%
O	11.56
Na	0.50
Al	20.35
Cl	0.50
K	0.38
Ca	0.71
Ti	28.83
Cr	33.22
Fe	3.96

DLC/TiAlN

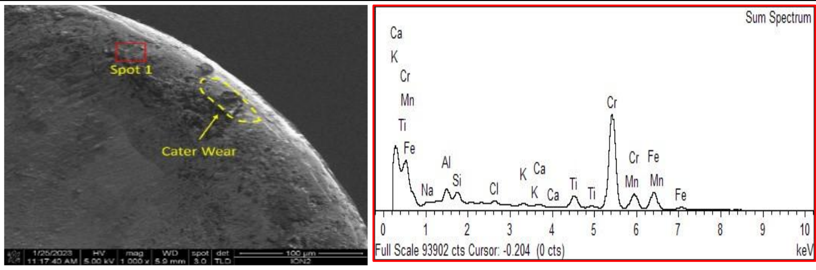

Element	Weight%
Na	0.63
Al	3.13
Si	2.31
Cl	0.85
K	0.65
Ca	0.62
Ti	5.29
Cr	64.95
Mn	2.86
Fe	18.70

DLC/CrN

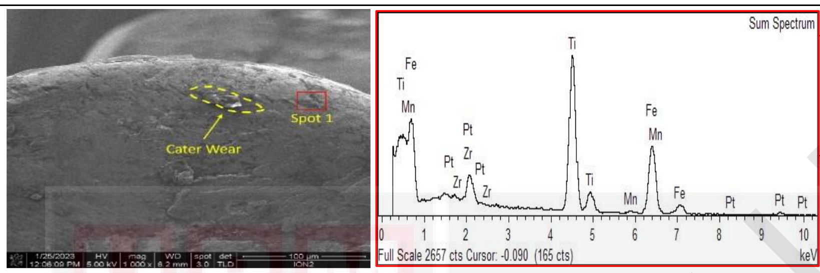

Element	Weight%
Ti	45.40
Mn	1.18
Fe	43.69
Zr	0.00
Pt	9.73

Figure 4.10: SEM-EDS analysis on both single- and double-layered coated tools after the orthogonal cutting of AISI4340 alloy steel

The SEM-EDS analysis results, depicted in Figure 4.9 and Figure 4.10, indicate that the dual-layer DLC/TiAlN coating significantly enhances the surface quality of both soft and brittle workpieces. Comparative SEM-EDs analyses, presented in Figure 4.11 and Figure 4.12, reveal the performance of DLC/TiAlN coated tools versus uncoated ones during the machining of Al6061 and AISI4340 materials. The DLC/TiAlN coated tool displayed a minor build-up edge (BUE), whereas the uncoated tool showed considerable adhesive wear and BUE, particularly after processing a soft workpiece. This difference is ascribed to the workpiece's inherent softness and the low heat production during cutting. In the context of machining brittle materials, the DLC/TiAlN coating exhibited minimal abrasive wear, which contributes to the overall degradation of cutting tools due to both abrasive and adhesive wear, as supported by reference Freitas et al., (2024). In contrast, uncoated tools were prone to chip breakage at the tool's edge.

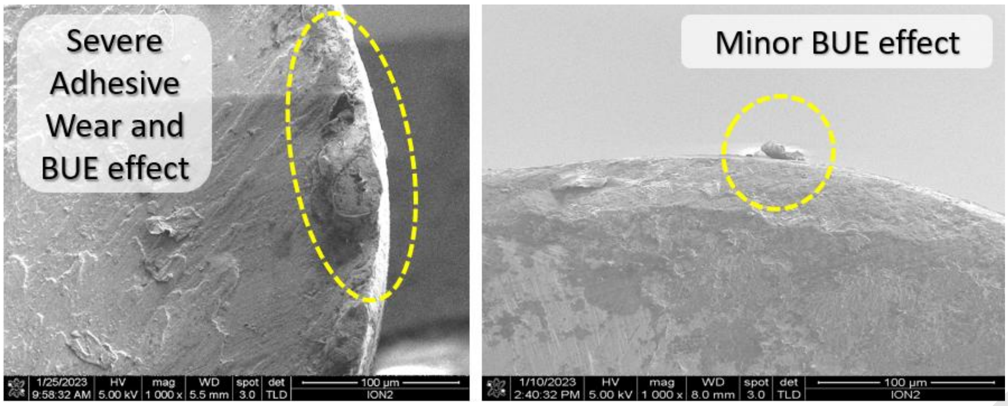

Uncoated tool DLC/TiAlN coated tool

Figure 4.11: Tool wear on uncoated (left) and double-layered DLC/TiAlN (right) coated tools after the orthogonal cutting of aluminium Al6061 using SEM-EDS analysis.

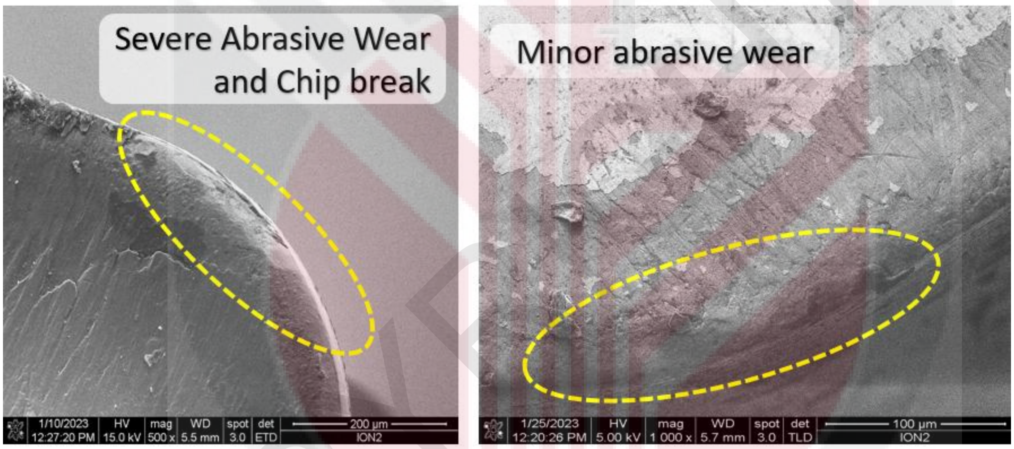

Uncoated tool DLC/TiAlN coated tool

Figure 4.12: Tool wear on uncoated (left) and double-layer DLC/TiAlN (right) coated tools after the orthogonal cutting of AISI4340 alloy steel using SEM-EDS analysis.

4.2.4 Raman analysis of top-layered DLC coatings

Raman analysis is important in characterizing the structural properties of DLC-based coatings, including DLC, DLC/TiAlN, DLC/TiAlSN, and DLC/CrN. This technique provides insight into the bonding structure and disorder in the carbon network by analyzing the D and G bands in the Raman spectrum. The

D band, located around 1350 cm^{-1}, represents the breathing mode of the sp^2-bonded carbon ring and is associated with structural defects or disorders in the DLC coating. The G band, at around 1580 cm^{-1}, corresponds to the stretching vibration of sp^2-bonded carbon atoms and indicates the presence of a graphitic or ordered structure. Figure 4.13 displays the double coating tools Raman spectra together with their peak characteristics. The G band, which is the vibrational mode of the sp2-bonded carbon atoms in the DLC film, is represented by a prominent peak in the DLC at about 1580 cm-1. The titanium aluminum nitride-integrated DLC/TiAlN variant displayed a wider peak about 1500 cm-1, which is similarly attributed to the G band. This suggests that the addition of titanium and aluminum may dilute the sp2 bonding, causing the peak to expand (Rao et al., 2020). The D band, which denotes a vibrational mode connected to defects or disorder in the carbon structure, was seen in peaks about 1350 cm-1 in DLC/CrN and DLC/TiAlSN, which include chromium nitride and titanium aluminum silicon nitride, respectively (Rao et al., 2020). As indicated by a more prominent D band peak, the addition of chromium and titanium aluminum silicon nitride is probably going to cause additional defects. The DLC coating had the maximum degree of sp2 bonding, according to Raman spectroscopy research, whereas the DLC/CrN and DLC/TiAlSN coatings showed a higher frequency of faults. The intermediate structure of the DLC/TiAlN coating represented a balance between the more defect-rich DLC/CrN and DLC/TiAlSN coatings and the pure DLC. These results were consistent with the expected properties of the coatings: DLC is known for its durability and hardness, whilst DLC/CrN and DLC/TiAlSN are known for their improved resistance to oxidation.

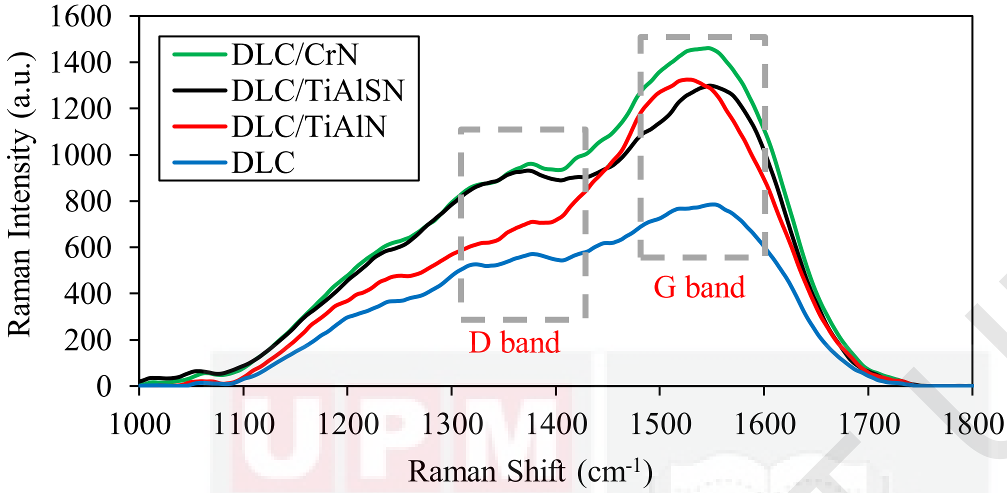

Figure 4.13: Raman analysis on DLC coating as top-layered to CrN-, TiAlSiN-, TiAlN coatings

4.2.5 Microstructural analysis of DLC/TiAlN coating

Figure 4.14 illustrates a cross-sectional view of a DLC/TiAlN coating, showing the DLC film as the top layer and the TiAlN film as the base layer, both applied to a cutting tool steel substrate. Morphological analysis of each layer revealed that the DLC coating measured 2.4 μm in thickness, while the TiAlN coating was 2 μm thick. SEM images prove a strong bond between the TiAlN film, the DLC layer, and the cutting tool steel substrate. The Cr interlayer, as evidenced by the Energy Dispersive Spectroscopy (EDS) findings in Figure 4.14, plays an important role in reducing the stress gradient at the interface between DLC and TiAlN (K. S. Kim et al., 2016). The integration of Cr and Ti, inferred from the EDS data, contributes to the increase in adhesion strength, which leads to a decrease in interfacial energy, the formation of strong chemical bonds, and a reduction of the stress gradient (Xiao et al., 2022, 2024). Moreover, the initial DLC layer is characterized by a clustered and rough texture, in stark contrast to the smooth and smooth appearance of the TiAlN layer. The detection of a large columnar grain structure in the CrCN/CrN interlayer, placed under the DLC layer, can explain the better adhesion properties noted in the DLC/TiAlN coating, as discussed in references (Sulaiman, 2017; Sulaiman et al., 2017b). The TiAlN coating exhibits a dense microstructure, evidenced by a consistent columnar shape with few pores and inclusions, as detailed in Figure 4.15 (bottom right). This structure, coupled with the high aluminum content displayed in Figure 4.15 (middle), plays an important role in increasing the hardness of the DLC/TiAlN coating. The TiAlN interlayer is susceptible to shear stress, which is beneficial in strengthening the bond strength between the DLC film and the cutting tool substrate. At the same time, the presence of the Cr interlayer serves to strengthen the adhesion by reducing the stress difference between the TiAlN and DLC layers. Therefore, the combined action of these layers is likely to reduce the surface tensile stress that occurs due to sliding, effectively minimizing wear and extending tool life.

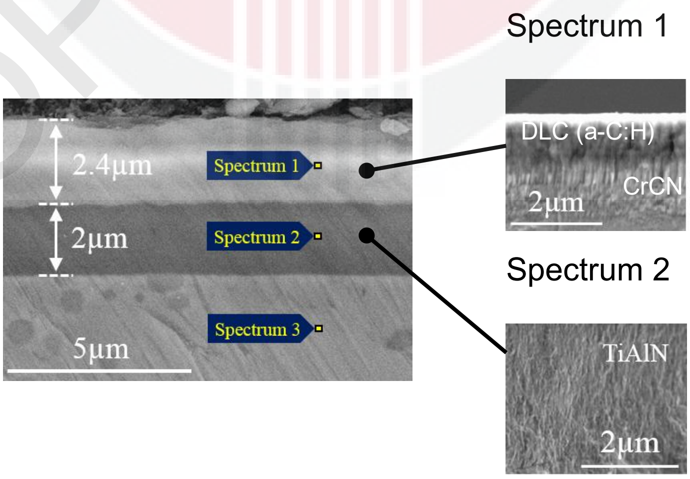

Figure 4.14: A cross-sectional view of the tool surface with deposited DLC/TiAlN coating (Note: Spectrum 1 – DLC, Spectrum 2 – TiAlN, and Spectrum 3 – Cutting tool surface).

DLC coating

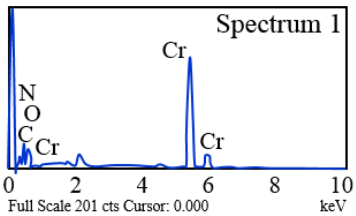

Elements	Weight%	Atomic%
Cr	73.54	41.92
N	13.88	29.38
C	8.77	21.63
O	3.81	7.07

TiAlN coating

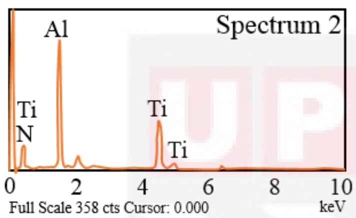

Element	Weight%	Atomic%
Ti	45.01	24.80
Al	31.33	30.64
N	23.65	44.56

Tool steel, Vanadis 4

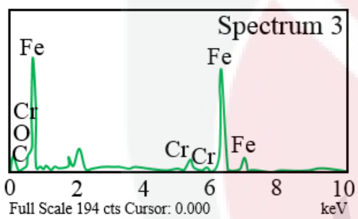

Element	Weight%	Atomic%
Fe	87.82	72.08
Cr	5.16	4.55
O	3.57	10.22
C	3.45	13.15

Figure 4.15 : Analysis of the elemental composition in DLC/TiAlN coating via SEM-EDX.

4.3 Evaluation of water-based lubricant

The objective 2 involves performing tribological tests using the block-on-ring method with various water-based lubricants (WBLs). A newly formulated WBL, enriched with MXene and an ionic liquid, has been proposed. To further enhance its properties, surfactants like carboxymethyl cellulose and xanthan gum are incorporated.

4.3.1 Influence of additive in water-based lubricant

The properties of WBLs are evaluated by measuring sedimentation and conducting kinetic viscosity analysis. Adding specific additives can significantly alter the chemical and physical characteristics of these lubricants. This affects their performance and suitability for various applications.

The stability of the WBLs dispersion was monitored for four days using the sedimentation test method. The photo capture of sedimentation of WBLs was captured at 24-hour intervals. Sedimentation test results, as depicted in Figure 4.16, include samples: (a) CMC_IL, (b) XG_IL (c) CMC_Mxene, (d) XG_Mxene (e) CMC_Mxene/IL, and (f) XG_Mxene/IL. WBL containing Ionic Liquid (IL) additives maintained consistent dispersion from day one to day four for both surfactants, CMC and XG. XG_IL appeared slightly cloudy, while CMC_IL remained clear from the first day to the fourth day. The XG surfactant exhibited a longer dispersion period for the Mxene additive than the CMC, with both lubricants appearing black. On the second day, CMC_Mxene showed some cleaning on the upper surface of the water lubricant, with Mxene particles settling to the bottom on the third day and remaining there until the fourth day. In contrast, XG_Mxene maintained dispersion until the second day, then began to show a cloudy black appearance on the top surface of the lubricant on the third and fourth day. The combination of Mxene and IL with CMC surfactant showed a pattern similar to CMC_Mxene. XG_Mxene/IL followed a similar pattern to XG_Mxene, with the onset of turbidity occurring on the third day, but to a greater extent than CMC_Mxene, which continued into the fourth day. The gel-forming ability of xanthan gum helps prevent phase separation, ensuring long-term stability in lubricants (Miryuk, 2024).

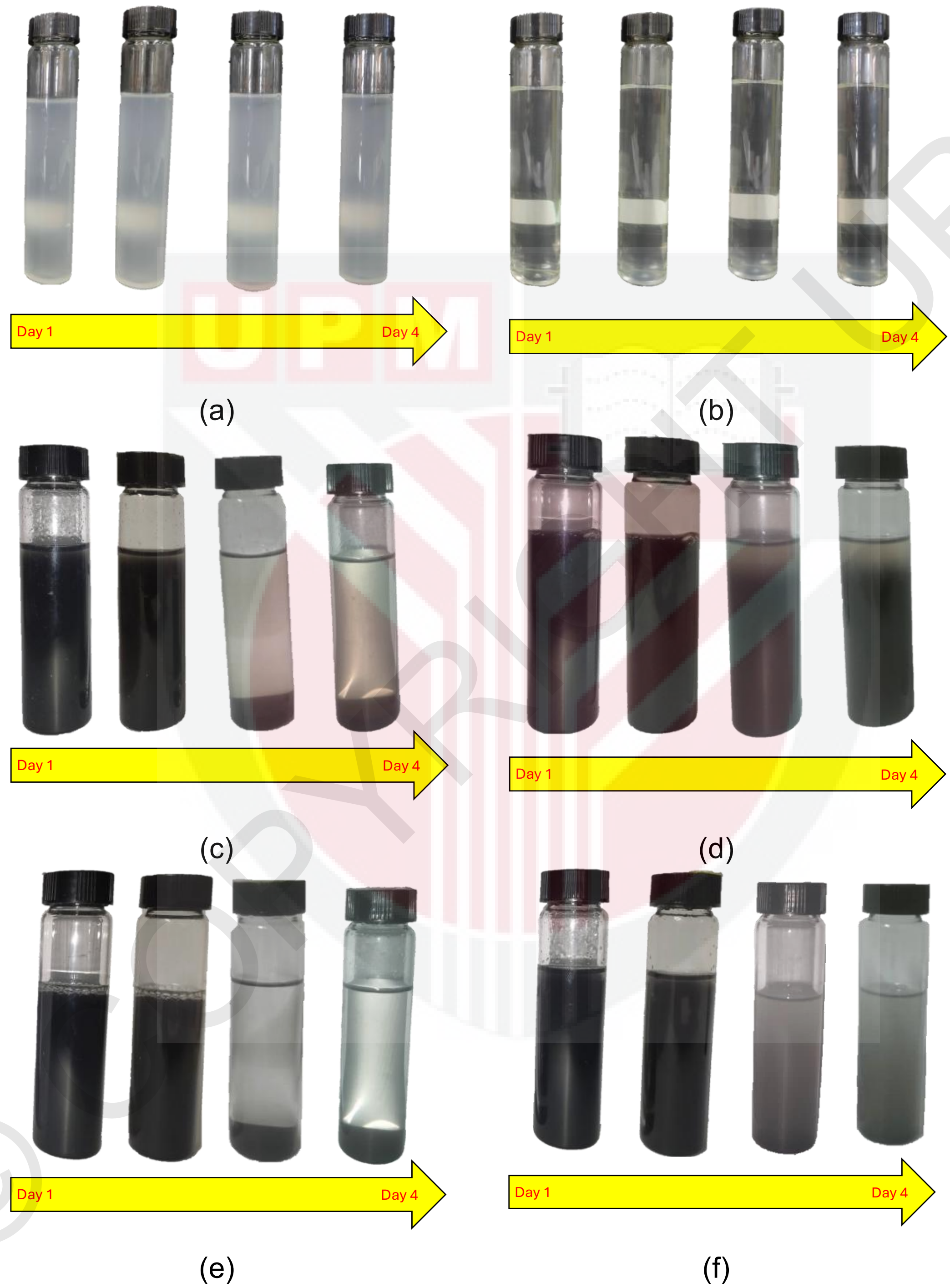

Figure 4.16: Sedimentation test of wate-based lubricants; (a) CMC_IL, (b) XG_IL (c) CMC_Mxene, (d) XG_Mxene (e) CMC_Mxene/IL, and (f) XG_Mxene/IL.

Figure 4.17 illustrates the dynamic viscosity of a WBLs formulated at 30 °C. The viscosity of these WBLs exceeds that of DI, mainly due to the incorporation of surfactants and nanoparticles. According to Y. Wang et al., (2017), the increased viscosity observed in nanofluids can be traced back to molecular interactions. This interaction results from the erratic movement of both nanoparticles and water molecules. The XG_IL exhibits the greatest viscosity, measuring 139.14 mPa.s, which is the highest recorded among WBLs. In contrast, the CMC_Mxene demonstrates the lowest viscosity within the same group, with a measurement of 6.29 mPa.s.

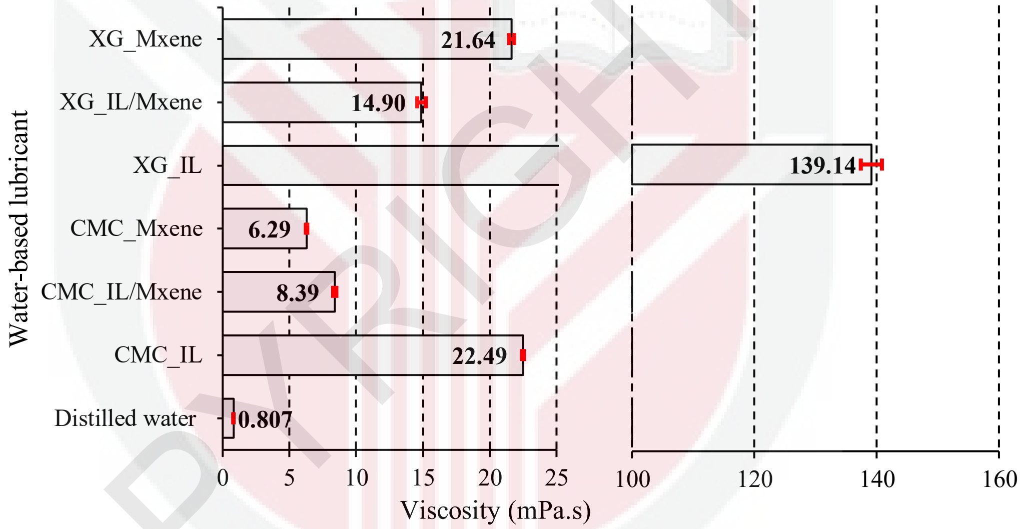

Figure 4.17: Viscosity of for the test WBLs

4.3.2 Coefficient of friction (COF)

The COF is a unitless measurement that indicates the resistance to movement between two contacting surfaces. In this research, COF will demonstrate the effectiveness of lubricants in maintaining a protective layer between block and ring during tribological evaluation. A reduced COF is better, as it helps minimize energy losses, often expressed as heat. Furthermore, a lower COF in mechanical systems generally signifies a longer equipment life. The COF values are plotted over the number of cycles and are displayed graphically, as shown in Figure 4.18.

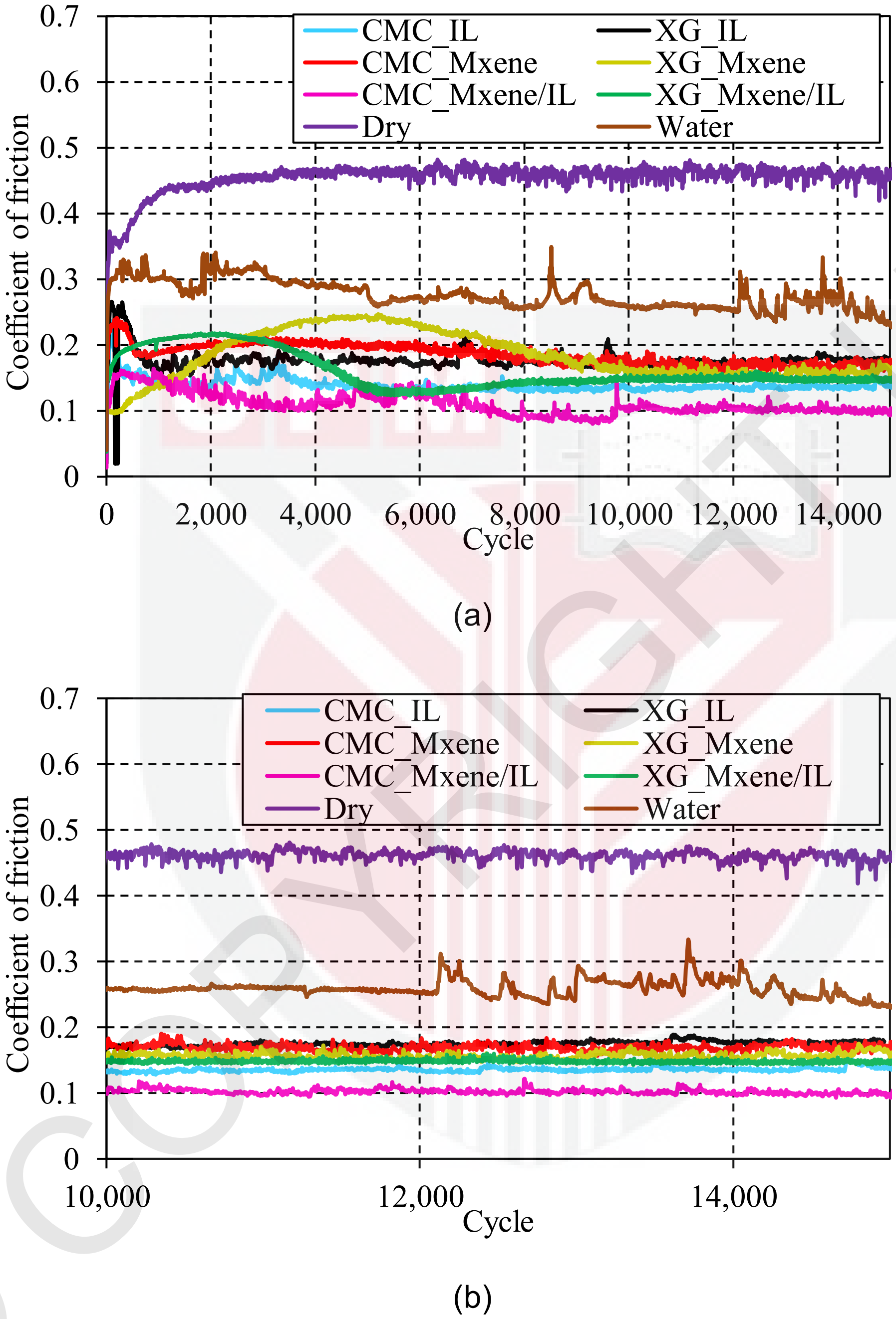

Figure 4.18: COF for all lubricants including dry condition for whole testing (a) 15000 cycle and (b) at steady state.

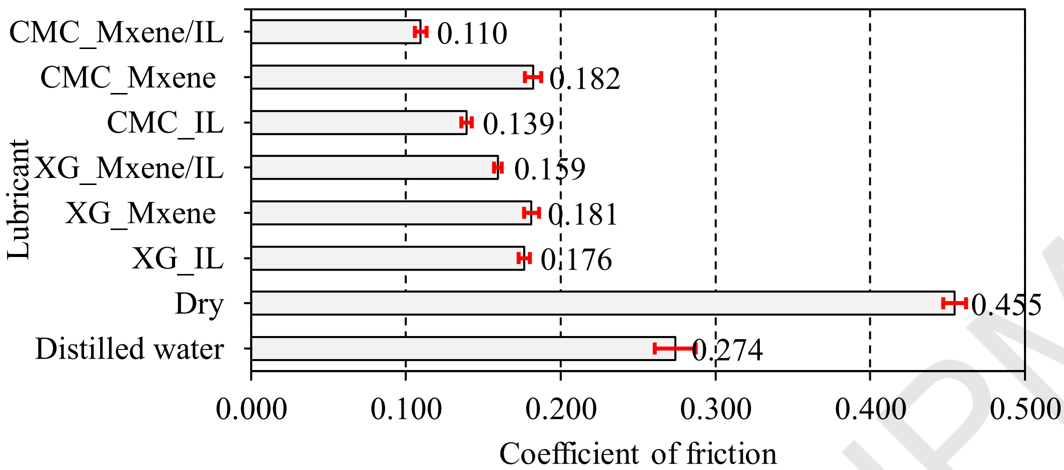

Figure 4.19: Average COF for different lubricant at 500 rpm

Based on Figure 4.19, dry condition and using distilled water showed the highest COF, followed WBLs. Generally, WBLs typically exhibit a lower COF indicating that the inclusion of nanoparticles has effectively enhanced their ability to reduce friction. This improvement in frictional performance underscores the potential of nanoparticles to optimize lubrication systems. Among all WBLs CMC_Mxene/IL have the lowest COF at 0.011 and reduce around 76 % relative to dry condition and around 60 % reduction compared to by using distilled water. The unique structure of MXene nanoflakes characterized by a layered structure that facilitates easy shear. This structure not only enhances lubrication but also forms a protective film Concurrently, ionic liquids (ILs) are noted for their exceptional thermal stability and their ability to the formation of a protective tribofilm on the metal surfaces (Grützmacher et al., 2024; R. Guo et al., 2024; Nguyen & Chung, 2020; Wijanarko et al., 2022a).

After measuring the viscosity of the lubricant, it becomes possible to calculate the minimum film thickness and the ratio film thickness and roughness, λ.

These can be determined using Equation 2.9 and Equation 2.10, respectively, and their values are tabulated in Table 4.1. Analysis of Table 4.1 reveals that λ shows a consistent relationship with lubricant viscosity. This is because viscosity is the only variable in the λ equation, with all other parameters held constant or assumed constant. For distilled water, a λ less 1 result in a minimum film thickness of 0.34 μm, which falls within the boundary lubrication regime. In the mixed lubrication regime, CMC_Mxene and CMC_IL exhibit λ values ranging from 1 to 3, with corresponding minimum film thicknesses of 1.45 μm and 1.77 μm, respectively. Other WBLs demonstrate λ values greater 3, indicating their operation in the hydrodynamic lubrication regime.

Table 4.1: Minimum film thickness and λ of lubricants

WBL	minimum film thickness (μm)	λ	Mode of lubrication
Distilled water	0.34	0.41	BL
CMC_Mxene	1.45	1.74	ML
CMC_IL	1.77	2.13	ML
XG_Mxene/IL	2.65	3.18	HL
XG_Mxene	3.44	4.13	HL
CMC_Mxene/IL	3.54	4.25	HL
XG_IL	12.66	15.20	HL

*Note: [Menezes et al., (2013)]
BL – Boundary Lubrication ($\lambda \leq 1$),
ML – Mixed Lubrication ($1 < \lambda < 3$),
HL – Hydrodynamic lubrication ($\lambda \geq 3$)

Figure 4.20 illustrates a graph plotting the average COF and minimum film thickness against the Hersey number, covering the lubrication region where viscosity is different, speed is constant at 500 rpm and normal load 42 N. This finding is supported by additional studies that have shown that an increase in viscosity leads to a thicker lubricating film. As a result, this reduces the interaction between surface asperities, thereby reducing the friction coefficient (Ahamed et al., 2020).

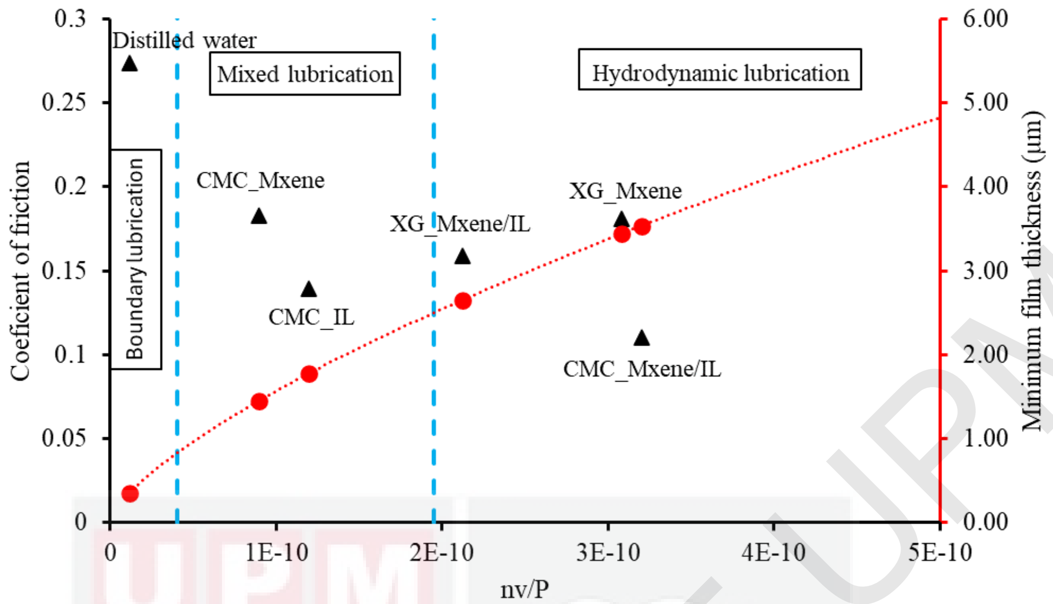

Figure 4.20: WLB in region of lubrication with COF and minimum film thickness where viscosity of lubricant is different at 500 rpm and normal load 42 N

4.3.3 Temperature

The temperature of testing over the cycles as shown in Figure 4.21. The average temperature and maximum temperature for each lubricant is plotted in Figure 4.22. The data indicates that the CMC_Mxene/IL WBL exhibits the lowest average temperature, recorded at 31.8 °C, with a maximum temperature of 34 °C. Starting from an ambient room temperature of approximately 28 °C, this represents a significant reduction in temperature. Specifically, there is a 41% decrease in the maximum temperature when compared to dry conditions after 15000 cycles, and a 32% reduction in the average temperature. This suggests that the CMC_Mxene/IL composite is highly effective in thermal management applications. Additives improve the tribological performance of WBLs by forming a durable lubricating film that prevents direct contact between friction surfaces (Zhao et al., 2019). This film not only reduces friction but also stabilizes the lubricant, effectively maintaining a lower temperature even under high load conditions (Bukvić et al., 2023).

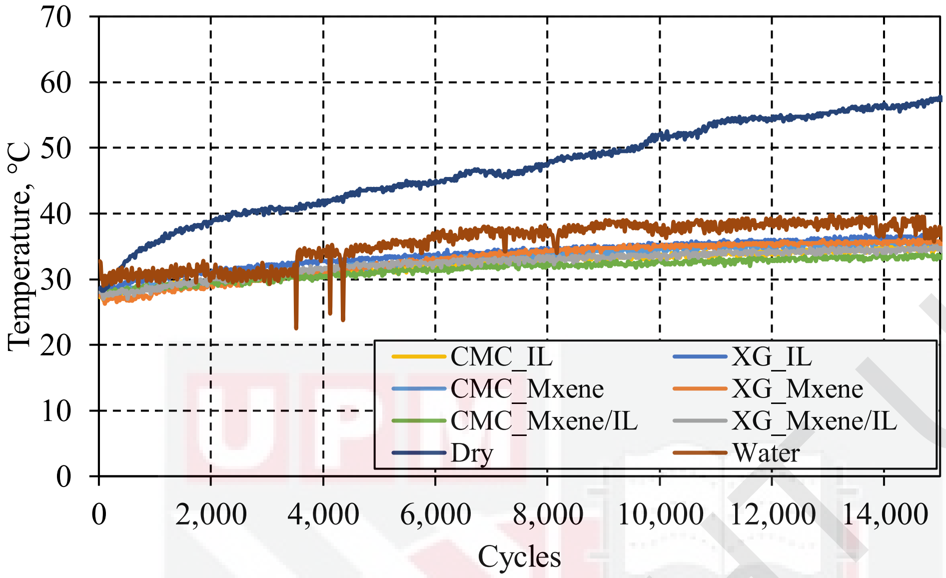

Figure 4.21: Temperature near to sliding surfaces for tribological experiment on block-on-ring test setup until 15,000 cycle.

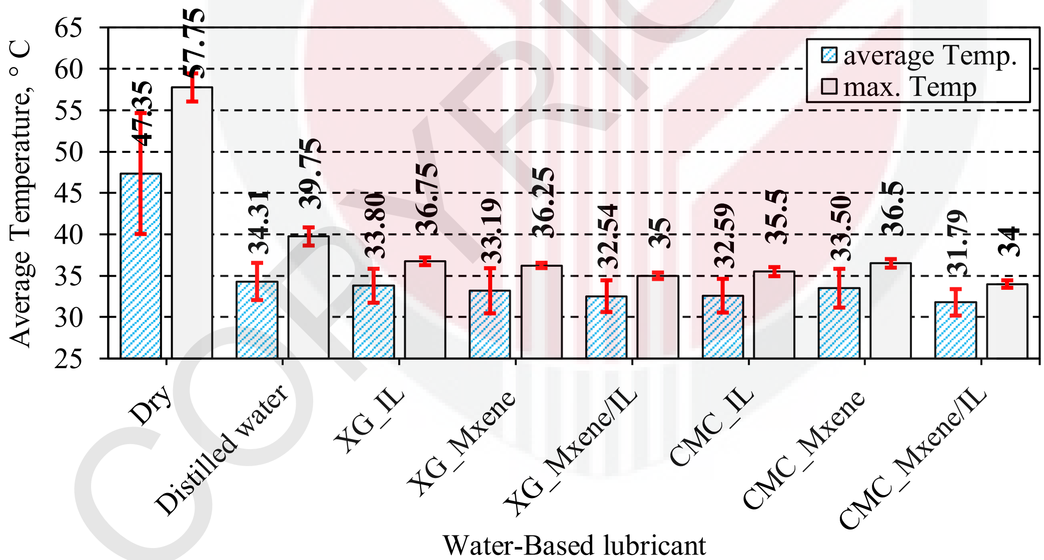

Figure 4.22: Measured average and maximum temperature near to sliding surfaces for tribological experiment on block-on-ring test setup until 15,000 cycle.

4.3.4 Wear

Figure 4.24 arranges images of block wear scars, captured with a Dino-Lite Microscope, in ascending order of wear area. This sequence visually represents the effectiveness of different lubricants, with larger wear areas correlating with increased wear rates. The wear area is determined by referring to Figure 4.23.

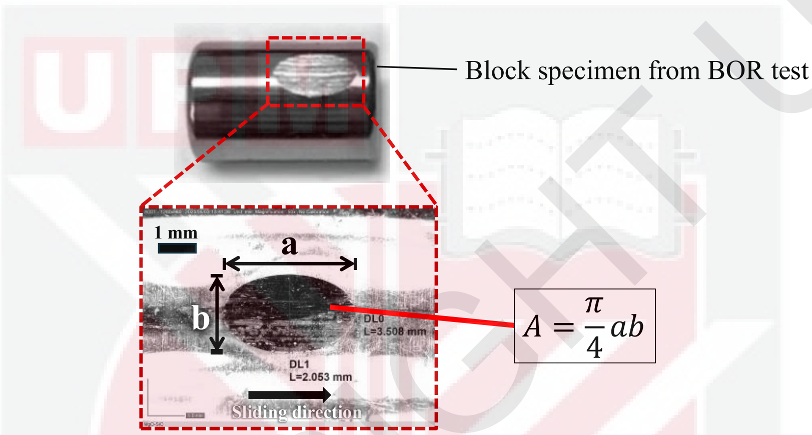

Figure 4.23: Area of Wear and the Calculation Formula

Least wear → Severe wear

Lubricants	CMC MXene/IL	XG Mxene/IL	XG_Mxene	CMC_IL	XG_IL	CMC Mxene	Distilled Water	Dry
Sliding direction	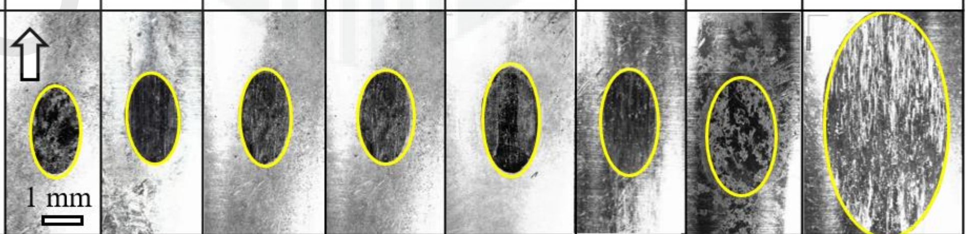							
Wear Area A (mm^2)	2.196	2.359	2.587	2.817	2.904	3.052	3.987	11.734

Figure 4.24: Wear scar of the block arranged ascendingly according to the wear area.

Based on Figure 4.24, integration of Mxene with IL has been shown to reduce wear. However, wear reduction is slightly different when CMC surfactant is used compared to XG surfactant. In particular, the CMC_Mxene/IL combination results in a wear area reduction of about 2.196 mm^2, which is an 81% decrease compared to the dry condition. In addition, this combination achieves a 45% reduction in wear compared to the use of distilled water, which has a wear area of 3.987 mm^2. During the processes of friction and wear, MXene material is deposited onto the worn surface under the influence of compressive stress, resulting in the formation of a self-laminating film, this acts as a barrier, preventing direct interaction between the contacting surfaces, thereby reducing friction (Gasni et al., 2024)

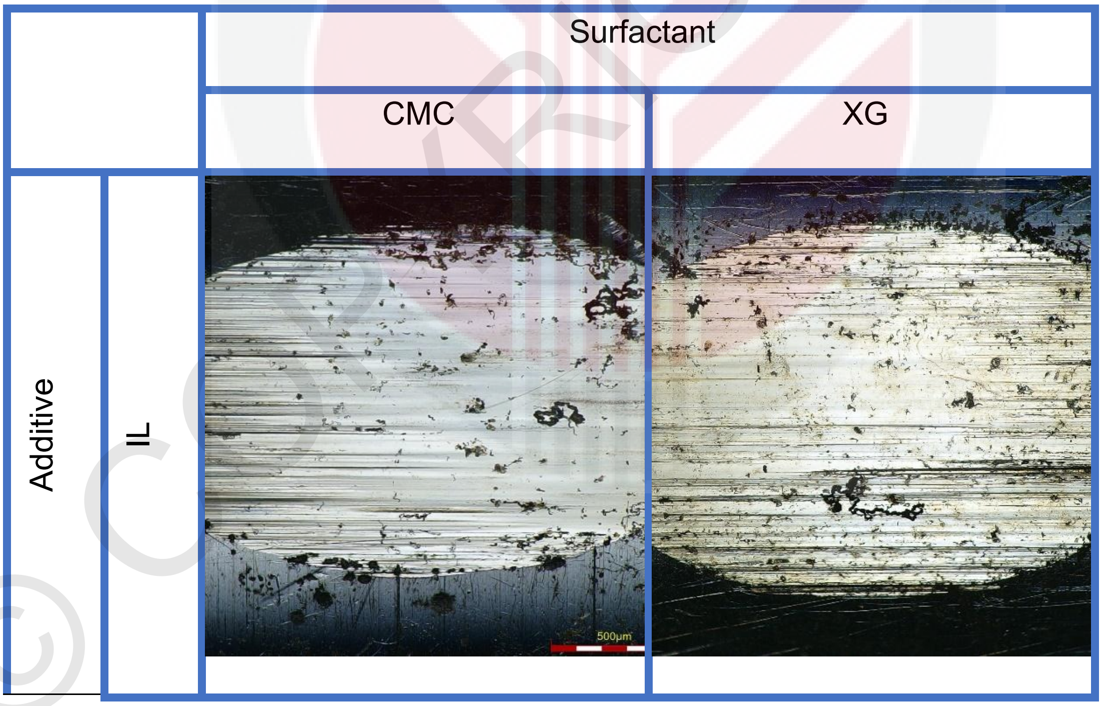

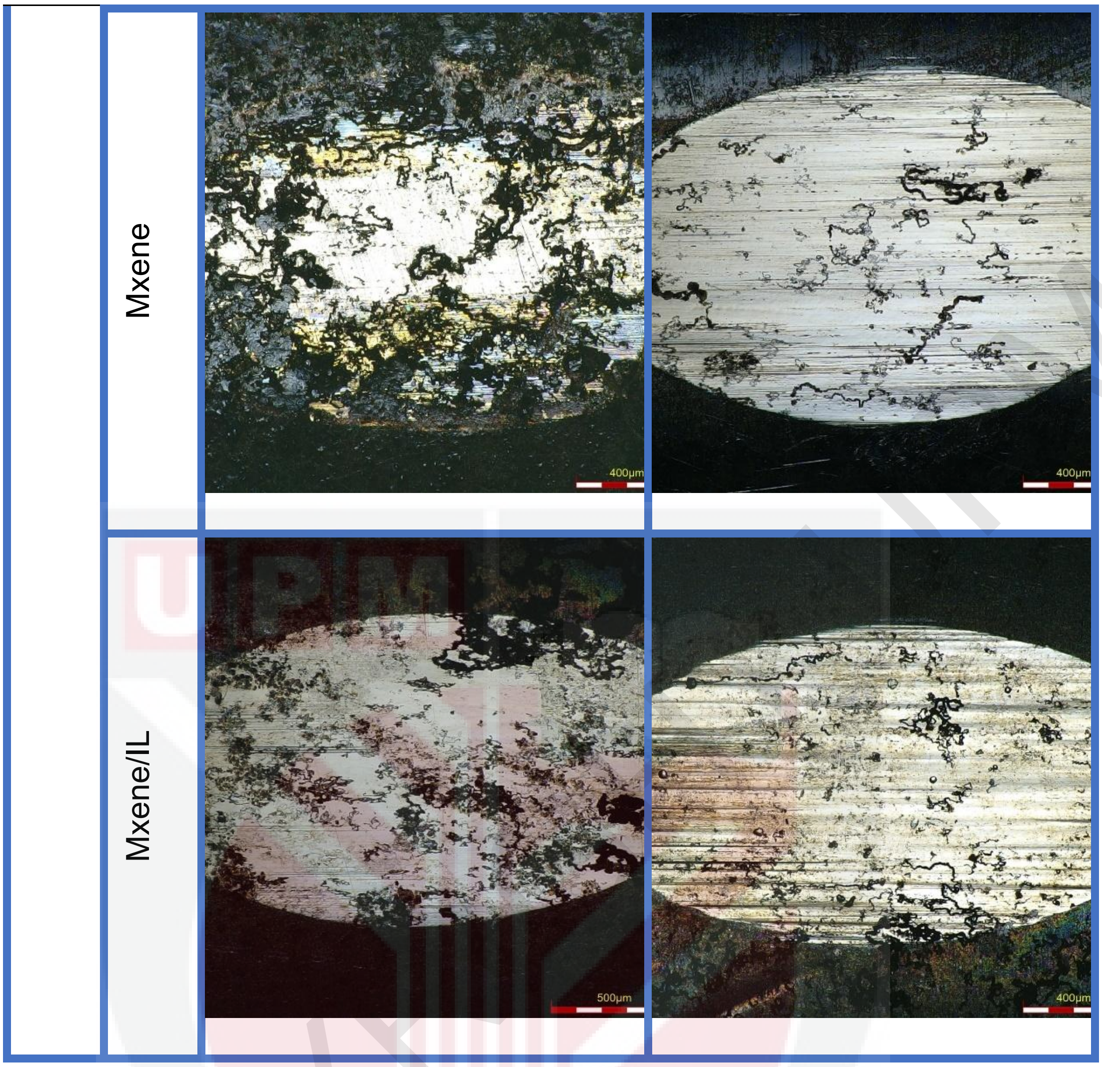

Figure 4.25: Close up of the wear on the block for every additive and surfactant.

4.3.5 Roughness of sliding surface

The roughness of the block Figure 4.25 after block-on-ring test, illustrated in Figure 4.26 and summarized in Table 4.2, show different variations in surface roughness (*Ra*) and (*Sa*) when using various WBLs. The parameters *Ra* (arithmetical mean height) and *Sa* (arithmetical mean height in area) indicate the degree of roughness on the block surface after testing.

WBL for CMC_IL exhibited moderate roughness values, with an average roughness (*Ra*) of approximately 3.016 µm and Sa roughly 4.466 µm. On the other hand, the CMC_Mxene sample showed the highest roughness among the lubricants tested, with a *Ra* value of 4.965 µm and a *Sa* value of 4.745 µm. However, incorporating CMC_Mxene/IL significantly reduced both *Ra* values, indicating improved smoothness, with *Ra* reduced to 1.108 µm and *Sa* to 1.441 µm.

The XG_IL sample shows relatively high surface roughness, indicated by *Ra* and Sa values of about 3.164 µm and 1.837 µm, respectively. In contrast, the XG_Mxene composite significantly reduced the surface roughness, reaching Ra and Sa values of nearly 1.361 µm and 1.941 µm, respectively. Mixing Mxene with IL results in an intermediate level of roughness, with Ra slightly above 2.05 µm and Sa approximately 2.061µm.

The findings of the study show that the integration of Mxene with IL generally leads to a decrease in surface roughness, which implies better lubrication and reduced wear. Notably, the CMC_Mxene/IL composite exhibited the most significant improvement in surface smoothness. On the other hand, the surface treated with CMC_Mxene alone showed higher roughness, which could be attributed to insufficient lubrication or increased friction encountered during the test.

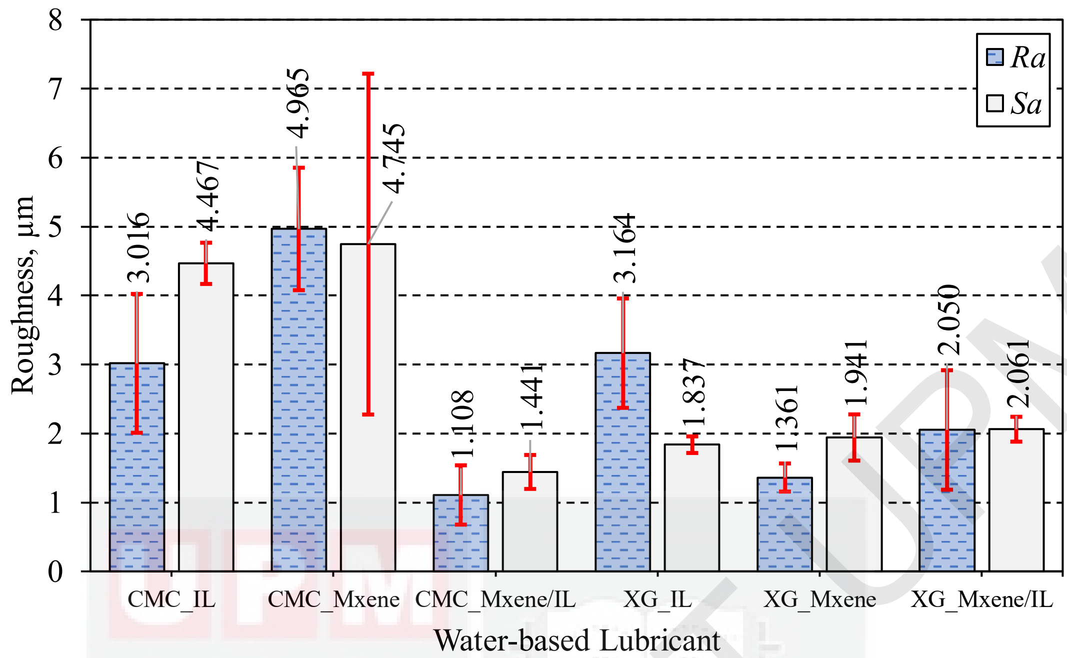

Figure 4.26: Line roughness (*Ra*) and Area surface roughness (*Sa*) on the block after BOR

Table 4.2: Summary of surface Roughness (*Ra* and *Sa*) on the block after BOR

	Ra (µm)	Sa (µm)
CMC_Mxene/IL	1.108	1.441
XG_Mxene	1.361	1.941
XG_Mxene/IL	2.050	2.061
CMC_IL	3.016	4.466
XG_IL	3.164	1.837
CMC_Mxene	4.965	4.745

4.3.6 Film thickness of test WBLs

Figure 4.27 show the Stribeck curve for the CMC_Mxene/IL lubricant, where the COF is shown to be dependent on variables such as viscosity, velocity and normal load. This graphical representation serves as an important tool in understanding the tribological performance of composites under various operating conditions. As speed increases, a thin lubricant film begins to form, reducing friction and moving into a mixed lubrication regime as show in Figure 2.16. Further increases in velocity and film thickness lead to hydrodynamic lubrication, where a complete lubricant film separates the surfaces, minimizing friction to its lowest point. However, at very high speeds or excessive film thickness, the viscous drag in the lubricant increases, causing increased friction. Therefore, while increasing velocity and film thickness generally reduces friction, beyond a certain point, it can lead to an increase in coefficient of friction because of hydrodynamic drag.

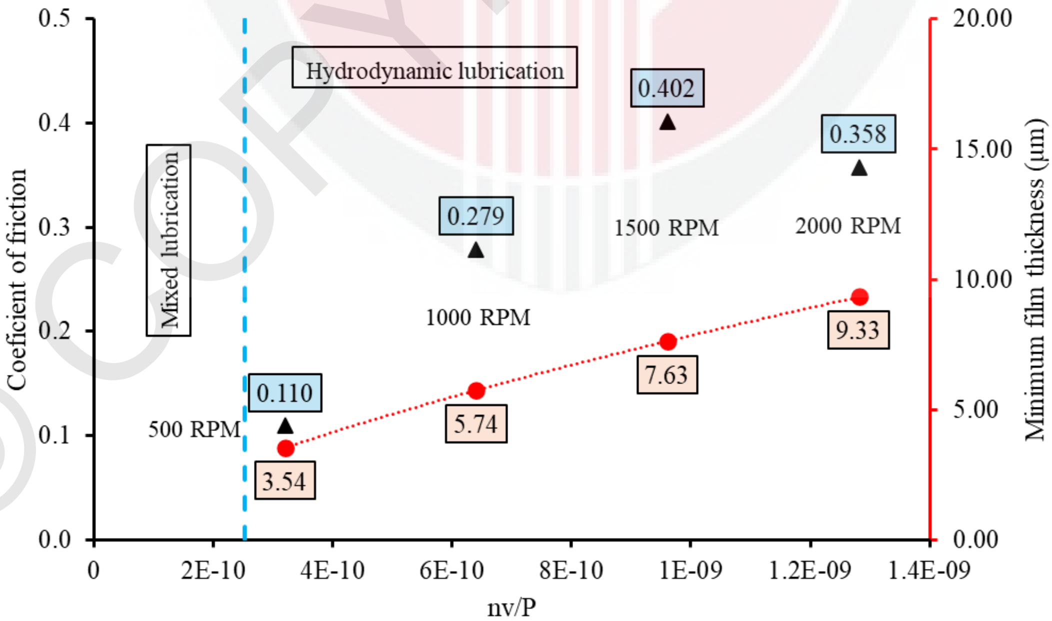

Figure 4.27 : COF and minimum thickness for CMC_Mxene/IL at various speeds.

4.4 Combined effect of coating and water-based lubricant in metal working

The objective 3 involves applying metal forming techniques, specifically the ironing process of stainless steel. The experimental setup incorporates the most effective coating identified in the first phase and the WBLs developed in the second phase.

4.4.1 Ironing force

Figure 4.28 shows the forces required for the ironing process under three different conditions: one involving dry friction, second involving DLC/TiAlN coating and three involving DLC/TiAlN coating together with a WBL that includes CMC as a surfactant, MXene, and an ionic liquid. (IL) as an additive. It shows the required force for every 5 strokes and provides a calculated average force for each condition.

Under dry friction conditions, the required force remains consistently high throughout all strokes, typically exceeding 400 N. Especially around 15th and 25th stroke, the force often approaches or even exceeds 500 N. This pattern indicates that there is significant friction between the tool and the workpiece in the absence of lubrication or protective coating. The ironing process using DLC/TiAlN coating shows the little lower than dry friction condition. Using WBLs and the DLC/TiAlN coating significantly reduces the force required for each stroke during the blanking process. This combination ensures that the applied force remains consistently low, mainly oscillating between 350 N and

450 N, except at 40th stroke 450 N. Such stability shows the effectiveness of the coating and lubricant in reducing friction and thus increasing the efficiency of the emptying operation. Compared to scenarios involving dry friction, this lubricating condition consistently requires less force, thereby increasing the interaction between the tool and the workpiece. This shows that the use of both lubricants and coatings can provide advantages in terms of extending tool life and improving the quality of the workpiece. This result underlines the advantages of applying advanced coatings like DLC/TiAIN, combined with an effective lubricant system, in reducing the operational forces and possibly leading to better energy efficiency and less wear in the blanking process.

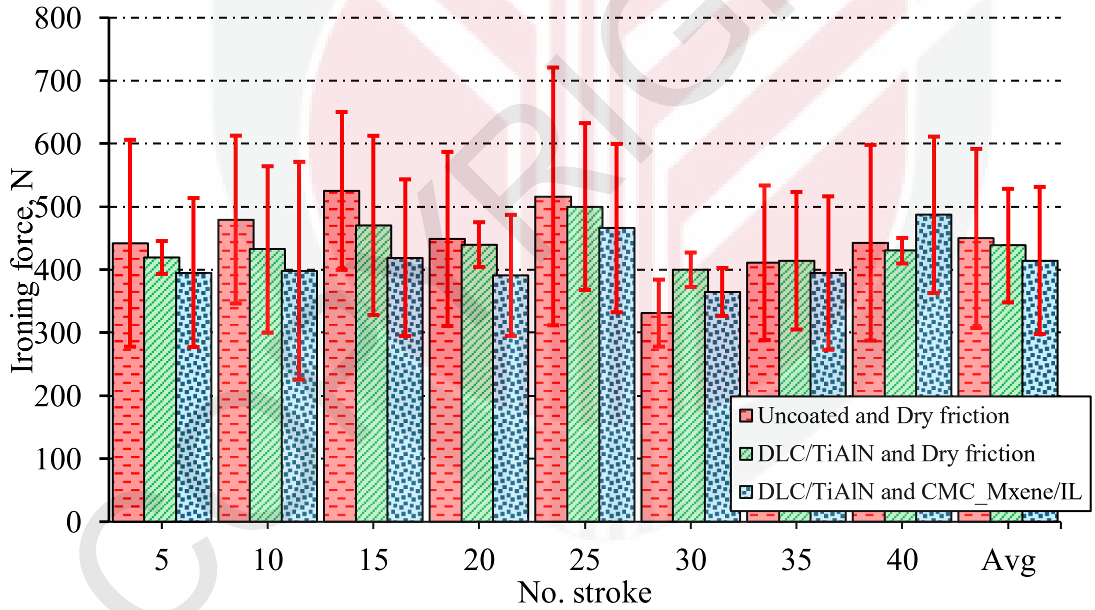

Figure 4.28: Force during blanking process every 5 strokes for dry frication and using DLC/TiAIN coating with lubricant CMC_Mxene/IL

4.4.2 Wear on the tool surface

The wear patterns observed on the punches during the ironing process show significant differences when comparing different lubrication and coating conditions. There is a significant difference among the dry friction condition (Figure 4.29) , tools coated with DLC/TiAlN (Figure 4.30) and tools coated with DLC/TiAlN with WBL that contain MXene/IL as an additive (Figure 4.31). In dry friction conditions, the surface of the tool shows significant rough wear. The severe scratching and plowing at most area indicate high material transfer between the tool and the workpiece, leading to extensive damage. This phenomenon is often caused by insufficient lubrication, which leads to direct metal-to-metal contact, which in turn causes adhesive wear and material removal from the surface of the punch. The grooves formed are deeper and exhibit a consistent pattern, indicating continuous wear during operation. In contrast, tools coated with DLC/TiAlN and lubricated with WBL infused with MXene/IL exhibited different wear mechanisms. This coating provides a protective barrier that reduces the intensity of wear. Although localized delamination and damage can be observed in the Figure 4.31 the overall level of wear is much lower than that caused by dry friction. The lubricant forms a barrier that prevents direct metal-to-metal contact between the tool and the workpiece, while MXene/IL additives may increase the effectiveness of the lubricant, thus reducing friction and wear. The presence of irregular wear patches indicates localized deterioration, which may result from isolated failures in the coating. However, the lack of extensive rough wear suggests that the combined effect of the coating and lubrication system is successful in reducing wear.

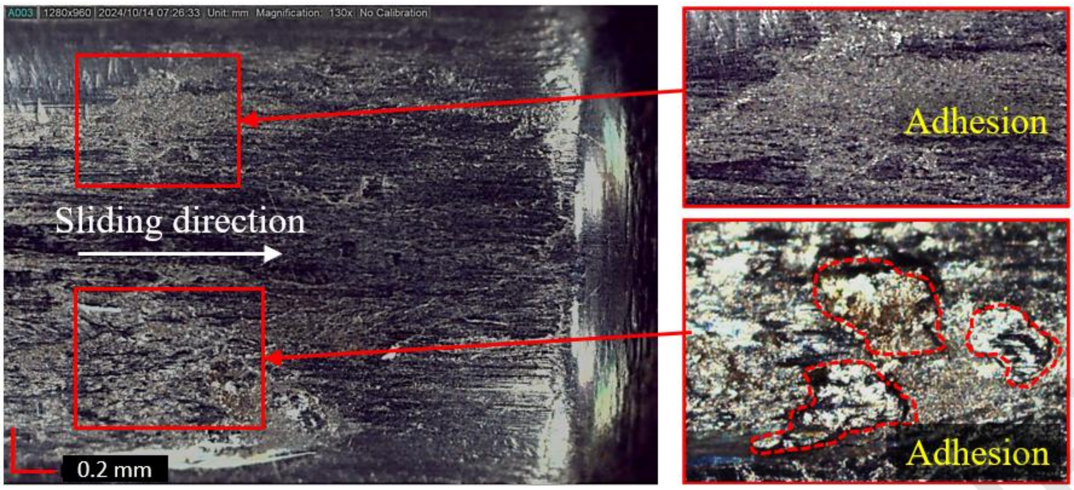

Figure 4.29: Wear visible on punch nose of uncoated tool performed in dry friction condition.

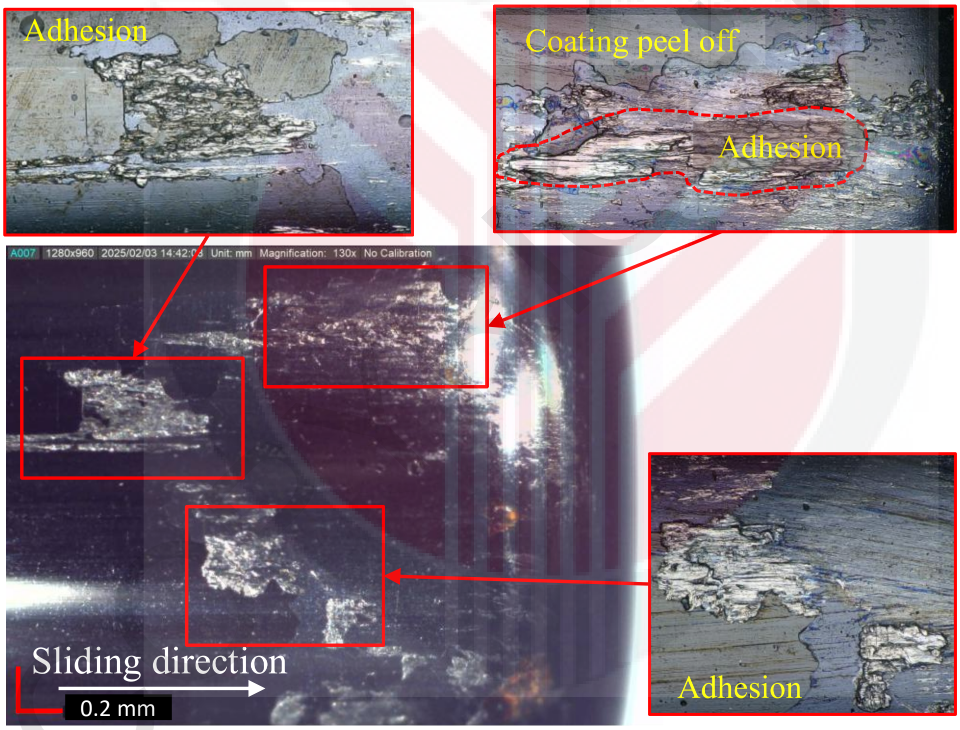

Figure 4.30: Wear occurred to punch nose for DLC/TiAlN coated punch with dry condition

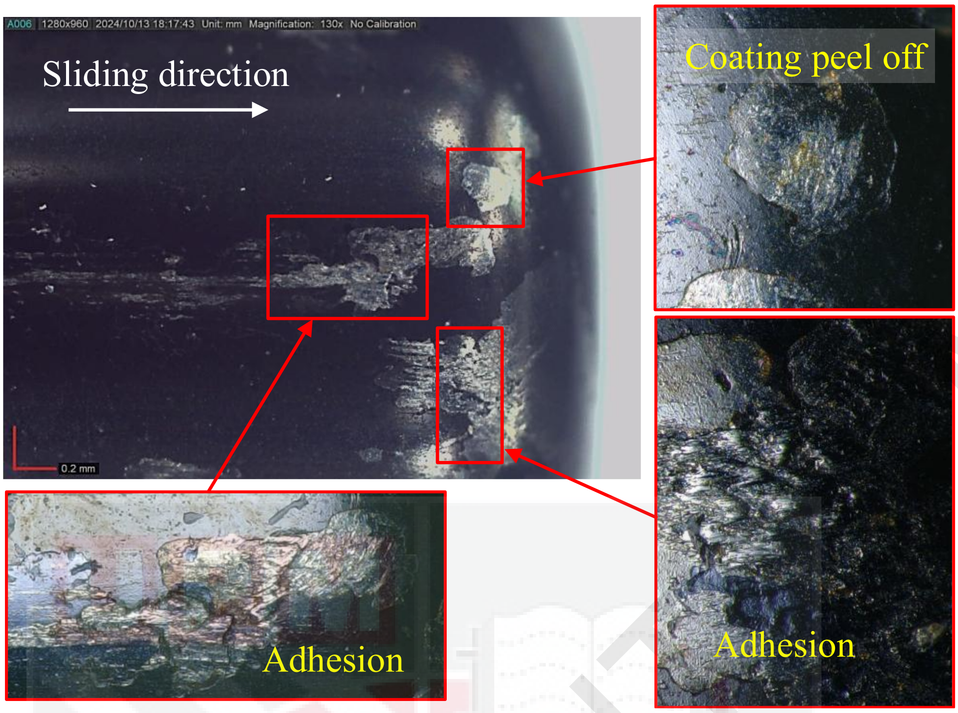

Figure 4.31: Wear occurred to punch nose for DLC/TiAlN coated punch lubricated with CMC_Mxene/IL WBL.

4.4.3 DLC/TiAlN and CMC_Mxene/IL testing

The combinations of CMC_Mxene/IL and DLC/TiAlN were subjected to a comprehensive friction analysis. This evaluation aimed to understand the tribological behavior of these advanced material pairings, which are pivotal in applications demanding high wear resistance and low friction coefficients. The setup was the same as the previous test but using a DLC/TiAlN coating on the block. The COF over cycles is presented in Figure 4.32, and the average COF is summarized in Figure 4.33, which includes measurements from the last 5000 cycles assumed to represent a steady state. The results show that using a DLC/TiAlN coating reduces COF from 0.110 (uncoated) to 0.081 (coated), amounting to a decrease of about 26%. This could be of wear-resistant qualities of the DLC coating could be the reason for this improvement. These qualities are enhanced by the superior adhesion strength provided by the TiAlN interlayer coating (Sulaiman et al., 2019).

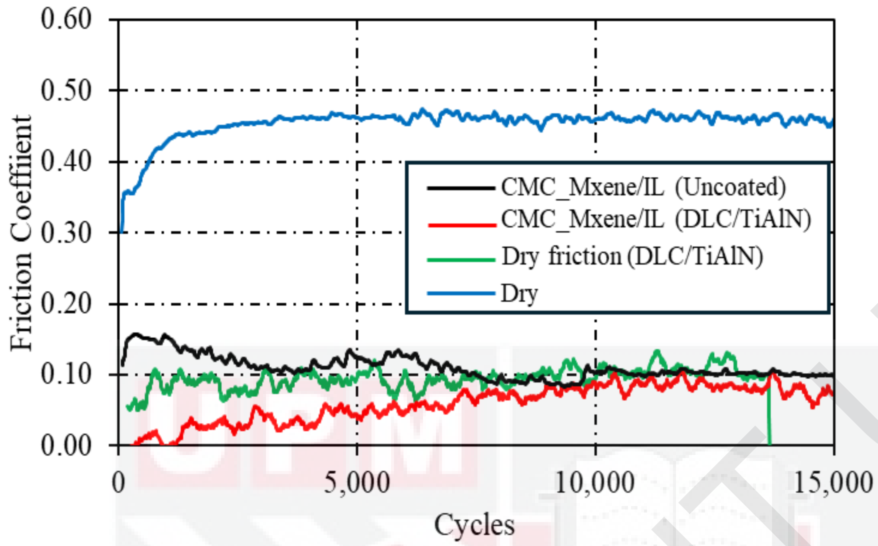

Figure 4.32: Measurement of friction for CMC_Mxene/IL with DLC/TiAlN coated and uncoated.

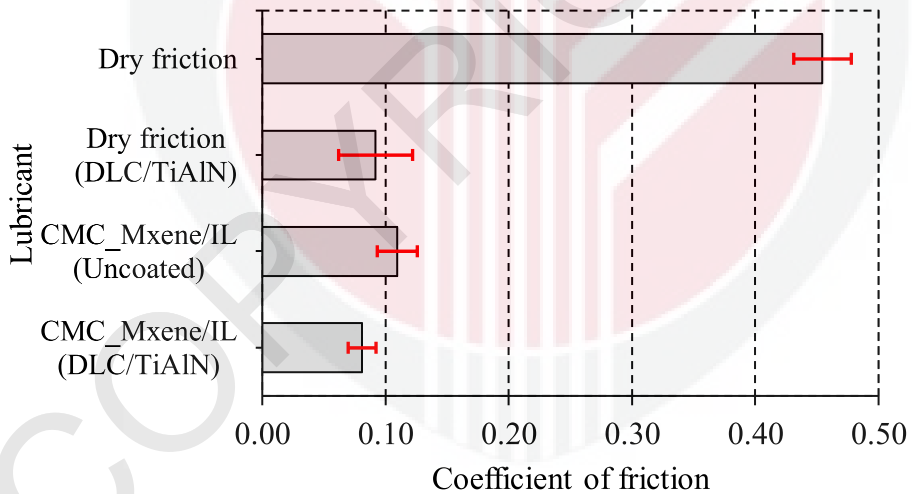

Figure 4.33: Average COF for CMC_Mxene/IL with DLC/TiAlN coated and uncoated at 500 rpm.

The average temperature and maximum temperature for WBL CMC_Mxene/IL with coating DLC/TiAlN and without coating is plotted in Figure 4.34. For temperature measurements, where WBL CMC_Mxene/IL with DLC/TiAlN coated sample experiences a bit higher maximum temperature than the uncoated with lubricant sample. This increase in temperature can be attributed to coating durability and wear resistance, which limits frictional heat dissipation by preventing significant lubricant damage or heat dissipation through wear. As a result, more heat accumulates at the interface, leading to a higher temperature but given the friction coefficient is reduced with the CMC_MXene/IL lubricant and the DLC/TiAIN coating.

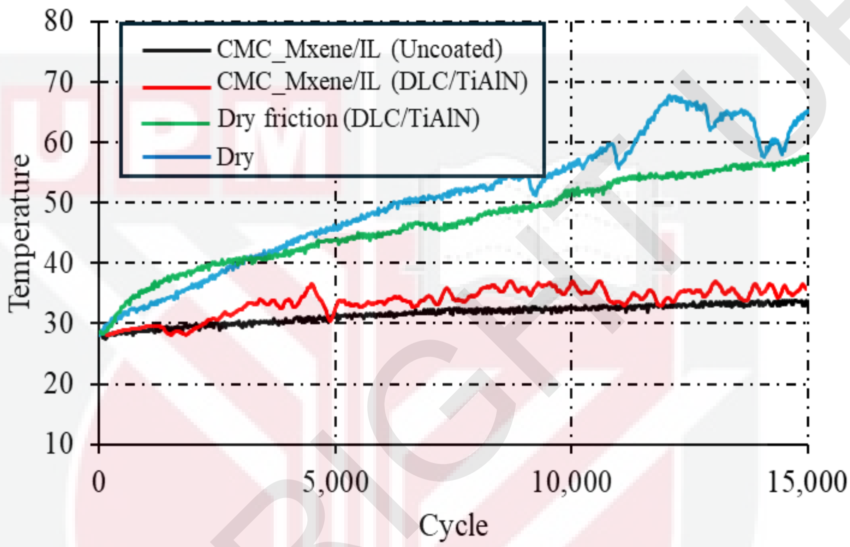

Figure 4.34: Average and maximum temperature near to sliding surfaces for WBL CMC_Mxene/IL with coating DLC/TiAIN and without coating.

The wear area is determined by referring to Figure 4.23 and is summarized in Table 4.3 which includes measurements from Figure 4.35. The results indicate that using WBL CMC_Mxene/IL with a DLC/TiAIN coating shows a marginally lower wear area compared to surfaces without the coating. Specifically, there is a 7.3% difference, with the DLC/TiAIN coated surface measuring 2.036 mm² and the uncoated surface measuring 2.196 mm². This reduction can be attributed to low friction coefficient and superior anti-adhesive properties of DLC coatings, which are advantageous for the sliding interaction between two contact surfaces (L. Wang et al., 2022). Additionally, the application of TiAIN over DLC films, along with intermediate layers, has been shown to significantly enhance the substrate's resistance to wear (Sousa et al., 2021).

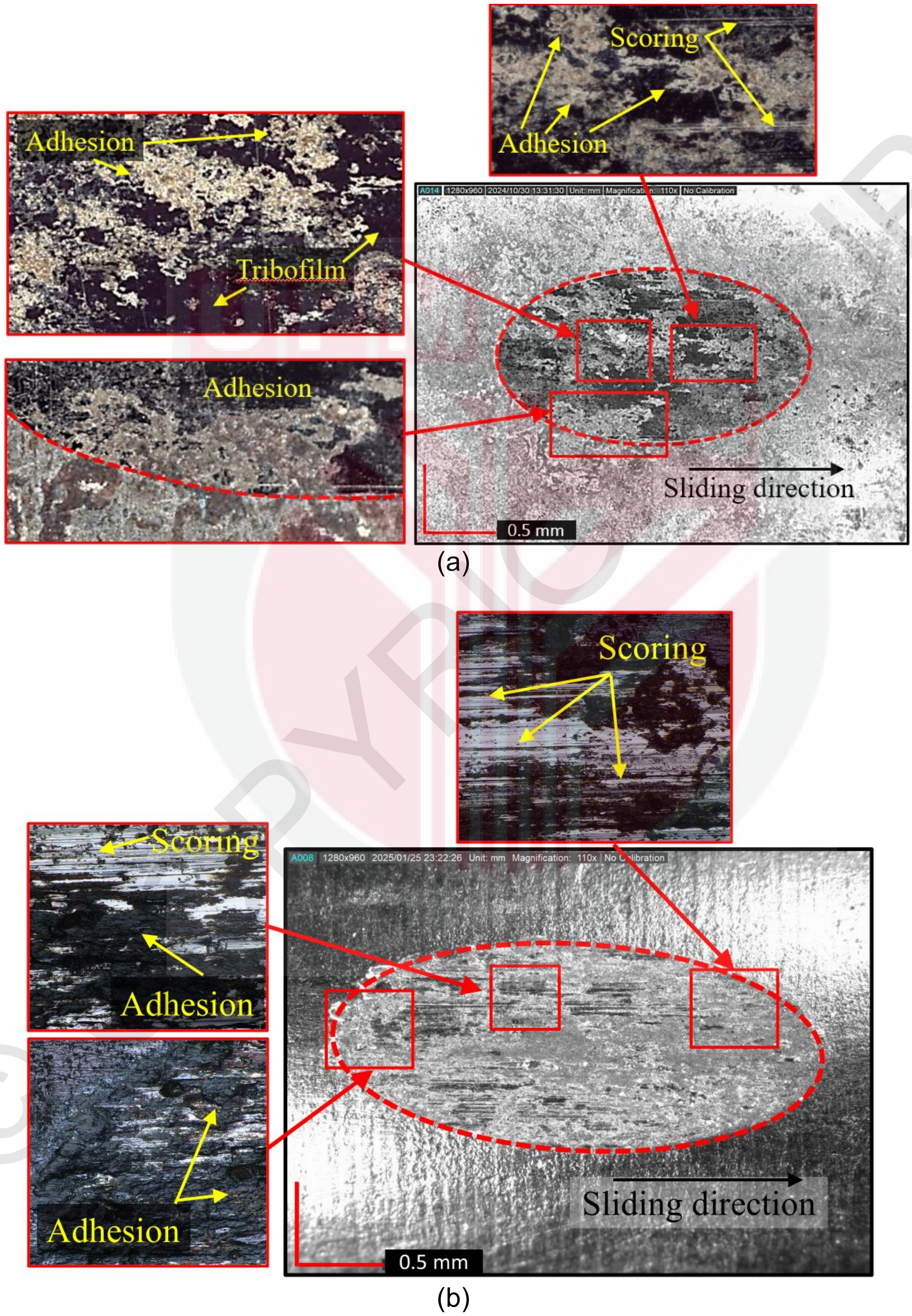

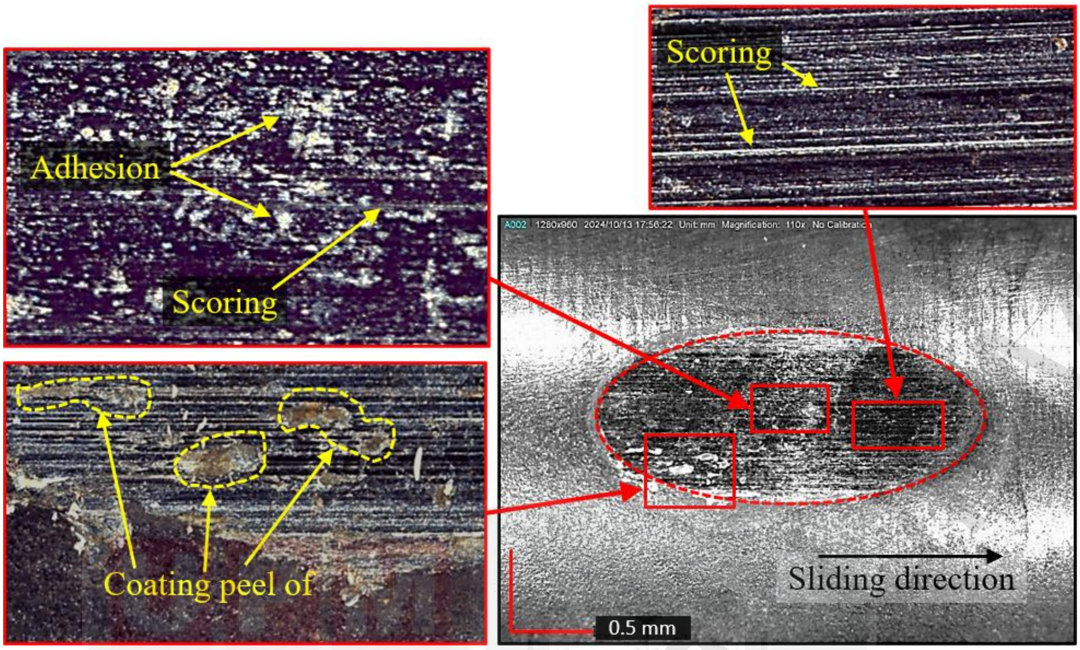

(c)

Figure 4.35: Wear area on the block using (a) DLC/TiAlN coating with CMC_Mxene/IL, (b) DLC/TiAlN coating with dry condition and (c) Uncoated steel surface.

Table 4.3: Wear area for CMC_Mxene/IL with coating DLC/TiAlN and without coating

Conditions	Wear area (mm^2)
DLC/TiAlN and CMC_Mxene/IL	2.036
DLC/TiAlN with Dry condition	2.879
Uncoated and CMC_Mxene/IL	2.196
Dry uncoated	14.248

* This wear area was calculated from the measured wear area, indicated by the red-coloured hidden line shown in Figure 4.35.

CHAPTER 5

CONCLUSION

5.1 Conclusion

In this study, the efficacy of a double-layered coating tool, specifically diamond-like carbon (DLC) as a top layer over TiAlSN, TiAlN, and CrN, were examined. The tribological performance of these coatings was systematically evaluated. Tools with no coating, a single coating, and a double coating were employed in the turning process of Al6061 aluminum and AISI4340 alloy steel under conditions of dry friction. It was observed that the DLC/TiAlN combination resulted in the lowest cutting forces for both materials, leading to reduced temperatures due to decreased friction. Furthermore, the surface roughness of the finished products was significantly improved, exhibiting the lowest values for both types of workpieces. This also extended to flank and crater wear, which demonstrated only minor BUE when machining Al6061 and minimal abrasive wear when machining AISI4340, using the DLC/TiAlN coated tool. This indicates that the double-layered DLC/TiAlN coating could enhance the durability and performance of cutting tools under dry machining conditions.

WBLs incorporating Ti_3C_2Tx Mxene multilayer nanoflakes (Titanium Carbide) and ionic liquid (IL) Tributyl(methyl)phosphonium dimethyl phosphate were successfully synthesized and evaluated. Six different WBL formulations, utilizing XG and CMC as surfactants, underwent testing to determine their physical, mechanical, and tribological properties. The λ calculations indicated the lubrication regime. When compared to dry conditions and distilled water

(DI), the addition of the additive significantly enhanced friction reduction, and wear resistance. The WBL containing DI, CMC, Mxene, and IL (CMC_Mxene/IL) demonstrated exceptional tribological performance, surpassing other formulations in friction and wear reduction. CMC_Mxene/IL reduced the COF by 76% compared to dry conditions and by 60% compared to DI, while wear area decreased by 81% against dry conditions and 45% compared to DI. These findings suggest that the use of additives can substantially improve the effectiveness of boundary lubrication. The development of WBLs with enhanced boundary lubrication properties as a new era of eco-friendly lubrication solutions for various engineering applications.

The tribosystem combining the effects of WBLs formulated with CMC_Mxene/IL and DLC/TiAlN coating has produced positive results, showing a significant reduction in the average forming force compared to the uncoated tool, which lead to less wear appear on tool coating compared to uncoated tool. Further examination through the tribological experiment using block-on-ring test setup on the use of this tribosytem with a combination of DLC/TiAlN coating and CMC_Mxene/IL WBL formulation, has found to reduce friction coefficient by approximately 26%, which is a significant improvement over the uncoated condition. This reduction in friction has a direct effect on wear formation, leading to a decrease in wear area. There is a 7.3% reduction in wear area when using CMC_Mxene/IL with a DLC/TiAlN coating, with measurements showing 2.036 mm² compared to 2.196 mm² without the coating and 29% % reduction in wear area when compared to coating at dry condition (2.879 mm²). This data underlines the effectiveness of the coating in improving the durability and performance of the tribosystem.

5.2 Recommendations

Several recommendations for future research could significantly improve the accuracy and scope of this study. Future investigations may explore various depths of cut during the machining process to determine their effect on material properties and tool performance. Additionally, multiple parameters, such as revolutions per minute (RPM) and different loads applied during tribological testing of WBLs, can be examined to understand their influence on friction and wear rates. In the field of sheet metal forming, it is beneficial to expand the scope of experiments to include other manufacturing processes such as bending, punching, and blanking, to obtain a comprehensive understanding of their effects on material behavior and final product quality. This expanded research can lead to more robust and efficient manufacturing practices, contributing to advancements in the field.

REFERENCES

Abdelrazek, A. H., Choudhury, I. A., Nukman, Y., & Kazi, S. N. (2020). Metal cutting lubricants and cutting tools: a review on the performance improvement and sustainability assessment. *The International Journal of Advanced Manufacturing Technology*, *106*(9–10), 4221–4245. https://doi.org/10.1007/s00170-019-04890-w

Ahamed, M. M., Basha, S. M. J., & Prasad, B. D. (2020). *Comparison of Thermo-Physical and Tribological Characteristics of Nanolubricant* (pp. 153–164). https://doi.org/10.1007/978-981-32-9931-3_16

Ahmed, Y. S., Paiva, J. M., Bose, B., & Veldhuis, S. C. (2019). New observations on built-up edge structures for improving machining performance during the cutting of superduplex stainless steel. *Tribology International*, *137*, 212–227. https://doi.org/10.1016/j.triboint.2019.04.039

Ai, X., Tan, J., Sun, H., Lu, L., Yang, Z., Yu, Z., Liao, G., Li, S., Jin, Y., Niu, Y., He, N., & Hao, X. (2022). Effect of Tool Coatings on Machining Properties of Compacted Graphite Iron. *Micromachines*, *13*(10), 1781. https://doi.org/10.3390/mi13101781

Aiman, Y., Syahrullail, S., & Hamid, M. K. A. (2024). Optimisation of friction surfacing process parameters for a1100 aluminium utilising different derivatives of palm oil based on closed forging test. *Biomass Conversion and Biorefinery*, *14*(7), 8857–8874. https://doi.org/10.1007/s13399-022-03178-6

Ajay, T., Mugendiran, V., Vasumathi, M., & Rashia Begum, S. (2024). Study of machining performance and tribological characteristics of monolayer, compound and bilayer Diamond-Like carbon (DLC) coated HSS drill bits. *Materials Today: Proceedings*. https://doi.org/10.1016/j.matpr.2024.02.011

Aleshin, V. V., & Papangelo, A. (2020). Friction-induced energy losses in mechanical contacts subject to random vibrations. *International Journal of Solids and Structures*, *190*, 148–155. https://doi.org/10.1016/j.ijsolstr.2019.10.026

Ali, I., Basheer, A. A., Kucherova, A., Memetov, N., Pasko, T., Ovchinnikov, K., Pershin, V., Kuznetsov, D., Galunin, E., Grachev, V., & Tkachev, A. (2019). Advances in carbon nanomaterials as lubricants modifiers. *Journal of Molecular Liquids*, *279*, 251–266. https://doi.org/10.1016/j.molliq.2019.01.113

Ali, M. K. A., & Xianjun, H. (2020). Colloidal stability mechanism of copper nanomaterials modified by bis(2-ethylhexyl) phosphate dispersed in polyalphaolefin oil as green nanolubricants. *Journal of Colloid and Interface Science*, *578*, 24–36. https://doi.org/10.1016/j.jcis.2020.05.092

Ali, M. K. A., & Xianjun, H. (2021). Role of bis(2-ethylhexyl) phosphate and Al2O3/TiO2 hybrid nanomaterials in improving the dispersion stability of nanolubricants. *Tribology International*, *155*, 106767. https://doi.org/10.1016/j.triboint.2020.106767

Ali, M. K. A., Xianjun, H., Elagouz, A., Essa, F. A., & Abdelkareem, M. A. A. (2016). Minimizing of the boundary friction coefficient in automotive engines using Al2O3 and TiO2 nanoparticles. *Journal of Nanoparticle Research*, *18*(12), 377. https://doi.org/10.1007/s11051-016-3679-4

Alojali, H. M., & Benyounis, K. Y. (2016). Advances in Tool wear in Turning Process. In *Reference Module in Materials Science and Materials Engineering*. Elsevier. https://doi.org/10.1016/B978-0-12-803581-8.04031-5

Angayarkanni, S. A., & Philip, J. (2015). Review on thermal properties of nanofluids: Recent developments. *Advances in Colloid and Interface Science*, *225*, 146–176. https://doi.org/10.1016/j.cis.2015.08.014

Arinbjarnar, Ú., Moghadam, M., & Nielsen, C. V. (2022). Application of Calcium Carbonate as Green Lubricant Additive in Sheet Metal Forming. *Key Engineering Materials*, *926*, 1133–1142. https://doi.org/10.4028/p-x87o62

Asadi, A., Aberoumand, S., Moradikazerouni, A., Pourfattah, F., Żyła, G., Estellé, P., Mahian, O., Wongwises, S., Nguyen, H. M., & Arabkoohsar, A. (2019). Recent advances in preparation methods and thermophysical properties of oil-based nanofluids: A state-of-the-art review. *Powder Technology*, *352*, 209–226. https://doi.org/10.1016/j.powtec.2019.04.054

Avilés, M. D., Carrión, F. J., Sanes, J., & Bermúdez, M. D. (2021). Bio-based ionic liquid crystal for stainless steel-sapphire high temperature ultralow friction. *Wear*, *484–485*, 204020. https://doi.org/10.1016/j.wear.2021.204020

Avilés, M.-D., Jiménez, A.-E., Pamies, R., Carrión-Vilches, F.-J., & Bermúdez, M.-D. (2022). Triprotic Ammonium Oleate Ionic Liquid Crystal Lubricant for Copper-Copper Friction and Wear Reduction. *Lubricants*, *10*(11), 290. https://doi.org/10.3390/lubricants10110290

Azman, N. F., & Samion, S. (2019). Dispersion Stability and Lubrication Mechanism of Nanolubricants: A Review. *International Journal of Precision Engineering and Manufacturing-Green Technology*, *6*(2), 393–414. https://doi.org/10.1007/s40684-019-00080-x

Azman, N. F., Samion, S., Paiman, Z., & Kameil Abdul Hamid, M. (2024). Tribological performance and mechanism of graphite, hBN and MoS2 as nano-additives in palm kernel oil-based lubricants: A comparative study. *Journal of Molecular Liquids*, *410*, 125616. https://doi.org/10.1016/j.molliq.2024.125616

Azman, N. F., Samion, S., & Sot, M. N. H. M. (2018). Investigation of tribological properties of CuO/palm oil nanolubricant using pin-on-disc tribotester. *Green Materials*, *6*(1), 30–37. https://doi.org/10.1680/jgrma.17.00026

Babar, H., & Ali, H. M. (2019). Towards hybrid nanofluids: Preparation, thermophysical properties, applications, and challenges. *Journal of Molecular Liquids*, *281*, 598–633. https://doi.org/10.1016/j.molliq.2019.02.102

Bai, Y., Wang, L., Ge, C., Liu, R., Guan, H., & Zhang, X. (2020). Atomically thin hydroxylation boron nitride nanosheets for excellent water-based lubricant additives. *Journal of the American Ceramic Society*, *103*(12), 6951–6960. https://doi.org/10.1111/jace.17088

Bay, N., Olsson, D. D., & Andreasen, J. L. (2008). Lubricant test methods for sheet metal forming. *Tribology International*, *41*(9–10), 844–853. https://doi.org/10.1016/j.triboint.2007.11.017

Bhushan, B. (2013). *Introduction to Tribology* (2nd ed.).

Blau, P. J. (2005). On the nature of running-in. *Tribology International*, *38*(11–12), 1007–1012. https://doi.org/10.1016/j.triboint.2005.07.020

Bukvić, M., Gajević, S., Skulić, A., Savić, S., Ašonja, A., & Stojanović, B. (2023). Tribological Application of Nanocomposite Additives in Industrial Oils. *Lubricants*, *12*(1), 6. https://doi.org/10.3390/lubricants12010006

Caliskan, H., Panjan, P., & Kurbanoglu, C. (2017). 3.16 Hard Coatings on Cutting Tools and Surface Finish. In *Comprehensive Materials Finishing* (pp. 230–242). Elsevier. https://doi.org/10.1016/B978-0-12-803581-8.09178-5

Cao, H., Xu, Z., Hu, Y., Zhong, M., & Liu, S. (2022). Research on Measurement Methods of Friction Coefficient. *Journal of Physics: Conference Series*, *2200*(1), 012022. https://doi.org/10.1088/1742-6596/2200/1/012022

Cappellini, C., & Abeni, A. (2022). Development and implementation of crater and flank tool wear model for hard turning simulations. *The International Journal of Advanced Manufacturing Technology*, *120*(3–4), 2055–2073. https://doi.org/10.1007/s00170-022-08885-y

Chen, C., Huang, B., Liu, Z., Li, Y., Zou, D., Liu, T., Chang, Y., & Chen, L. (2023). Additive manufacturing of WC-Co cemented carbides: Process, microstructure, and mechanical properties. *Additive Manufacturing*, *63*, 103410. https://doi.org/10.1016/j.addma.2023.103410

Chen, J., & Zhao, W. (2021). Simple method for preparing nanometer thick Ti3C2TX sheets towards highly efficient lubrication and wear resistance. *Tribology International*, *153*, 106598. https://doi.org/10.1016/j.triboint.2020.106598

Chen, W., Fu, X., Cao, L., Gao, S., & Wan, Y. (2021). Ultralow friction of copper by a green water-based lubricant containing phytic acid. *Journal of Molecular Liquids*, *338*, 116704. https://doi.org/10.1016/j.molliq.2021.116704

Choi, S. U. S., & Eastman, J. A. (2001). *Enhanced heat transfer using nanofluids*.

Chowdhury, M. S. I., Bose, B., Rawal, S., Fox-Rabinovich, G. S., & Veldhuis, S. C. (2021). Investigation of the Wear Behavior of PVD Coated Carbide Tools during Ti6Al4V Machining with Intensive Built Up Edge Formation. *Coatings*, *11*(3), 266. https://doi.org/10.3390/coatings11030266

Cui, Y., Ding, M., Sui, T., Zheng, W., Qiao, G., Yan, S., & Liu, X. (2020). Role of nanoparticle materials as water-based lubricant additives for ceramics. *Tribology International*, *142*, 105978. https://doi.org/10.1016/j.triboint.2019.105978

Dai, W., Kheireddin, B., Gao, H., & Liang, H. (2016). Roles of nanoparticles in oil lubrication. *Tribology International*, *102*, 88–98. https://doi.org/10.1016/j.triboint.2016.05.020

David, H., Robert, R., & Jearl, W. (2021). *Fundamentals of Physics* (12th ed., Vol. 1). Wiley.

Davim, J. P. (2011). *Modern Machining Technology: A Practical Guide*. Woodhead Publishing in Mechanical Engineering.

Del Sol, I., Gámez, A. J., Rivero, A., & Iglesias, P. (2019). Tribological performance of ionic liquids as additives of water-based cutting fluids. *Wear*, *426–427*, 845–852. https://doi.org/10.1016/j.wear.2019.01.109

Di Puccio, F., Di Pietro, A., & Mattei, L. (2024). Pin-on-Plate vs. Pin-on-Disk Wear Tests: Theoretical and Numerical Observations on the Initial Transient Phase. *Lubricants*, *12*(4), 134. https://doi.org/10.3390/lubricants12040134

Dou, S., & Xia, J. (2019). Analysis of Sheet Metal Forming (Stamping Process): A Study of the Variable Friction Coefficient on 5052 Aluminum Alloy. *Metals*, *9*(8), 853. https://doi.org/10.3390/met9080853

Du, S., Sun, J., & Wu, P. (2018). Preparation, characterization and lubrication performances of graphene oxide-TiO2 nanofluid in rolling strips. *Carbon*, *140*, 338–351. https://doi.org/10.1016/j.carbon.2018.08.055

Dunn, A. C., Krick, B. A., Liechti, K. M., & DelRio, F. W. (2021). Special Issue on Tribology of Advanced Materials. *Experimental Mechanics*, *61*(9), 1503–1505. https://doi.org/10.1007/s11340-021-00760-3

Elomaa, O., Singh, V. K., Iyer, A., Hakala, T. J., & Koskinen, J. (2015). Graphene oxide in water lubrication on diamond-like carbon vs. stainless steel high-load contacts. *Diamond and Related Materials*, *52*, 43–48. https://doi.org/10.1016/j.diamond.2014.12.003

Fatima, N., Minami, I., Holmgren, A., Marklund, P., Berglund, K., & Larsson, R. (2015). Influence of water on the tribological properties of zinc dialkyl-dithiophosphate and over-based calcium sulphonate additives in wet clutch contacts. *Tribology International*, *87*, 113–120. https://doi.org/10.1016/j.triboint.2015.02.006

Freitas, F. R. S., Casais, R. C. B., Silva, F. J. G., Sebbe, N. P. V., Martinho, R. P., Sousa, V. F. C., Sales-Contini, R. C. M., & Fernandes, F. (2024). Wear Behavior of TiAlN/DLC Coating on Tools in Milling Copper–Beryllium Alloy AMPCOLOY® 83. *Coatings*, *14*(11), 1354. https://doi.org/10.3390/coatings14111354

Gasni, D., Rahmadiawan, D., Irwansyah, R., & Khalid, A. E. (2024). Composite of Carboxymethyl Cellulose/MXene and Span 60 as Additives to Enhance Tribological Properties of Bio-Lubricants. *Lubricants*, *12*(3), 78. https://doi.org/10.3390/lubricants12030078

Grützmacher, P. G., Neuhauser, R., Stagel, K., Bica-Schröder, K., Boidi, G., Gachot, C., & Rosenkranz, A. (2024). Combining Tailored Ionic Liquids with Ti3C2Tx MXenes for an Enhanced Load-Carrying Capacity Under Boundary Lubrication. *Advanced Engineering Materials*, *26*(4). https://doi.org/10.1002/adem.202300721

Gulzar, M., Masjuki, H. H., Kalam, M. A., Varman, M., Zulkifli, N. W. M., Mufti, R. A., Zahid, R., & Yunus, R. (2017). Dispersion Stability and Tribological Characteristics of TiO2/SiO2 Nanocomposite-Enriched Biobased Lubricant. *Tribology Transactions*, *60*(4), 670–680. https://doi.org/10.1080/10402004.2016.1202366

Guo, J., Ma, S., & Zhang, X. (2020). Review of Design Theory of Ceramic Cutting Tools for High Speed Cutting. *2020 International Conference on Artificial Intelligence and Electromechanical Automation (AIEA)*, 412–415. https://doi.org/10.1109/AIEA51086.2020.00092

Guo, R., Liu, Z., Chen, X., Dou, X., Ye, Q., & Liu, X. (2024). Synergistic tribological performance of Ti3C2Tx MXene functionalized with ionic liquids. *Tribology International*, *194*, 109526. https://doi.org/10.1016/j.triboint.2024.109526

Gupta, B. R. (2023). Friction and wear mechanism of polymers, their composites and nanocomposites. In *Tribology of Polymers, Polymer Composites, and Polymer Nanocomposites* (pp. 51–117). Elsevier. https://doi.org/10.1016/B978-0-323-90748-4.00012-1

Gupta, M. K., Niesłony, P., Sarikaya, M., Korkmaz, M. E., Kuntoğlu, M., Królczyk, G. M., & Jamil, M. (2022). Tool wear patterns and their promoting mechanisms in hybrid cooling assisted machining of titanium

Ti-3Al-2.5V/grade 9 alloy. *Tribology International*, *174*, 107773. https://doi.org/10.1016/j.triboint.2022.107773

Gupta, R. N., & Harsha, A. (2018). Antiwear and extreme pressure performance of castor oil with nano-additives. *Proceedings of the Institution of Mechanical Engineers, Part J: Journal of Engineering Tribology*, *232*(9), 1055–1067. https://doi.org/10.1177/1350650117739159

Hao, Y., Biswas, S., Hawkes, E. W., Wang, T., Zhu, M., Wen, L., & Visell, Y. (2021). A Multimodal, Enveloping Soft Gripper: Shape Conformation, Bioinspired Adhesion, and Expansion-Driven Suction. *IEEE Transactions on Robotics*, *37*(2), 350–362. https://doi.org/10.1109/TRO.2020.3021427

He, J., Sun, J., Meng, Y., & Yan, X. (2019). Preliminary investigations on the tribological performance of hexagonal boron nitride nanofluids as lubricant for steel/steel friction pairs. *Surface Topography: Metrology and Properties*, *7*(1), 015022. https://doi.org/10.1088/2051-672X/ab0afb

Huang, S., He, A., Yun, J.-H., Xu, X., Jiang, Z., Jiao, S., & Huang, H. (2019). Synergistic tribological performance of a water based lubricant using graphene oxide and alumina hybrid nanoparticles as additives. *Tribology International*, *135*, 170–180. https://doi.org/10.1016/j.triboint.2019.02.031

Huang, S., Kumar, P., Yeong, W. Y., Narayan, R. L., & Ramamurty, U. (2022). Fracture behavior of laser powder bed fusion fabricated Ti41Nb via in-situ alloying. *Acta Materialia*, *225*, 117593. https://doi.org/10.1016/j.actamat.2021.117593

Huang, S., Lin, W., Li, X., Fan, Z., Wu, H., Jiang, Z., & Huang, H. (2021). Roughness-dependent tribological characteristics of water-based GO suspensions with ZrO2 and TiO2 nanoparticles as additives. *Tribology International*, *161*, 107073. https://doi.org/10.1016/j.triboint.2021.107073

Hwang, G. B., Huang, H., Wu, G., Shin, J., Kafizas, A., Karu, K., Toit, H. Du, Alotaibi, A. M., Mohammad-Hadi, L., Allan, E., MacRobert, A. J., Gavriilidis, A., & Parkin, I. P. (2020). Photobactericidal activity activated by thiolated gold nanoclusters at low flux levels of white light. *Nature Communications*, *11*(1), 1207. https://doi.org/10.1038/s41467-020-15004-6

Ideris, M. H., Kamaruddin, S., Sulaiman, M. H., Sukindar, N. A., Ahmad Azhar, A. Z., & Md Yasir, A. S. H. (2023). Effects of Coating and Lubrication on Friction and Wear for Metal-to Metal Application. *Journal of Advanced Research in Applied Mechanics*, *110*(1), 52–62. https://doi.org/10.37934/aram.110.1.5262

Ijaz Malik, M. A., Kalam, M. A., Mujtaba, M. A., & Almomani, F. (2023). A review of recent advances in the synthesis of environmentally friendly, sustainable, and nontoxic bio-lubricants: Recommendations for the future implementations. *Environmental Technology & Innovation*, *32*, 103366. https://doi.org/10.1016/j.eti.2023.103366

Isaka, M. (2020). *Coated cutting tool*.

İşleyen, Ü. K., & Karamanoğlu, M. (2019). The influence of machining parameters on surface roughness of MDF in milling operation. *BioResources*, *14*(2), 3266–3277. https://doi.org/10.15376/biores.14.2.3266-3277

Janssen, C. P., Donker, S. F., Brumby, D. P., & Kun, A. L. (2019). History and future of human-automation interaction. *International Journal of Human-Computer Studies*, *131*, 99–107. https://doi.org/10.1016/j.ijhcs.2019.05.006

Jieming, Y., Hsu-Ming, L., & Filippo, M. (2023). Linking Molecular Structure and Lubrication Mechanisms in Tetraalkylammonium Orthoborate Ionic Liquids. *Research Square*. https://doi.org/https://doi.org/10.21203/rs.3.rs-2463794/v1

Jiménez, A.-E., Avilés, M.-D., Pamies, R., Bermúdez, M.-D., Carrión-Vilches, F.-J., & Sanes, J. (2022). Ecofriendly Protic Ionic Liquid Lubricants for Ti6Al4V. *Lubricants*, *11*(1), 5. https://doi.org/10.3390/lubricants11010005

Kapsiz, M., Geffroy, S., Holzer, A., & Schmitz, K. (2023). Tribological Performances of Diamond-Like Carbon Coatings for Hydraulic Applications. *Chemical Engineering & Technology*, *46*(1), 118–127. https://doi.org/10.1002/ceat.202200459

Kashyap, A., Harsha, A. P., Kondaiah, P., & Barshilia, H. C. (2022). Study on galling behaviour of HiPIMS deposited Mo/DLC multilayer coatings at ambient and elevated temperature. *Wear*, *498–499*, 204327. https://doi.org/10.1016/j.wear.2022.204327

Khan, H., Mahmood, N., Zavabeti, A., Elbourne, A., Rahman, Md. A., Zhang, B. Y., Krishnamurthi, V., Atkin, P., Ghasemian, M. B., Yang, J., Zheng, G., Ravindran, A. R., Walia, S., Wang, L., Russo, S. P., Daeneke, T., Li, Y., & Kalantar-Zadeh, K. (2020). Liquid metal-based synthesis of high performance monolayer SnS piezoelectric nanogenerators. *Nature Communications*, *11*(1), 3449. https://doi.org/10.1038/s41467-020-17296-0

Khan, S. A., Ameer, M. F., Uddin, G. M., Ali, M. A., Anwar, S., Farooq, M. U., & Alfaify, A. (2022). An in-depth analysis of tool wear mechanisms and surface integrity during high-speed hard turning of AISI D2 steel via novel inserts. *The International Journal of Advanced Manufacturing Technology*, *122*(9–10), 4013–4028. https://doi.org/10.1007/s00170-022-10151-0

Khatai, S., Kumar Sahoo, A., Kumar, R., & Panda, A. (2022). On Machining behaviour of various cutting Inserts: A review on hardened steel.

Materials Today: Proceedings, *62*, 3485–3492. https://doi.org/10.1016/j.matpr.2022.04.301

Khatun, N., & Roy, S. C. (2022). Optimization of etching and sonication time to prepare monolayer Ti3C2T MXene flakes: A structural, vibrational, and optical spectroscopy study. *Micro and Nanostructures*, *167*, 207256. https://doi.org/10.1016/j.micrna.2022.207256

Khonsari, M. M., Ghatrehsamani, S., & Akbarzadeh, S. (2021). On the running-in nature of metallic tribo-components: A review. *Wear*, *474–475*, 203871. https://doi.org/10.1016/j.wear.2021.203871

Kim, E. J., Choi, M., Park, H. Y., Hwang, J. Y., Kim, H.-E., Hong, S. W., Lee, J., Yong, K., & Kim, W. (2019). Thorn-like TiO2 nanoarrays with broad spectrum antimicrobial activity through physical puncture and photocatalytic action. *Scientific Reports*, *9*(1), 13697. https://doi.org/10.1038/s41598-019-50116-0

Kim, K. S., Kim, H. K., La, J. H., & Lee, S. Y. (2016). Effects of interlayer thickness and the substrate material on the adhesion properties of CrZrN coatings. *Japanese Journal of Applied Physics*, *55*(1S), 01AA02. https://doi.org/10.7567/JJAP.55.01AA02

Klüber Lubrication. (2018, October 17). *Hydro Lubricants: Water-based lubricants for hydropower applications*.

Lee-Niinioja, H. S. (2022). *The Continuity of Pre-Islamic Motifs in Javanese Mosque Ornamentation, Indonesia*. Archaeopress Publishing Ltd. https://doi.org/10.2307/j.ctv2b07tsb

Li, Z., Wu, L., Wang, H., Zhou, W., Liu, H., Cui, H., Li, P., Chu, P. K., & Yu, X.-F. (2019). Synergistic Antibacterial Activity of Black Phosphorus Nanosheets Modified with Titanium Aminobenzenesulfanato Complexes. *ACS Applied Nano Materials*, *2*(3), 1202–1209. https://doi.org/10.1021/acsanm.8b02065

Lian, W., Mai, Y., Liu, C., Zhang, L., Li, S., & Jie, X. (2018). Two-dimensional Ti3C2 coating as an emerging protective solid-lubricant for tribology. *Ceramics International*, *44*(16), 20154–20162. https://doi.org/10.1016/j.ceramint.2018.07.309

Liao, P.-H., Jian, J.-W., & Tsay, L.-W. (2023). The Corrosion and Wear-Corrosion of the Iron-Base Amorphous Coating Prepared by the HVOF Spraying. *Metals*, *13*(6), 1137. https://doi.org/10.3390/met13061137

Lijesh, K. P., & Khonsari, M. M. (2020). Characterization of multiple wear mechanisms through entropy. *Tribology International*, *152*, 106548. https://doi.org/10.1016/j.triboint.2020.106548

Liu, Y., Yu, S., Shi, Q., Ge, X., & Wang, W. (2022). Multilayer Coatings for Tribology: A Mini Review. *Nanomaterials*, *12*(9), 1388. https://doi.org/10.3390/nano12091388

Lu, T., Wang, L., Jiang, Y., liu, Q., & Huang, C. (2016). Hexagonal boron nitride nanoplates as emerging biological nanovectors and their potential applications in biomedicine. *Journal of Materials Chemistry B*, *4*(36), 6103–6110. https://doi.org/10.1039/C6TB01481J

Lu, X., Gu, X., & Shi, Y. (2023). A review on the synthesis of MXenes and their lubrication performance and mechanisms. *Tribology International*, *179*, 108170. https://doi.org/10.1016/j.triboint.2022.108170

Mandali, H., Ghasemi, F., Farshad, A. A., Moradi Hanifi, S., Abedi, K., Ghorbani, M., & Ebrahimi, H. (2023). Risk and Reliability Assessment of Metal Lathe Machining Operation with DBN-FFTA Hybrid Approach. *Mathematical Problems in Engineering*, *2023*(1). https://doi.org/10.1155/2023/8873531

MatWeb LLC. (2024). *MatWeb: Online Materials Information Resource*. http://www.matweb.com

Mello, V. S., Faria, E. A., Alves, S. M., & Scandian, C. (2020). Enhancing Cuo nanolubricant performance using dispersing agents. *Tribology International*, *150*, 106338. https://doi.org/10.1016/j.triboint.2020.106338

Menezes, P. L., Nosonovsky, M., Ingole, S. P., Kailas, S. V., & Lovell, M. R. (2013). *Tribology for Scientists and Engineers*. Springer.

Michaelis, J. U., Kiese, S., Amann, T., Folland, C., Asam, T., & Eisner, P. (2023). Thickening Properties of Carboxymethyl Cellulose in Aqueous Lubrication. *Lubricants*, *11*(3), 112. https://doi.org/10.3390/lubricants11030112

Mir, I. A., Radhakrishanan, V. S., Rawat, K., Prasad, T., & Bohidar, H. B. (2018). Bandgap Tunable AgInS based Quantum Dots for High Contrast Cell Imaging with Enhanced Photodynamic and Antifungal Applications. *Scientific Reports*, *8*(1), 9322. https://doi.org/10.1038/s41598-018-27246-y

Miracle, A. A., & Olaleke, M. O. (2020). Predictive Model for Thermal Response During Dry Machining of Al 6082-T6 using Fem. *International Journal of Engineering Research & Technology (IJERT) Www.Ijert.Org*, *9*. www.ijert.org

Miryuk, O. A. (2024). Magnesia composite materials for layered products. *Kompleksnoe Ispol'zovanie Mineral'nogo Syr'â/Complex Use of Mineral Resources/Mineraldik Shikisattardy Keshendi Paidalanu*, *328*(1), 5–12. https://doi.org/10.31643/2024/6445.01

Morshed, A., Wu, H., & Jiang, Z. (2021). A Comprehensive Review of Water-Based Nanolubricants. *Lubricants*, *9*(9), 89. https://doi.org/10.3390/lubricants9090089

Ngaile, G., Montmitonnet, P., & Dohda, K. (2022). *Tribology in Manufacturing Processes* (Vol. 414). Trans Tech Publications Ltd. https://doi.org/10.4028/b-73JFhe

Nguyen, H. T., & Chung, K.-H. (2020). Assessment of Tribological Properties of Ti3C2 as a Water-Based Lubricant Additive. *Materials*, *13*(23), 5545. https://doi.org/10.3390/ma13235545

Nguyen, T. T., & Trung, N. D. (2021). On the thinning variations in hydrostatic forming of sheet metal. *Journal of Mechanical Engineering and Sciences*, *15*(1), 7824–7836. https://doi.org/10.15282/jmes.15.1.2021.17.0617

Nogueira, F. R., Pedroso, A. F. V., Silva, F. J. G., Campilho, R. D. S. G., Sales-Contini, R. C. M., Sebbe, N. P. V., & Casais, R. C. B. (2023). A Comparative Study on the Wear Mechanisms of Uncoated and TiAlTaN-Coated Tools Used in Machining AMPCO® Alloy. *Coatings*, *14*(1), 4. https://doi.org/10.3390/coatings14010004

Nowak, P., Kucharska, K., & Kamiński, M. (2019). Ecological and Health Effects of Lubricant Oils Emitted into the Environment. *International Journal of Environmental Research and Public Health*, *16*(16), 3002. https://doi.org/10.3390/ijerph16163002

Öpöz, T. T., & Chen, X. (2016). Chip Formation Mechanism Using Finite Element Simulation. *Strojniški Vestnik - Journal of Mechanical Engineering*, *62*(11), 636–646. https://doi.org/10.5545/sv-jme.2016.3523

Osman, O. A., Merah, N., Abdul Samad, M., Baig, M. M. A., Samuel, R., Alshalan, M., & Alshaarawi, A. (2022). Casing Wear and Wear Factors: New Experimental Study and Analysis. *Materials*, *15*(19), 6544. https://doi.org/10.3390/ma15196544

Otsuki, T., Okita, K., & Sasahara, H. (2022). Evaluating surface quality by luminance and surface roughness. *Precision Engineering*, *74*, 147–162. https://doi.org/10.1016/j.precisioneng.2021.10.013

Parida, A. K., Rao, P. V., & Ghosh, S. (2020). Influence of cutting speed and nose radius in the machining of Al-6061: FEM and experimental validation. *Materials Today: Proceedings*, *27*, 2569–2573. https://doi.org/10.1016/j.matpr.2019.10.142

Parra-Muñoz, N., Soler, M., & Rosenkranz, A. (2022). Covalent functionalization of MXenes for tribological purposes - a critical review. *Advances in Colloid and Interface Science*, *309*, 102792. https://doi.org/10.1016/j.cis.2022.102792

Pereira Falcón, J. C., Echeverría, A., Afonso, C. R. M., Zambrano Carrullo, J. C., & Amigó Borrás, V. (2019). Microstructure assessment at high temperature in NiCoCrAlY overlay coating obtained by laser metal deposition. *Journal of Materials Research and Technology*, *8*(2), 1761–1772. https://doi.org/10.1016/j.jmrt.2018.12.006

Podgornik, B. (2022). Adhesive Wear Failures. *Journal of Failure Analysis and Prevention*, *22*(1), 113–138. https://doi.org/10.1007/s11668-021-01322-4

Popov, V. L. (2010). *Contact Mechanics and Friction*. Springer Berlin Heidelberg. https://doi.org/10.1007/978-3-642-10803-7

Preedawiphat, P., Koowattanasuchat, P., Mahayotsanun, N., & Mahabunphachai, S. (2020). Sheet thinning prediction method based on localized friction effect in deep-drawing. *Advances in Mechanical Engineering*, *12*(9). https://doi.org/10.1177/1687814020953941

Qian, L., Zhang, Y., Zhang, S., Zhuang, L., & Zhang, J. (2020). Development and Status of Tool Coating. *International Journal of Engineering Research & Technology*, *9*(12), 189–191. www.ijert.org

Qiang, Z., Zhang, S., Zhuang, L., Zhang, J., & Zhang, Y. (2020). Development of Tool Coating. *International Journal of Engineering Research & Technology*, *9*(09), 959–962. www.ijert.org

Radhika, P., Sobhan, C. B., & Chakravorti, S. (2021). Improved tribological behavior of lubricating oil dispersed with hybrid nanoparticles of functionalized carbon spheres and graphene nano platelets. *Applied Surface Science*, *540*, 148402. https://doi.org/10.1016/j.apsusc.2020.148402

Rahmadiawan, D., & Shi, S.-C. (2024). Enhanced Stability, Superior Anti-Corrosive, and Tribological Performance of Al2O3 Water-based Nanofluid Lubricants with Tannic Acid and Carboxymethyl Cellulose over SDBS as Surfactant. *Scientific Reports*, *14*(1), 9217. https://doi.org/10.1038/s41598-024-59010-w

Rao, X., Yang, J., Chen, Z., Yuan, Y., Chen, Q., Feng, X., Qin, L., & Zhang, Y. (2020). Tuning C–C sp2/sp3 ratio of DLC films in FCVA system for biomedical application. *Bioactive Materials*, *5*(2), 192–200. https://doi.org/10.1016/j.bioactmat.2020.02.009

Ratoi, M., Niste, V. B., Walker, J., & Zekonyte, J. (2013). Mechanism of Action of WS2 Lubricant Nanoadditives in High-Pressure Contacts. *Tribology Letters*, *52*(1), 81–91. https://doi.org/10.1007/s11249-013-0195-x

Ren, Z., Jiang, H., Zou, Z., & Yuan, S. (2023). Simulation Prediction and Experiment of Brittle Damage of Cemented Carbide Microgroove Turning Tools Based on Peridynamics. *Processes*, *11*(2), 520. https://doi.org/10.3390/pr11020520

Rohlmann, P., Watanabe, S., Shimpi, M. R., Leckner, J., Rutland, M. W., Harper, J. B., & Glavatskih, S. (2021). Boundary lubricity of phosphonium bisoxalatoborate ionic liquids. *Tribology International*, *161*, 107075. https://doi.org/10.1016/j.triboint.2021.107075

Sami, U. K., & Wasim, J. (2023). Finite Element Analysis and Wear Rate Analysis of Nano Coated High Speed Steel Tools for Industrial Application. *Babylonian Journal of Mechanical Engineering*, *2023*, 13–19. https://doi.org/10.58496/BJME/2023/002

Schmid, S. R. (2013). Manufacturing Tribology. In *Encyclopedia of Tribology* (pp. 2159–2164). Springer US. https://doi.org/10.1007/978-0-387-92897-5_606

Schmid, S. R., Saha, P. K., Wang, J., & Schmitz, T. (2020). Developments in Tribology of Manufacturing Processes. *Journal of Manufacturing Science and Engineering*, *142*(11). https://doi.org/10.1115/1.4047723

Sebbe, N. P. V., Fernandes, F., Silva, F. J. G., Pedroso, A. F. V., Sales-Contini, R. C. M., Barbosa, M. L. S., Durão, L. M., & Magalhães, L. L. (2024). Wear Behavior of TiAlVN-Coated Tools in Milling Operations of INCONEL® 718. *Coatings*, *14*(3), 311. https://doi.org/10.3390/coatings14030311

Shailesh Rao, A., & Rao, S. (2024). Effect of alloy composition on machining parameters and surface quality through comprehensive analysis. *Frontier Materials & Technologies*, *4*, 97–110. https://doi.org/10.18323/2782-4039-2024-4-70-9

Sharifahmadian, O., & Mahboubi, F. (2019). A comparative study of microstructural and tribological properties of N-DLC/DLC double layer and single layer coatings deposited by DC-pulsed PACVD process. *Ceramics International*, *45*(6), 7736–7742. https://doi.org/10.1016/j.ceramint.2019.01.076

Sharma, A. K., Tiwari, A. K., Dixit, A. R., Singh, R. K., & Singh, M. (2018). Novel uses of alumina/graphene hybrid nanoparticle additives for improved tribological properties of lubricant in turning operation. *Tribology International*, *119*, 99–111. https://doi.org/10.1016/j.triboint.2017.10.036

Shaw, Z. L., Kuriakose, S., Cheeseman, S., Dickey, M. D., Genzer, J., Christofferson, A. J., Crawford, R. J., McConville, C. F., Chapman, J., Truong, V. K., Elbourne, A., & Walia, S. (2021). Antipathogenic properties and applications of low-dimensional materials. *Nature Communications*, *12*(1), 3897. https://doi.org/10.1038/s41467-021-23278-7

Shuai, J., Zuo, X., Wang, Z., Guo, P., Xu, B., Zhou, J., Wang, A., & Ke, P. (2020). Comparative study on crack resistance of TiAlN monolithic and Ti/TiAlN multilayer coatings. *Ceramics International*, *46*(5), 6672–6681. https://doi.org/10.1016/j.ceramint.2019.11.155

Sidh, K. N., Jangra, D., & Hirani, H. (2023). An Experimental Investigation of the Tribological Performance and Dispersibility of 2D Nanoparticles as Oil Additives. *Lubricants*, *11*(4), 179. https://doi.org/10.3390/lubricants11040179

Silva, K. H. S., Brito, P. P., Santos, I. B., Câmara, M. A., & Abrão, A. M. (2020). The behaviour of AISI 4340 steel coatings on low carbon steel substrate produced by friction surfacing. *Surface and Coatings Technology*, *399*, 126170. https://doi.org/10.1016/j.surfcoat.2020.126170

Singh, A., Chauhan, P., & Mamatha, T. G. (2020). A review on tribological performance of lubricants with nanoparticles additives. *Materials Today: Proceedings*, *25*, 586–591. https://doi.org/10.1016/j.matpr.2019.07.245

SKF Group. (2021). *Water-based lubricants make the vehicles of the future ready to roll*.

Sousa, V. F. C., Da Silva, F. J. G., Pinto, G. F., Baptista, A., & Alexandre, R. (2021). Characteristics and Wear Mechanisms of TiAlN-Based Coatings for Machining Applications: A Comprehensive Review. *Metals*, *11*(2), 260. https://doi.org/10.3390/met11020260

Stachowiak, G., & Batchelor, A. W. (2013). *Engineering Tribology* (4th Edition). Butterworth-heinemann.

Stephenson, D. A., & Agapiou, J. S. (2018). *Metal Cutting Theory and Practice*. CRC Press. https://doi.org/10.1201/9781315373119

Sulaiman, M. H. (2017). *Development and Testing of Tailored Tool Surfaces for Sheet Metal Forming* [PhD. Thesis, Technical University of Denmark]. https://core.ac.uk/download/pdf/154332245.pdf

Sulaiman, M. H., Christiansen, P., & Bay, N. (2017). A study of DLC coatings for ironing of stainless steel. *Journal of Physics: Conference Series*, *896*, 012031. https://doi.org/10.1088/1742-6596/896/1/012031

Sulaiman, M. H., Farahana, R. N., Bienk, K., Nielsen, C. V., & Bay, N. (2019). Effects of DLC/TiAlN-coated die on friction and wear in sheet-metal forming under dry and oil-lubricated conditions: Experimental and numerical studies. *Wear*, *438–439*, 203040. https://doi.org/10.1016/j.wear.2019.203040

Sulaiman, M. H., Farahana, R. N., Mustaffa, M. N., & Bienk, K. (2019). Tribological properties of DLC coating under lubricated and dry friction condition. *IOP Conference Series: Materials Science and Engineering*, *670*(1), 012052. https://doi.org/10.1088/1757-899X/670/1/012052

Tang, W., Huang, Z., & Wang, B. (2018). Synthesis of ionic liquid functionalized graphene oxides and their tribological property under water lubrication. *Fullerenes, Nanotubes and Carbon Nanostructures*, *26*(3), 175–183. https://doi.org/10.1080/1536383X.2017.1422246

Tang, W., Wang, B., Li, J., Li, Y., Zhang, Y., Quan, H., & Huang, Z. (2019). Facile pyrolysis synthesis of ionic liquid capped carbon dots and subsequent application as the water-based lubricant additives. *Journal of Materials Science*, *54*(2), 1171–1183. https://doi.org/10.1007/s10853-018-2877-0

Terwey, J. T., Fourati, M. A., Pape, F., & Poll, G. (2020). Energy-Based Modelling of Adhesive Wear in the Mixed Lubrication Regime. *Lubricants*, *8*(2), 16. https://doi.org/10.3390/lubricants8020016

TriboMAN. (2024). *Friction in Orthogonal Cutting*. Tribology Innovations for Manufacturing.

Trzepieciński, T. (2023). Approaches for Preventing Tool Wear in Sheet Metal Forming Processes. *Machines*, *11*(6), 616. https://doi.org/10.3390/machines11060616

Val, S., Lambán, M. P., Lucia, J., & Royo, J. (2024). Analysis and Prediction of Wear in Interchangeable Milling Insert Tools Using Artificial Intelligence Techniques. *Applied Sciences*, *14*(24), 11840. https://doi.org/10.3390/app142411840

Valdes, M. J., Marín, J. G. A., Rodriguez-Cabal, M. A., & Betancur, J. D. (2020). Tribometry: How is friction research quantified? a review. In *International Journal of Engineering Research and Technology* (Vol. 13, Issue 10, pp. 2596–2610). International Research Publication House. https://doi.org/10.37624/IJERT/13.10.2020.2596-2610

Valizade, N., & Farhat, Z. (2024). A Review on Abrasive Wear of Aluminum Composites: Mechanisms and Influencing Factors. *Journal of Composites Science*, *8*(4), 149. https://doi.org/10.3390/jcs8040149

Verma, J., Nagdeve, L., & Kumar, H. (2022). Tribological investigations into pin-on-disc tribometer under dry sliding conditions at various temperature ranges. *Proceedings of the Institution of Mechanical Engineers, Part E: Journal of Process Mechanical Engineering*, *236*(1), 178–186. https://doi.org/10.1177/09544089211042954

Wang, B., Tirado, A., Yang, F., Moran, C., Vander Woude, M., Song, Y., Wang, X., Qiao, R., Bai, S., Guo, Q., Tang, H., & Li, L. (2022). A functionalized ionic liquid as the next-generation nano-lubricant. *Droplet*, *1*(2), 192–201. https://doi.org/10.1002/dro2.28

Wang, L., Liu, Y., Chen, H., & Wang, M. (2022). Modification Methods of Diamond like Carbon Coating and the Performance in Machining Applications: A Review. *Coatings*, *12*(2), 224. https://doi.org/10.3390/coatings12020224

Wang, N., Wang, H., Ren, J., Gao, G., Chen, S., Zhao, G., Yang, Y., & Wang, J. (2020). Novel additive of PTFE@SiO2 core-shell nanoparticles with superior water lubricating properties. *Materials & Design*, *195*, 109069. https://doi.org/10.1016/j.matdes.2020.109069

Wang, Y., Li, C., Zhang, Y., Yang, M., Zhang, X., Zhang, N., & Dai, J. (2017). Experimental evaluation on tribological performance of the wheel/workpiece interface in minimum quantity lubrication grinding with different concentrations of Al2O3 nanofluids. *Journal of Cleaner*

Production, *142*, 3571–3583. https://doi.org/10.1016/j.jclepro.2016.10.110

Wang, Y., & Wang, Q. J. (2013). Stribeck Curves. In *Encyclopedia of Tribology* (pp. 3365–3370). Springer US. https://doi.org/10.1007/978-0-387-92897-5_148

Waqas, M., Zahid, R., Bhutta, M. U., Khan, Z. A., & Saeed, A. (2021). A Review of Friction Performance of Lubricants with Nano Additives. *Materials*, *14*(21), 6310. https://doi.org/10.3390/ma14216310

Wijanarko, W., Khanmohammadi, H., & Espallargas, N. (2022a). Ionic Liquid Additives in Water-Based Lubricants for Bearing Steel – Effect of Electrical Conductivity and pH on Surface Chemistry, Friction and Wear. *Frontiers in Mechanical Engineering*, *7*. https://doi.org/10.3389/fmech.2021.756929

Wijanarko, W., Khanmohammadi, H., & Espallargas, N. (2022b). Ionic liquids as boundary additives in water-based and PAO lubricants. *Friction*, *10*(9), 1405–1423. https://doi.org/10.1007/s40544-021-0550-0

Xiao, L., Xu, Y., & Chen, Z. (2022). Fretting tribological performance of DLC, TiAlN and DLC/TiAlN coatings deposited on carburized 18CrNi4A steel. *Surface Topography: Metrology and Properties*, *10*(1), 015009. https://doi.org/10.1088/2051-672X/ac4ab8

Xiao, L., Xu, Y., Chen, Z., & Xu, H. (2024). Tribological Properties of Diamond-Like Carbon, TiAlN, and Diamond-Like Carbon/TiAlN Coatings Deposited on Carburized 18CrNi4A Steel for Heavy-Duty Aerospace Transmission Components. *Journal of Materials Engineering and Performance*, *33*(2), 601–617. https://doi.org/10.1007/s11665-023-07996-1

Xu, J., Jiang, Q., Yang, J., Cui, J., Zhao, Y., Zheng, M., Oliveira, J. P., Zeng, Z., Pan, R., & Chen, S. (2023). A Review on Ultrafast Laser Microwelding of Transparent Materials and Transparent Material–Metals. *Metals*, *13*(5), 876. https://doi.org/10.3390/met13050876

Xu, Y., & Stokes, J. R. (2020). Soft lubrication of model shear-thinning fluids. *Tribology International*, *152*, 106541. https://doi.org/10.1016/j.triboint.2020.106541

Xu, Y., Wen, W., & Wu, J.-M. (2018). Titania nanowires functionalized polyester fabrics with enhanced photocatalytic and antibacterial performances. *Journal of Hazardous Materials*, *343*, 285–297. https://doi.org/10.1016/j.jhazmat.2017.09.044

Yang, L., Ji, W., Mao, M., & Huang, J. (2020). An updated review on the properties, fabrication and application of hybrid-nanofluids along with their environmental effects. *Journal of Cleaner Production*, *257*, 120408. https://doi.org/10.1016/j.jclepro.2020.120408

Yi, S., Li, J., Liu, Y., Ge, X., Zhang, J., & Luo, J. (2021). In-situ formation of tribofilm with Ti3C2Tx MXene nanoflakes triggers macroscale superlubricity. *Tribology International*, *154*, 106695. https://doi.org/10.1016/j.triboint.2020.106695

Yogesh Dileep Lande. (2024). Tool Coating Development: A Historical Overview. *International Journal of Advanced Research in Science, Communication and Technology*, 155–161. https://doi.org/10.48175/IJARSCT-17624

Zhai, W., Srikanth, N., Kong, L. B., & Zhou, K. (2017). Carbon nanomaterials in tribology. *Carbon*, *119*, 150–171. https://doi.org/10.1016/j.carbon.2017.04.027

Zhang, Y., Biboulet, N., Venner, C. H., & Lubrecht, A. A. (2020). Prediction of the Stribeck curve under full-film Elastohydrodynamic Lubrication. *Tribology International*, *149*, 105569. https://doi.org/10.1016/j.triboint.2019.01.028

Zhang, Y., Chan, C., Li, Z., Ma, J., Meng, Q., Zhi, C., Sun, H., & Fan, J. (2019). Nanotoxicity of Boron Nitride Nanosheet to Bacterial Membranes. *Langmuir*, *35*(18), 6179–6187. https://doi.org/10.1021/acs.langmuir.9b00025

Zhao, J., Yang, G., Zhang, C., Zhang, Y., Zhang, S., & Zhang, P. (2019). Synthesis of water-soluble Cu nanoparticles and evaluation of their tribological properties and thermal conductivity as a water-based additive. *Friction*, *7*(3), 246–259. https://doi.org/10.1007/s40544-018-0209-7

APPENDINCES

Appendix A: Viscosity of WBLs at ~ 30 °C

Lubricant	Viscosity (mPa.s)
Distilled water	0.806952
CMC_IL	22.48571
CMC_IL/Mxene	8.394762
CMC_Mxene	6.285238
XG_IL	139.1429
XG_IL/Mxene	14.89524
XG_Mxene	21.64286

Appendix B: Roughness measurement on the surface

Lubricant	Roughness	
	Ra [μm]	Sa [μm]
CMC_IL	3.016	4.467
CMC_Mxene	4.965	4.745
CMC_Mxene/IL	1.108	1.441
XG_IL	3.164	1.837
XG_Mxene	1.361	1.941
XG_Mxene/IL	2.050	2.061

Appendix C: ionic liquid tributyl(methyl)phosphonium dimethyl phosphate

with >95 % form Tokyo Chemical Inc, Japan

Appendix D: $Ti_3C_2T_x$ MXene multilayer Nanoflake with Purity 99.9 % from Nanoshell, India

Appendix E: Homogenizer process

Appendix F: Magnetic stirrer process

Appendix G: DLC/TiAlN coating of ironing process

BIODATA OF STUDENT

Muhammad Shuhaimi bin Ibrahim, born in 1999 and originally from Kelantan, is the seven of seven siblings. He graduated with a bachelor's degree with Honors in mechanical and manufacturing from Universiti Putra Malaysia (UPM) in 2022 and is currently pursuing a master's degree at the same university. His research focuses on metal working, additive in lubricant, and water-based lubrication, with plans to further his studies by pursuing a PhD in the future.

LIST OF PUBLICATIONS

Ibrahim, M. S., Sulaiman, M. H., Samin, R., Yaakob, Y., Kamis, S. L., Ridzuan, M. J. M., Pauzi, A. A., Sukindar, N. A, & Bienk, K. (2024). Tool wear of DLC coating as top-layered to CrN-, TiAlSiN-, TiAlN coatings in machining of steel and aluminum alloys. *Wear*, 205574. https://doi.org/10.1016/j.wear.2024.205574.

Ibrahim, M. S., Sulaiman, M. H., & Ismail, M. I. S. S. (2024). Enhancing wear resistance in blanking and punching of stainless-steel sheets under dry friction and solid lubrication conditions using single-layer ceramic-and carbon-based hard coatings. *Jurnal Tribologi*, *40*, 139-147.

Rui, L. M., Sulaiman, M. H., Ashman, M. A. H. A., **Ibrahim M. S.,** and Jamie, M. R. M. (2024). Enhancing physical, mechanical, tribological and contact characteristics of water-based lubrication using ceramic nanomaterials MgO and SiC for metal-to-metal sliding interfaces. *Jurnal Tribologi*, *39,* 51-68.

LIST OF PUBLICATIONS (SUBMITTED TO JOURNAL/ACCEPTED):-

Muhammad Shuhaimi Ibrahim, Mohd Hafis Sulaiman, Mohd Idris Shah Ismai. Influence of oil-based and water-based lubrication on tool wear of DLC/TiAlN-coated punches in blanking of stainless steel. Jurnal Tribologi, (*Submission ID: JTRIB-00751-2024-03*) [*Accepted: 17-10-2024*].

Muhammad Shuhaimi Ibrahim, Mohd Hafis Sulaiman. Assessment of lubricant performance enhanced with nanoadditive in punching and blanking of aluminium. Jurnal Tribologi, (*Submission ID: JTRIB-00761-2024-02*) [*Accepted: 27-9-2024*].

M.A.H. Azizana, **M.S. Ibrahim**, M.H. Sulaimanaa, Y. Yaakobb. Dispersion and tribological behaviours of modified functionalized surfaces of single and hybrid nanoparticles in water-based lubrication. Tribology Transactions, (*Submission ID: UTRB-6094*) [*Under first revision, Submission: 27-Oct-2024*].

A.F.M. Zainudina, **M.S. Ibrahim**, M.A.H. Azizana, M.H. Sulaimana. Assessment of boundary water-based lubrication enhanced with Ionic Liquid, MXene, t-GO, Al_2O_3, MgO, SiC and TiO_2 nanoadditives. Tribology Transactions, (*Submission ID: UTRB-6346*) [*Under review, Submission: 06-Sep-2024*].

LIST OF PAPERS PRESENTATION AT CONFERENCES: -

1. 5th MYTRIBOS International Symposium 2023
    - Title: Enhancing wear resistance in blanking and punching of stainless-steel sheets under dry friction and solid lubrication conditions using single-layer ceramic-and carbon-based hard coatings.
    - 24 August 2023.
    - Faculty of Engineering, Universiti Putra Malaysia, Selangor, Malaysia.

2. The 4th Malaysian International Tribology Conference (MITC2024)
    - Title: Influence of oil-based and water-based lubrication on tool wear of DLC/TiAlN-coated punches in blanking of stainless steel.
    - 2 – 3 September 2024.
    - The Pacific Sutera Hotel, Kota Kinabalu, Sabah, Malaysia.

3. 6th Malaysia-Japan Tribology Symposium 2024 (MJTS2024)
    - Title: Effects of parameter settings on tool wear in metal cutting of steel and aluminium alloys.
    - 29 August 2024.
    - Malaysia-Japan International Institute of Technology, Universiti Teknologi Malaysia (UTM), Kuala Lumpu